MODEL VALIDATION AND DESIGN FOR THE DYNAMIC ENVIRONMENT SIMULATOR

Jon A. van Poppel, MSME
David J. Pancratz, MSME
Mike H. Rangel, B.Sc.
Brian J. Barton, MSME
Robert D. Banks, BENG, MD
John B. Bomar, Jr., Ph.D.

September 1998

Final Report for period May 96 to September 1998

Prepared for:
Department of the Air Force
AFRL Human Effectiveness Directorate
United States Air Force
Brooks AFB, Texas 78235-5352

TABLE OF CONTENTS

TABLE OF CONTENTS (continued)

FIGURES

FIGURES (continued)

TABLES

ACKNOWLEDGMENTS

The members of the research team express their deep appreciation to the many individuals and organizations making contributions to this research program. Without the timely assistance given so generously by everyone, the research program and this report could not possibly have been accomplished.

The research team wishes to express their gratitude for the cooperation, support, and guidance of the Air Force Technical Project Manager Dr. William Albery, Dr. Daniel Repperger and Dr. Tamara Chalette of the Human Effectiveness Directorate, USAF Research Laboratory (AFRL). The excellent studies provided by Jeff Bird and Marvin Roark both of Veridian, Inc., were essential to our success.

Finally, the research team gives a very special thank you to the support staff at BRC. Without the effort of Celina Canales in operations support, this research program could not have been reported effectively. Appreciation is also due to Darrin Smith for research engineering support, John Martini and Adolph Mena for illustration support, and Patricia Riley for information services support.

1.0 Summary.

Biodynamic Research Corporation (BRC) of San Antonio, TX completed an SBIR Phase II project to validate a PC-based mathematical model of an Air Force centrifuge and to conduct a design improvement study of the centrifuge. The impetus for this project was the desire to faithfully replicate high agility aircraft accelerations using a ground-based simulator. Specifically, the model and design study were conducted to improve the utility of the Dynamic Environment Simulator (DES), located at Wright-Patterson Air Force Base.

In Phase I, BRC designed the centrifuge model software with two basic functions: (1) to permit the creation of centrifuge acceleration profiles from a desired set of crewmember motions, and (2) to simulate the effect of centrifuge motions on a crewmember. Part of the objectives in Phase II was to validate the model initiated in Phase I so that DES personnel could rely on the software for predicting the accelerations on a crewmember. To validate the software, BRC and subcontractor Veridian Inc. of Dayton, OH, conducted multiple test runs with the DES. In some of the tests, BRC predicted the accelerations at the crewmember location before the simulation to prove the validity of the software model.

The PC-based software model was developed using The Mathworks Matlab® version 5.1 for Windows, an interactive software package designed for numeric computation and visualization. The main model code was written in Matlab's interpreted expression language. Matlab interprets this code from text files, called m-files. In addition to this code, BRC engineers also developed certain numerical routines in C++ and Fortran to speed the analysis of centrifuge profiles.

A second part of the Phase II effort was to conduct a design study for improving the capabilities of the DES. BRC had subcontractor Veridian Inc. study the feasibility of upgrading the main arm drive system, new fork and cab drive systems, some of the centrifuge controls, the cab interior, and other systems. Veridian prepared the upgrade study according to different levels of cost for the Air Force. The benefits from upgrading to each level are described, and the cost to achieve the level are defined.

Using the improved performance levels from the Veridian design study, BRC conducted a cost-benefit study to allow the different upgrades to be compared from the standpoint of preparing the DES for future simulation needs. Major conclusions from this study were that arm G-onset improvements above 3.5 G/sec will not improve the DES simulation of high-agility aircraft maneuvers and that the addition of a fourth degree of freedom in the DES cab is likely to improve simulation fidelity in many profiles of interest.

Finally, BRC studied the commercial potential of using the DES for simulating the acceleration conditions prevalent in passenger car rollovers. Based on this study, it was evident that the DES could be used to model the early segments of a rollover.

Table 1-1 summarizes the results of the Phase II effort.

Table 1-1 Summary of DES Results

• Operates with Matlab for Windows software. • Provides tools for the creation of custom DES acceleration profiles. • Features two algorithms for computing the kinematics and motor commands necessary to simulate an agile flight maneuver. • Permits the forward computation of crewmember acceleration knowing centrifuge motions. • Has been verified to be an accurate and useful tool for predicting crewmember acceleration and designing acceleration profiles. • Features a graphical user interface. • Permits the visualization of simulation output.
• BRC tested simulations with the software and by hand to verify the software was coded properly. • DES tests were conducted and acceleration was measured to compare to the predicted motions from the DES software.
• A study of main arm upgrades, ranging from an increase in G onset to 1.5 G/sec to as high as 5 G/sec. • A fork upgrade study that would seek to improve its reliability and control. • Studies of upgrading the cab performance and interior. • A study of primary controller upgrades that would improve some of the control components for the DES. • A study of instrumentation and data transmission systems.
• Upgrading the arm to a G onset above 3.5 G/sec would be of no additional benefit. • Adding the fourth degree of freedom, a rotating pilot seat, would improve fidelity for many DES simulations.
• Potential for the DES to be used in simulations of early stages of a passenger car rollover.

2.0 Introduction.

This report describes an SBIR Phase II effort to validate a mathematical model and conduct a design study of the Air Force Dynamic Environment Simulator. The Dynamic Environment Simulator, or DES, is a three degree-of-freedom centrifuge operated by Armstrong Laboratories at Wright-Patterson AFB. The effort was conducted under Contract #F41624-96-C-6027 through the Armstrong Laboratory and was entitled "Model Validation and Design Study of the Dynamic Environment Simulator."

This Phase II project had four primary objectives, which were to:

1. Validate the Phase I software model of the DES;
2. Conduct a design study of DES improvements;
3. Perform a cost/benefit analysis of the possible DES improvements; and
4. Demonstrate the commercial potential of the model and the DES.

In order to achieve these objectives, BRC proposed a work plan that included the following steps:

1. Establishment of a model validation methodology;
2. Development of a testing protocol;
3. Conducting series of tests with the DES and evaluating the model performance;
4. Conduct a design improvement study;
5. Conduct a cost/benefit analysis of proposed improvements; and
6. Demonstrate the commercial potential of the software model and DES.

This final report documents and summarizes the work generally according to the objectives and work plan outlined above. Table 2-1 shows an outline of this report.

Table 2-1 Content of the DES Final Report

Section		Description
1.	Summary	This section summarizes the work done for this Phase II project.
2.	Introduction	This section describes the layout and organization of the final report.
3.	Technical Background and Literature Review	This section describes the technical background considerations and all literature reviewed in preparation for work on this project.
4.	Mathematical Model of the DES	This section describes the mathematics of how the DES was modeled.
5.	DES Testing and Validation of the DES Modeling	This section describes the testing that was conducted to validate model.
6.	Rollover Simulations Using the DES	This section describes simulations of automotive rollovers that would be a potential commercial application for the DES.
7.	Design Study of DES Improvements	This section describes the efforts of Veridian to design improvements for the DES that improve the performance or enhance the utility of the centrifuge.
8.	Cost/Benefit	This section describes a cost/benefit analysis of possible design improvements.
9.	Recommendations	This section presents recommendations for DES improvements and further studies.

3.0 Technical Background and Literature Review.

The Dynamic Environment Simulator, or DES, is a 3 degree-of-freedom centrifuge operated by Armstrong Laboratories at Wright-Patterson AFB, OH.

Figure 3-1 shows a schematic of the DES. Powered gimbals at the end of its 19-foot arm provide the two additional degrees of freedom, enabling the cab to pitch and roll. To simulate flight maneuvers, programmed commands are sent to each of the DES motors, producing motion along each of the three axes. As a result, the centrifuge crewmember receives both linear and angular accelerations. The primary objective of this project was the development of a software tool for the prediction and simulation of the optimal DES command signals.

Figure 3-1 Schematic of DES Centrifuge

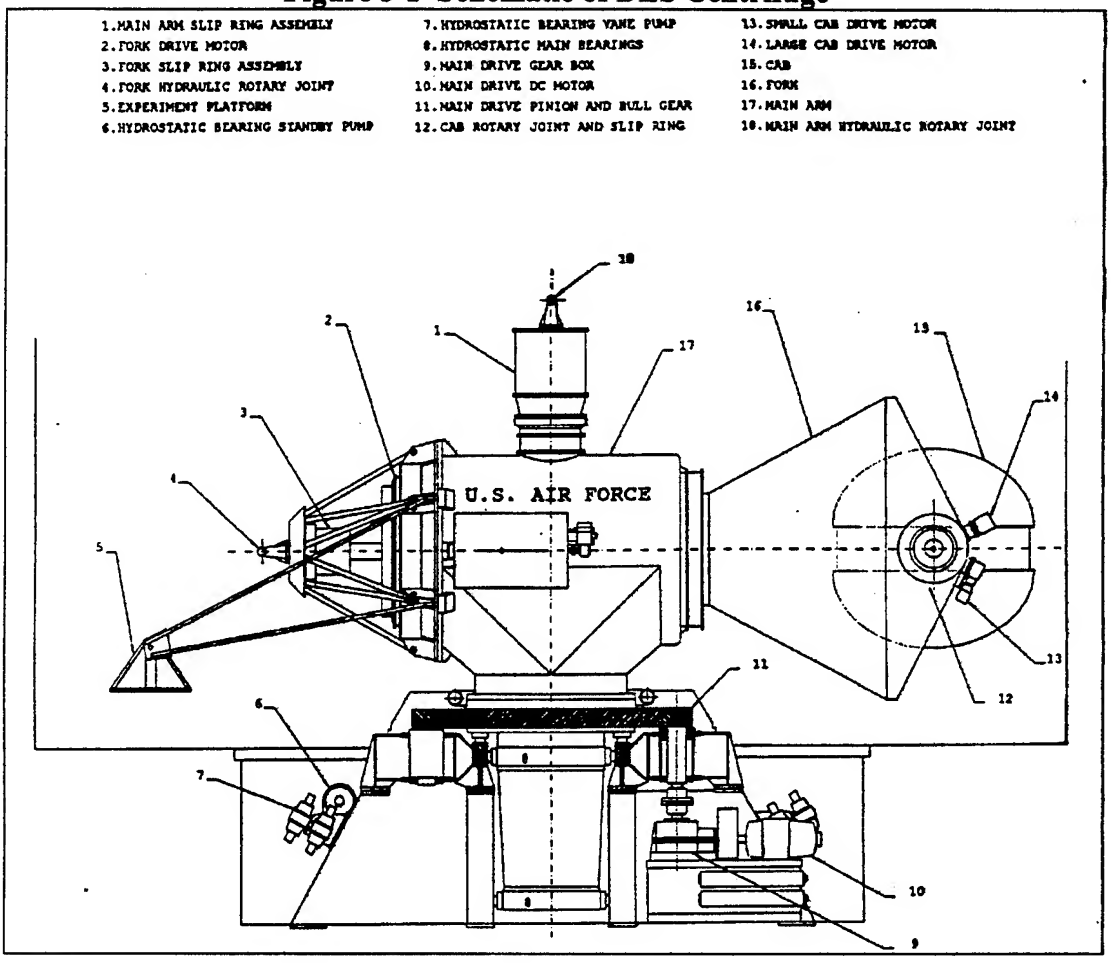

To accomplish that objective, BRC first conducted a literature review. BRC reviewed current literature on centrifuges and agile flight maneuvers, much of which was compiled from previous SBIR projects. In addition, BRC supplemented its library with recent literature in the areas of robot control and optimization theory, and with multiple publications related to the operation and performance of the DES.

3.1 Background and Literature Review.

The aim of this section is to review the nature of high-agility flight, the likely effects that high-agility flight will have on humans, and outline a rationale for research. This will lay the groundwork to show how an improved performance DES could contribute to innovative and aggressive research aimed at closing the time lag that now exists between high-agility technology and human factors technology, and will prevent predictable loss of life and scarce resources.

3.2 Agile Flight Technology.

The F-22 Raptor, now in flight testing, will be the first production thrust-vectored fighter in aviation history[1]. While capable of +/- 20 degrees of pitch thrust-vectoring (TV)[2], the F-22 will open a new era in aviation that will be characterized by pitch rates 2-3 times those of conventional aircraft[1] and angles-of-attack (AOA) up to 70-degrees[3]. Planned for operational deployment after 2003[1], the effect on humans of this capability will be defined in flight testing and early operations.

F-22 RAPTOR

- first production thrust-vectored fighter in history
- pitch rates 2-3 times those of conventional aircraft
- angles-of-attack up to 70-degrees
- will expose pilots to accelerations not previously experienced
- time-lag between F-22 development and human factors knowedge-base is significant

The F-22 will expose pilots to combinations of translational and rotational accelerations not previously experienced in fighter aircraft. Conceived in 1987 in response to a United States Air Force (USAF) statement of requirements, the YF-22 prototype was chosen as the next generation air superiority fighter in 1990 after a fly-off competition against the YF-23[2]. The rapid advance from concept to production aircraft has left the F-22 with a G-protection system little changed in concept from previous, non-agile aircraft. Also, F-22 flight instrument technology may prove ineffective in preventing loss of situational awareness among pilots during high-AOA maneuvering. The time-lag between F-22 technology development and development of human life support technologies is very significant. If not addressed, losses of aircraft and life will predictably occur.

3.2.1 Thrust Vectored Propulsion.

Thrust vectored propulsion (TVP) is the redirection of engine thrust in flight. With the development of high thrust/weight ratios, TVP systems have redefined the balance of forces on aircraft. Mature TVP systems can augment, and in some cases, eliminate the need for flight control surfaces. TVP adds energy to directional control and can provide for tight, highly agile movement of aircraft in flight. Thrust vectored control (TVC) has been used to describe this capability[4].

TVP enhanced maneuvering has variously been termed "high agility," "superagility," "supermanueverability," or "enhanced fighter maneuverability (EFM)[5]." The general concept was first described by Wolfgang Herbst and colleagues at Messerschmitt-Boelkow-Blohm (MBB) through research conducted in the 1970s. In exploring the concept of EFM, Herbst conceived the idea that controlled flight was feasible at high AOAs, at speeds less than the stall speed for condition of flight[6]. Using TVP, he postulated that it would be possible to deeply penetrate this previously forbidden part of the flight envelope, and maintain control throughout. This capability was termed post-stall maneuvering (PST)[7].

As conceived by Herbst, high AOAs during PST would allow unprecedented maneuvering potential that could include the ability to quickly "point" the nose of the aircraft at an adversary

THRUST VECTORED PROPULSION (TVP)

- redirection of engine thrust in flight
- provides for tight, highly agile maneuvering of aircraft in flight
- termed "high agility," "superagility," "super maneuverability," "enhanced fighter maneuverability."
- controlled flight possible below the stall speed
- allows pilot the ability to "point" the aircraft nose at an adversary

while maintaining complete control. Since the stall-AOA was previously considered the limit of low speed aircraft control, a new term, 'high alpha,' was introduced to describe pitch angles beyond the stall-AOA[8].

TVP was not limited to pitch thrust vectoring. By redirecting the thrust vector into the yaw plane, it was possible to introduce a lateral "pointing." At MBB, Herbst and his colleagues conceived several novel flight maneuvers that exploited pitch and yaw TVP. An example was the "Herbst" maneuver, which used pitch TVP to achieve high alpha and PST, then lateral TVP to yaw (or roll) the aircraft around the direction of flight (or velocity vector). This maneuver had the tactical advantage of allowing the aircraft to change direction quickly.

3.2.2 Enhanced Maneuverability Flight (EFM).

The tactical advantages of a point-first capability arose from the development of all aspect missiles[9,10,11], that is, missiles that could lock on the forward aspect of a target. Since fighter pilots would no longer need to tail-chase into a '6 o'clock position', just pointing at the adversary would be sufficient to achieve a kill[6]. With improved fire control systems, missile launch opportunities for all aspect weapons would be directed forward, along the aircraft longitudinal axis and aircraft "pointing" would be important in minimizing missile flight duration, essential in order to escape mutual destruction[11]. Herbst projected exchange ratios of at least 2:1 in air-to-air combat involving EFM aircraft flown against current modern fighter aircraft[7]. His prediction proved to be an underestimation.

Nevertheless, some thought short range air-to-air combat capability was unimportant in an era of beyond-visual-range weapons. The need for short range air-to-air combat capability arose when considering an extended conflict, after beyond-visual-range weapons were expended or electronic countermeasures neutralized intelligence and command capabilities. The conflict would then close to medium and short-range engagements[12]. Survivability would then depend on the "point-first" capability, use of all-aspect missiles, and the ability to avoid threats, including the threat of mutual destruction. Rapid pitch maneuvers would be required[1]. New tactics that traded energy for agility would emerge. Medium-range engagements would still take place at supersonic speed and involve the moderate sustained-G maneuvers seen in current operational aircraft. Thus, the successful future combat aircraft would need designs incorporating the high speed capabilities of current fighters with lower speed high agility[13].

The advantages of EFM would not be limited to short range, air-to-air combat. The majority of aircraft losses in recent wars have been due to ground attack[14]. Low level tactical maneuvering or automated systems, such as the Automatic Maneuver and Attack System (AMAS), would enhance EFM-capable fighters ability to escape ground or air threats. The dive attack would remain an important tactical option that would be improved by EFM[14], and EFM would allow strike fighters to avoid potential ground/air threats[15]. While future ground attack aircraft, such as the Joint Strike Fighter (JSF), might eventually use unmanned fighter versions in this role[16], no existing combination of computers and simulators of appropriate size can yet duplicate the capabilities of a pilot in real-world conditions[17]. Pilots will remain in the ground attack role for the foreseeable future.

There are two particular disadvantages associated with EFM: 1) low energy states following the PST maneuver, leaving the fighter vulnerable to reattack; 2) the spin-like characteristic of the PST roll maneuver[9]. Energy decay will be reduced by minimizing the time spent at PST. Herbst has predicted average PST durations of 5 s[7]. With the possibility of pitch rotations of 400 degrees per second, it is possible that EFM maneuvers will involve completion of pitch-up to greater than 70 degrees AOA and recover to straight and level flight in considerably less than 5 s[1]. While the design of such a capability may be possible, the pilot will experience both impact and sustained acceleration and the effect of the combination of these accelerations is largely unknown. The effects of an abrupt spin-like maneuver, such as a rapid Herbst maneuver, during high and changing +Gz acceleration, is also unknown.

ENHANCED FIGHTER MANEUVERABILITY (EFM)

- advent of the F-22 signifies acceptance of concept
- there is an affirmation of the need for EFM in future war
- future development is inevitable
- can be applied to helicopters, transports, unmanned air vehicles

3.3 Historical Perspective.

Prior to 1987, the conceptual framework and early design of EFM was conducted using simulations[7]. Proof of concept flights, using a variety of unmanned scaled models, began in 1987[11]. These models included TVP-modified F-15, F-16s and tailless aircraft. These flights confirmed the concept, and the value of the earlier work, and demonstrated that TVP could double pitch rate[18] and triple turning rate of the F-15[11]. PST flight tests of an F-22 model were conducted[11]. The advantages of tailless flight using TVC were demonstrated in models[2,4].

In the face of continued skepticism regarding the advantages of EFM, a manned flight research program involving the first international X-plane, the X-31, was undertaken to address the issue[6]. The goal of this work was to demonstrate high agility in flight and produce design guidelines that would allow future aircraft to excel in close combat without sacrificing beyond-visual-range capabilities[19]. Notably, the X-31 program was out of phase with the Advanced Tactical Fighter (ATF) program which already had the YF-22 and YF-23 prototypes flying[20].

The X-31 demonstrated several unique maneuvers, including enhanced PST flight, pitch-up from inverted flight, and the "Herbst" maneuver. In air combat maneuvering, the X-31 dominated comparable conventional adversaries by an exchange ratio of 3:1, although results were more mixed against superior fighters[21]. Kill ratios in excess of 32:1 were reported in offensive mode with TVP activated (the X-31 always won offensively in this series). Exchange ratios against the F-14 were 8:1[22].

EFM gained popular attention at the 1989 Paris show when the Russian Su-27 demonstrated a maneuver that became known as the Cobra maneuver[23]. Analysis of this maneuver demonstrated a shortfall in Western fighter technology. Only the F-16 could somewhat duplicate the maneuver, although with loss of lateral stability[23]. It was estimated that the Su-27 had at least three more basic fighter maneuvers not available to Western fighter pilots: loaded roll, post-stall pointing (Herbst), and improved pitch rate below 300 knots[23].

Subsequently, the Su-27 demonstrated previously unknown high levels of transient agility[23,24]. A subsequent version of the Su-27, the Su-37, had fully independent, fully moveable thrust nozzles for each of its two engines. The Su-37 demonstrated superior agility that included backward flight during post-stall loops[2]. The Russians are currently flight testing the Su-35, capable of TVP of +/- 15 degrees in yaw and pitch, and have indicated their intention to market the aircraft internationally[22]. An additional maneuver, the 'hook' - or sideways Cobra, was introduced using

the Su-35[11]. The Russians have sold 50 Su-27s to the Chinese since the early 1990s[25]. The Indian air force is currently purchasing 40 Su-30MKI fighters equipped with pitch-yaw nozzles capable of +/- 15 deg and +/- 32 deg respectively[26].

As the USAF and United States Navy (USN) became more active in assessing the merits of TVP[27], additional flight based programs were approved. Using the Calspan NF-16D variable stability in-flight test aircraft (VISTA)[28], multi-axis thrust vectoring (MATV) demonstrated the tactical advantages of TVP. The heavily modified F-16 demonstrated the Cobra, J-turn maneuver, split-S, and Herbst maneuvers[29]. Another maneuver, the "helicopter" consisted of a flat-spin that allowed continuous pointing at any adversary in any position in the sky[2]. The USN funded similar research involving the F/A-18 High Angle of Attack Research Vehicle (HARV)[27]. Work involving a tailless aircraft (X-36) was also conducted[2,30]. While the role of TVP in the future Joint Strike Fighter (JSF) remains unclear, the requirement for short take-off and landing capability is an indication that capability for highly agile flight will exist. Future flights of the JSF prototypes, the Boeing X-32 and the Lockheed Martin X-35, will ultimately define new JSF capabilities[15].

The advent of the F-22 signifies an acceptance of the concept of TVP and affirmation of the need for EFM in future war. Driven by the competitive work of potential adversaries, and the likelihood of future tactical encounters with EFM-capable aircraft, future development is inevitable[2,10,21,30]. While essential to fighters, TVP may also be applied to helicopters, transport aircraft, and unmanned air vehicles[11,31].

3.4 Acceleration Stress During High-Agility Flight.

Very few pilots have experienced high agility flight. Moreover, there is very little data in the published literature that relates to the effects of Gx, Gy or Gz associated with EFM flight. However, it is possible to speculate on the acceleration stress that will be encountered by pilots during EFM.

The primary physiological effects of EFM on pilots will relate to abrupt changes in magnitude and/or direction of acceleration experienced by the pilot. Acceleration has been categorized as "impact" (less than 1-second duration) or "sustained" acceleration (greater than 1-second duration). Sustained acceleration is experienced in aircraft as a result of centrifugal force during high velocity turns. Previously, impact acceleration was associated with collisions (crashes), turbulence, or ejection escape. Pilots of EFM-capable aircraft will experience both impact and sustained acceleration during maneuvers that may be complete in several seconds[2].

ACCELERATION STRESS DURING EFM

- very few pilots have experienced EFM
- there is little data in existence on the effects on humans of EFM
- +Gz will likely be less than current aircraft, but more frequent
- -Gz will be much more frequent
- 0 Gz will be more frequent
- Gy exposure will become frequent
- Gx exposures will increase in magnitude
- angular acceleration will be superimposed on translational acceleration

While it is possible that peak Gz loads will be higher then those currently experienced, very short G durations might preclude physical harm[10] and some have claimed that peak +Gz may actually decrease during EFM[32]. Nevertheless, angular acceleration will be a new, potentially dangerous feature[33]. Herbst predicted the following maneuver characteristics: 1) 5 s PST average duration; 2) 10% of total engagement time in PST; 3) lower G-level by about 1 G, and; 4) lower maneuvering speeds by about 0.1 M[7].

Some prediction of the nature of acceleration stress can be made by considering several defined EFM maneuvers. The Herbst maneuver consists of an abrupt pitch-up to a high-alpha in the PST envelope followed by a 180 degree yaw leading to a nose-down inverted attitude and low airspeed. Recovery then allows the aircraft to reverse direction within a very short turning radius. The pilot would start the Herbst from +Gz, experience increased +Gz of short duration due to pitch, and experience additional increased +Gz due to aircraft decelerating profile drag. Then, depending on entry speed, seat back angle, and time at high alpha, the pilot would experience 0 Gz or -Gz before +/-Gy begins during the yaw phase. If stable velocity is achieved prior to yaw, the pilot would experience +1 Gx (gravity). Tamrat has compared the Herbst maneuver to a spin[9]. The magnitude of yaw-induced Gy would vary with the distance of the cockpit from the center of aircraft rotation[34]. On completion of the yaw, in the nose down attitude, the pilot would experience 0 Gz and increased +Gx during energy recovery, and +Gz during dive recovery (possible "push-pull" effect). Current aircraft attitude flight instrument depictions would make spatial orientation a problem during this maneuver, especially during low visibility conditions. These projected G changes are summarized in Table 3-1.

During a Cobra maneuver, the pilot would start from +Gz and experience rapidly increased +Gz due to pitch and drag (similar to the Herbst maneuver). When stable at high-alpha, with no pitch movement, 0 or -Gz would occur. On recovery, nose down pitch would result in increased -Gz that would vary with the distance of the pilot from the center of pitch rotation[34]. The ability to recover from the Cobra may be limited by the pilot's -Gz tolerance. Negative AOA might occur during energy recovery with increased +Gz as the aircraft accelerates out of the maneuver (again, possible push-pull effect). Depending on exit speed, the maneuver could be repeated, or the pilot might unload to 0 Gz to recover energy. These projected G changes are displayed in Table 1. As with the Herbst maneuver, spatial orientation will be a problem in poor visibility conditions. In-flight recordings from a TVP modified F-15 showed G variations during pitch of -1.5 Gz to

+4 Gz, -1 Gy to +1 Gy, and - 1 Gx[22].

The so-called standard agility maneuvers (SACOMs), devised to provide common objective measures of agility between aircraft, offer additional insight into the acceleration stress that will be encountered during EFM. Gal-Or has proposed seven SACOMs:

1) Voll (post-stall roll around the velocity vector) reversal post-stall acceleration/deceleration;
2) pure pitch reversal post-stall rotation acceleration/deceleration;
3) pure yaw reversal rotation acceleration/deceleration;
4) pure roll reversal rotation acceleration/deceleration;
5) pure axial reversal translational acceleration/deceleration;
6) pure lateral reversal translational Jink-Track acceleration/deceleration;
7) pure 'vertical' reversal translational Jink-Track acceleration/deceleration[22].

The following stresses will predictably be experienced:

SACOM #1 (voll reversal): Starting from straight and level flight (+1 Gz), the pilot will experience increased +Gz due to pitch and drag, 0 Gz at 90 deg AOA in level flight with constant velocity (and +1 Gx), then increased + /-Gy during voll and voll-reversal which will be accentuated by the gravity vector during yaw.

SACOM #2 (pitch reversal): Similar to Cobra.

SACOM #3 (yaw reversal): This is a pure yaw pointing maneuver. Depending on entry speed, significant magnitude +/-Gy accelerations will occur.

SACOM #4 (roll reversal): Pure roll reversal is a property of current fighter aircraft. The pilot rolls, then reverses. The pilot will experience angular acceleration.

SACOM #5 (axial reversal): This is Gx acceleration test that measures the ability of the aircraft to accelerate and decelerate. The pilot is exposed to +/-Gx accelerations.

SACOM #6: Pure lateral translational jink-track acceleration/deceleration. The pilot will be subjected to +/-Gy loads.

SACOM #7: Pure vertical translational jink-track acceleration/deceleration. Possible high, short duration +/-Gz loads.

The projected acceleration associated with these maneuvers is charted at Table 3-1.

Table 3-1 Anticipated Acceleration Variations Associated with Currently Projected High-Agility Flight Maneuvers

Maneuver	+Gx	+/-Gy	+Gz (entry)	Angular Acceleration direction	Transitions	Comments
Herbst	↘ then ↗	↗ then ↘	↗↗ then ↘ to 0 or -Gz	Lateral	1. 0 Gy → +/-Gy 2. +Gz → 0 Gz (or -Gz) → +Gz 3. 0 Gx → +/- Gx 4. +/- ang accel	1. Spatial orientation 2. Push-pull effect (PPE)
Cobra	↘ then ↗	N/A	1. ↗↗ then ↘ to 0 or -Gz 2. -Gz then +Gz	Pitch	1. +Gz → -Gz → Gz	1. Spatial orientation 2. PPE
Voll reversal	↘ then ↗	1. ↗ then ↘ 2. ↘ then ↗	↗↗ then ↘ to 0 or -Gz	Lateral	1. 0 Gy → +/-Gy 2. +1 Gz → +Gz → 0 Gz (or -Gz) → +Gz 3. 0 Gx → +/- Gx 4. +/- ang/trans accel	1. Spatial orientation 2. Possible PPE
Pitch reversal	↘ then ↗	N/A	1. ↗↗ then ↘ to 0 or -Gz then ↗ Gz 2. ↘↘ to -Gz then ↗ 0 or +Gz	Pitch	+Gz → -Gz → Gz	1. Spatial orientation 2. Possible PPE
Yaw reversal	N/A	↗ then ↘	N/A	z-axis	0 Gy → +/-Gy → 0 Gy	
Roll reversal	N/A	N/A	N/A	Roll	Angular acceleration changes	
Axial reversal	1. ↘↘ then ↗↗ 2. ↗↗ then ↘↘	N/A	N/A	N/A	+/- Gx	
Lateral jink	N/A	↗↗ then ↘↘	N/A	Inertial	+/- Gy	
Vertical jink	N/A	N/A	1. ↗ then ↘ to 0 or -Gz then ↗ Gz 2. ↘ to -Gz then ↗ 0 or +Gz	Inertial	+/-Gz	

Review of Table 3-1 offers some idea of future acceleration stress patterns in EFM-capable aircraft. While +Gz will be less than current aircraft, and of shorter duration, it will be more frequent. Negative Gz exposure will be much more frequent than currently experienced. Zero Gz will be frequently experienced, both as an energy recovery tactic and during maneuver transitions. Gy exposure, now rarely experienced, will become frequent during pointing and escape maneuvers. Gx exposures will increase in magnitude as propulsion systems and air braking systems improve. Because of the unprecedented degree of controllability afforded by thrust vectoring, rapid changes in magnitude and direction involving these accelerations will occur. Superimposed on translational accelerations will be angular accelerations.

3.5 Human Factors and EFM.

Very little research exists that addresses human factors and high agility flight. The large body of knowledge that exists in the fields of vestibular and acceleration physiology was gathered with reference to the flight characteristics of non-agile aircraft, and did not include many of the acceleration patterns seen at Table 3-1. Laboratory tools used in this work, such as the human centrifuge, were usually capable of generating +Gz only, and incapable of -Gz. Gx and Gy were generally uncontrolled and regarded as artifact. While a small fund of current knowledge might be applicable to EFM, with caution, properly controlled studies on the vestibular and acceleration effects of multi-axis acceleration in EFM have yet to be done. The lack of

understanding of the problems of spatial disorientation and G-incapacitation in EFM will accelerate aircraft and pilot attrition during peacetime, and limit tactical capability in war.

3.6 Vestibular Concerns.

Pilots rely on flight instruments as their primary defense against visual and vestibular illusion and loss of situational awareness. The various heads up display (HUD) designs, attitude indicators (AI), and associated primary flight instruments allow the pilot to determine spatial orientation relative to the earth in degraded visibility. Translational and rotational accelerations are known to affect spatial orientation through induced vestibular and proprioceptive illusions. Loss of spatial orientation can lead to loss of situational awareness. Never solved previously, aircraft crashes attributed to loss of situational awareness continue to occur[35].

Current AI/HUDs display a two dimensional depiction of the aircraft attitude relative to the horizon. Neither instrument effectively displays the yaw or velocity vector. Most airspeed indicators are pneumatically driven and become unreliable below the stall speed. Thus, the pilot of an EFM-capable aircraft, flying at high-AOA during PST, employing current flight instrument displays, would receive inadequate orientation and velocity information. A HUD design in the X-31 depicting the velocity vector has proven confusing[6]. Vestibular illusions, not yet identified, will lead to pilot misperceptions of flight orientations that may be difficult to counter with existing instrument displays. Improved instrumentation will be needed to counter the severe vestibular illusions that will certainly be associated with EFM[36]. Cord discussed the problem of situation awareness and the need to better integrate the pilot with the aircraft[10].

Spatial orientation of pilots will be especially challenged by lateral accelerations (Gy) that will be experienced during angular acceleration in voll reversal maneuvers such as the Herbst maneuver. Similar forces are experienced by civilian light aircraft aerobatic pilots, with an important difference - high agility fighter pilots will experience lateral Gy in combination with long radius angular acceleration. The effects of this combination are unknown and will likely be associated with currently unidentified vestibular illusions[36]. While the natural tendency of any pilot might be to reposition the head in the direction of rotation (thus converting lateral angular motion to pitch motion), preoccupation with tactics may not allow orienting compensating movements. Thus, there will be a large combination of possible disorienting stimuli.

Short radius yaw rotational movements that occur in helicopter flight and vertical take off and landing (VTOL) fixed wing aircraft, subject pilots to rotation around the z-axis. The NF-16D MATV 'helicopter' maneuver is an example of a similar high-agility yaw maneuver[2]. The speed of rotation in EFM-capable fighters may be significantly greater than that seen previously, and may be combined with other acceleration stress. Head movements during z-axis rotation may provoke disorientation and motion sickness[35,37].

Several important illusions in non-agile aircraft were identified only after the loss of aircraft, a notable example being the somatogravic illusion which occurs during take-off or rapid acceleration in fighter aircraft[35]. Spatial orientation can be expected to be a serious limitation in EFM-capable fighters.

VESTIBULAR PROBLEMS

- current flight instrument displays are inadequate for preventing disorientation in EFM aircraft
- vestibular illusions, not yet identified, will cause pilot misperceptions
- there is a potentially large combination of disorienting stimuli
- incidents and accidents attributed to push-pull effect are emerging

3.7 Cardiovascular Concerns.

Despite lower peak Gz levels, G-induced loss of consciousness (G-LOC) as a result of cardiovascular decompensation during +Gz will become a greater threat. EFM will involve more frequent transitions from -Gz to greater than +1 Gz (Table 3-1). Transitions between zero or -Gz and +Gz are known to decrease human Gz tolerance. This decrease in tolerance has been termed the "push-pull effect"[38]. The possibility of diminished +Gz tolerance following zero-G was first investigated during an in-flight study by von Beckh in 1959. Using an F-94F jet, he demonstrated significantly diminished +Gz tolerance in all 6 subjects following 35 to 45 s at zero-G[39]. Despite these findings, and a growing appreciation of the problem among pilots[40,41] and physiologists/flight surgeons[42,43], no further work was undertaken until 1992. Since then, several laboratory experiments and in-flight studies have confirmed the push-pull effect[44,45,46,47,48]. The 'push' phase may involve any Gz less than +1 Gz. The 'pull' phase involves +Gz.

Risk factors associated with the push-pull effect are poorly understood. It is known that push-pull effect becomes worse as time at -Gz increases[46]. However, suggestions that increased height, gender, and age are independent risk factors[49] have not yet been confirmed by well designed studies. The role of positive pressure breathing anti-G suits in preventing push-pull effect remains uncertain[50] although standard anti-G suits have been shown to improve, but not eliminate push-pull effect[51].

In flight incidents of push-pull effect leading to pilot incapacitation have emerged. Mohler documented incidents of incapacitation in civilian aerobatic pilots during vertical eight maneuvers when the +G phase of the maneuver followed the -G phase[41]. Diedrichs documented a case of G-LOC at +2-3 G in a push-pull type maneuver[43]. The Canadian Forces (CF) recently reported that 17% of all G-LOC episodes were related to push-pull effect, several involving CF-18 pilots who were in control of the aircraft[52]. Williams and colleagues reported incidents in civilian aerobatic pilots[53]. The Israelis have documented incidents[54]. Several anecdotal reports from pilots and flight surgeons have described incidents of partial or full incapacitation caused by push-pull effect. One report involved a CF-18 pilot who experienced a G-LOC at +5 Gz after a sustained dive attack. Michaud has confirmed that push-pull effect maneuvers are commonly flown by USAF fighter pilots[55].

Push-pull effect was identified as causing the loss of an F-18 and pilot[56] and is suspected of

causing others. The CF Defence and Civil Institute of Environmental Medicine (DCIEM) conducted a reassessment of CF aircraft mishaps from 1976 to 1997 to determine if push-pull effect might have caused other accidents. Five accidents were determined to be "likely" caused by push-pull effect. Three other accidents were determined to be "possible" (Capt Brush, DCIEM - personal communication). A similar review of United States Air Force (USAF) accident records determined that three F-16s, two F-15s, one A-10 and one T-37 were likely lost in recent years because of G-LOC due to push-pull effect (Maj. Michaud, USAF, publication pending).

Aside from the problem of push-pull effect, the direct effects of -Gz remain poorly understood. Relatively little research has been conducted on the effects of -Gz. It was estimated that about 30 good studies exist on the effects of -Gz, most conducted during WW II or soon after. These studies illustrate the role of the parasympathetic nervous system in adapting to -Gz. The physiology of -Gz was partly reviewed in 1992 in a discussion paper on bradycardia during –Gz[57]. A previously unidentified problem, persistent vertigo following -Gz (termed the "wobblies"), was recently described[53].

CARDIOVASCULAR PROBLEMS

- G-induced loss of consciousness (G-LOC) will become a greater problem
- more transitions between -Gz and +Gz will result in the push-pull effect and G-LOC
- risk factors for push-pull effect are poorly understood
- incidents and accidents attributed to push-pull effect are emerging
- the physiology of –Gz is poorly understood

3.8 The Problem with Current Anti-G Suits.

Pilots of current EFM-capable aircraft, such as the F-22, will wear anti-G suits designed for previous, non-agile aircraft. Pneumatic, anti-G trousers were first developed and used operationally in WWII[58]. Changes following the war led to the anti-G suit becoming standard equipment on many fighters by the time of the Korean War. The original anti-G suit design remains operational today, with minor changes only[58].

The basic design of all anti-G systems includes an anti-G valve that controls the flow of pressurized air into inflatable compartments in the G-trousers. By inflating the G-trousers during +Gz, a measure of cardiovascular protection is achieved. As +Gz increases, pressure delivery to the trousers increases. Optimum protection requires that the trousers inflate within 1 s of +Gz application[58], but inflation delays of 1-3 s are typical.

PROBLEM WITH CURRENT G-SUITS

- pilots of EFM-capable aircraft, such as the F-22, are using G-suits designed for non-agile aircraft
- optimized G-trouser coverage, positive pressure breathing, and air pressure scheduling will produce the most effect G protection possible
- these components must be designed to be appropriate for the conditions of flight
- there is no current G-suit that has been designed for EFM conditions

The addition of positive-pressure breathing (PPB) during +Gz as a means of countering fatigue[58] was a comparatively recent innovation. First expressed operationally in the USAF Combat Edge design, other PPB systems are operational or in design. PPB works in conjunction with the standard anti-G suit and valve. Enhancing the effectiveness of the G-trousers by increasing area of coverage of the lower limbs (a return to early WWII designs) has also occurred. Optimization of trouser coverage, PPB, and pressure scheduling will likely produce the most effective G protection possible. However, like any design, these components must be appropriate to the actual conditions of flight. Currently there is no G-suit that is designed for EFM conditions.

Current anti-G valve pressure scheduling is effective in human centrifuges. Because of the inability of most human centrifuges to produce -Gz, G-research has been conducted in the +Gz direction only, usually from baselines of +1.4 Gz to +1.8 Gz, a condition almost never encountered in flight. The 0.4 to 0.8 Gz baseline difference from +1 Gz (normal physiologic state), constitutes an experimental bias. This bias pervades the literature, and is entrenched and generally unacknowledged[59].

With the exception of Lambert's classic work[60,61,62] little effort has gone towards validating the human centrifuge as a research tool. The importance of baseline Gz was illustrated during a recent experiment. Speculation that human +Gz tolerance is less when starting from +1.0 Gz compared to +1.4 Gz was supported by several observations made during push-pull research (Dr. Fred Buick, DCIEM, personal communication). It is likely that currently accepted estimates of human +Gz tolerance are high. This overestimation may explain why anti-G suits have been only partially successful in solving the problem of G-LOC.

Current anti-G protective systems, based on +Gz-only research, will be particularly ineffective in the presence of increased pitch rates and more frequent +/- Gz changes. Current mechanical or

electrical pre-programmed pressure schedules could even reduce protection in some circumstances during EFM. For example, an air pressure delivery lag time of 1-3 seconds during oscillations in pitch, or rapid serial changes between -Gz and +Gz, could lead to G-trousers and PPB pressure increases/decreases that are out of phase with need. Pressure could be cycling out of the suit while +Gz in increasing. This dangerous possibility should be considered by anyone authorizing use of current G-suits in EFM-capable aircraft.

3.9 Current Research Initiatives in -/+Gz Protection.

There are two research initiatives underway that will lead to improvements in +Gz protection during highly agile flight. Neither is specific to the needs of the F-22 or EFM. The CF, through DCIEM, is conducting tilt-table, multi-gimbaled centrifuge, and in-flight studies aimed at understanding and countering the push-pull effect. Because the DCIEM centrifuge is limited to accelerations greater than +1 Gz, they have recruited partners with -Gz centrifuge capabilities. Two primary partners have been the USAF, through use of the Wright-Patterson AFB Dynamic Environment Simulator (DES) and Veda Corporation (now part of Veridian Corporation) which operates the former USN Human Centrifuge and Dynamic Flight Simulator (DFS) at Warminster. Studies conducted on these devices are beginning to reach publication[48]. Across several studies, push-pull effect has been shown to occur in all subjects, but with high variation between individuals (Capt Wright, DCIEM - personal communication). Incapacitation has been observed in subjects during in-flight CF-18 studies (Dr. Fred Buick, DCIEM - personal communication).

The second research initiative is a USN sponsored research effort that aims to provide closed-loop sensory feedback control of protective systems, including the G-suit. Termed the Smart Aircrew Integrated Life Support System (SAILSS), a bi-national research team is developing sensors for detecting the physiological status of pilots[63] and applying this information to neural net technologies in order to create smart, adaptive life support systems[64]. Computer modeling will be essential to the maturation of this approach[65,66] as a basis for algorithm development. This technology will have direct applicability to EFM-capable aircraft.

Uniting these two efforts is the need for a new anti-G valve. A prototype valve is in development that will produce rapid and continuous changes in the G-suit pressure in order to adapt to the frequent changes of G. Such a valve will create pressure scheduling based on G

CURRENT RESEARCH INITIATIVES

- Two initiatives underway, neither specific to the needs of F-22 or EFM
- Canadian study aimed at understanding and countering the push-pull effect
- US-Canadian study aimed at developing future sensor-based technology
- major partners include Wright-Patterson AFB Dynamic Environmental Simulator (DES) and Veda Corporation centrifuge

time-history. When SAILSS technology matures, changes to the pressure schedule will be based on the immediate changing physical state of the pilot.

3.10 Defining the Need for Research and Training.

The lack of understanding of the physical demands imposed by high-agility flight has been described as the "forbidden human space-time agility domains."[34] "Understanding these complex rigid-body translational, rotational, gyration, and gyroscopic phenomenon, requires reassessment of well-established concepts."[34] While some speculation has occurred on the effects of G in high-agility flight[18], it is based on gradual or rapid G-onset studies not representative of high-agility accelerations. Gal-Or, one of the few engineer-researchers who has shown an appreciation of human factor limitations in these aircraft has strongly recommended DES-centrifuge research into these problems[18], and has included the need for research into pilot tolerances as part of his methodology[34]. Tedor has described the problems that could be anticipated and the lack of resources to solve them. He emphasized the problems of G-LOC and visual/vestibular illusion[67].

Central to acquiring future understanding of human factors in EFM is the need for validated laboratory tools and proven experimental methods. Acceleration devices capable of -Gz, Gy, and Gx are needed. Two such research devices exist in the USA today, the DES and Veda centrifuges. The DES can simulate the accelerations of EFM. The DES can also be used to study spatial disorientation during EFM. However, both the DES and Veda centrifuges are dated and have technical limitations (See Table 3-2). Newer designs are currently under construction overseas. A need exists for a family of modern human centrifuges that can closely simulate the accelerations of EFM. With the continued absence of such devices, upgrading and maintenance of the DES and Veda centrifuges is essential in solving the approaching EFM human factors problems.

Table 3-2 Existing US Man-Rated Centrifuges

Device	Location	Radius [ft]	Crew station motion	Acceleration Onset [G sec^{-1}]
Dynamic Environment Simulator (DES)	Armstrong Laboratory, Wright-Patterson AFB, OH	19	powered gimbals	< 1
Brooks Centrifuge	Armstrong Laboratory, Brooks AFB, TX	20	passive roll gimbal	6
Dynamic Flight Simulator (DFS)	Naval Air Warfare Center, PA	50	powered gimbals	> 6

What remains, within the context of EFM, is providing the right protection at the right time. Appropriate pneumatic scheduling of air pressure into protective pneumatic garments will provide transparent G-protection throughout EFM envelopes. Proof of concept studies and centrifuge testing of new designs will require -Gz capable centrifuges. Current and future

DEFINING FUTURE RESEARCH NEEDS

- dependence on human factors technology designed for non-agile aircraft will prove disastrous
- central to future research will be proper laboratory tools such as Gx, Gy, Gz-capable human centrifuges
- the DES can simulate EFM, but has technical limitations
- newer centrifuge designs are in construction overseas future acceleration research requires -Gz-capable centrifuges

aircraft designs will require an unprecedented degree of physical and computer modeling in order to contain costs and accurately forecast problems[68]. While the capabilities of new aircraft are rapidly improving, human tolerances to anticipated EFM stresses remain poorly understood.

The advent of high agility flight has challenged the established assumptions of fixed wing flight. Aeronautical terms and thought has evolved. Tactical concepts, once thought inviolate, are changing. New terms are emerging and the very nature of flight is evolving. Radical and revolutionary concepts are emerging.

A similar evolution is required in our understanding of the human physiology of flight. While engineering concepts have led to advanced aircraft that now defy established flight doctrine, forth generation fighter test pilots continue to rely on protective systems based on the capabilities of Korean War and Vietnam-era fighters. The threats of loss of situational awareness and G-LOC, never solved on older aircraft, will increase if the need for change and evolution is not confronted. While new terms, such as "voll" are developed to describe new, previously unflown flight maneuvers, new terms and thought need to evolve to describe new elements of physiology and human factors of EFM.

3.11 References.

[1] Gal-Or, B., Western vs Eastern fighter technologies beyond 2000. International Journal of turbo and Jet Engines, 1994. 11: p. 113-8.

[2] Discovery, Wings: Air Dominance, . 1998, Discovery Channel.

[3] Dornheim, M. and S. Kandebo, F-22 test flights begin at Edwards. Aviation Week & Space Technology, 1998(May 25, 1998): p. 23-4.

[4] Proctor, P., Israelis test thrust vectoring. Aviation Week and Space Technology, 1998: p. 81.

[5] Herbst, W., Breaking the stall barrier. Aerospace Engineering, 1987(November 1987): p. 27-9.

[6] Dornheim, M., X-31 flight tests to explore combat agility to 70 deg AOA. Aviation week and Space Technology, 1991(March 11, 1991): p. 38-41.

[7] Herbst, W., Supermaneuverability, . 1983, Messerschmitt-Bolkow-Blohm GMBH: Ottobrunn bei Munchen.

[8] Lynn, N., High alpha: key to combat survival?, in Flight International. 1987. p. 29-31.

[9] Tamrat, B. Fighter aircraft agility assessment concepts and their implication on future agile fighter design. in AIAA/AHS/ASEE Aircraft Design, Systems and Operations Meeting. 1988. Atlanta, Georgia: American Institute of Aeronautics and Astronautics.

[10] Cord, T., M. Detroit, and D. Multhopp, Is an agility requirement needed for fighter aircraft? (manuscript), . 1990, Wright Research and Development Centre.

[11] Gal-Or, B., Thrust vectoring for flight control and safety: a review. International Journal of turbo and Jet Engines, 1994. 11: p. 119-36.

[12] Gallaway, C. and R. Osborn. Aerodynamics perspective of supermaneuverability. in AIAA 3rd Applied Aerodynamics Conference. 1985. Colorado Springs, Colorado: AIAA.

[13] Herbst, W., Dynamics of air combat. Journal of Aircraft, 1982. 20: p. 594-9.

[14] Herrick, P. Air-to-ground attack fighter improvements through multi-function nozzles. in SAE Aerospace Atlantic. 1990. Dayton, Ohio: Society of Automotive Engineers.

[15] Brown, D., Joint strike fighter: one aircraft, many missions. Aviation Week and Space Technology, 1998(May 25, 1998): p. S3 - S18.

[16] Fulghum, D., JSF to spawn black derivatives. Aviation Week and Space Technology, 1998(March 9): p. 55.

[17] Zaloga, S., UAVs gaining credibility. Aviation Week and Space Technology, 1998(January 12, 1998): p. 93-5.

[18] Gal-Or, B., Tailless Vectored Fighters. Theory, Laboratory and Flight Tests, . 1991, Technion - Isreal Institute of Technology: Technion City, Haifa, Israel.

[19] Lynn, N., X-31: breaking the stall barrier. Flight International, 1987: p. 27-8.

[20] DeMeis, R., X-31 will turn on a dime. Aerospace America, 1990(October 1990): p. 26-9.

[21] Francis, M., X-31: An international success story. Aerospace America, 1995(February 1995): p. 20-32.

[22] Gal-Or, B., Proposed flight testing standards for engine thrust vectoring to maximize kill ratios, post-stall agility and flight safety. International Journal of turbo and Jet Engines, 1995. 12: p. 252-268.

[23] Skow, A. An analysis of the Su-27 flight demonstration at the 1989 Paris airshow. in SAE Technical Paper Series. 1990. Dayton, Ohio: SAE.

[24] North, D., Aviation Week editor flies top Soviet fighter, in Military Aircraft Pilot Reports, D. North, Editor. 1990, McGraw-Hill: New York. p. 58-68.

[25] Proctor, P., Basic defense work still on track in Asia, in Aviation Week and Space Technology. 1998. p. 66-7.
[26] Novichkov, N., Pitch-yaw nozzles to be used on Su-30MKs for Indian Air Force. Aviation Week and Space Technology, 1998(June 29, 1998): p. 34-5.
[27] Smith, B., USAF to press thrust-vectoring tests on limited budget, in Military Aircraft Pilot Reports, D. North, Editor. 1996, McGraw-Hill: New York. p. 177-80.
[28] North, D., VISTA primed for research, training, in Military Aircraft Pilot Reports, D. North, Editor. 1995, McGraw-Hill: New York. p. 162-8.
[29] North, D., MATV F-16 displays high alpha benefits, in Military Aircraft Pilot Reports, D. North, Editor. 1994, McGraw-Hill: New York. p. 169-76.
[30] Scott, W., X-36 testing gives Boeing jump on UCAV work. Aviation Week and Space Technology, 1998(March 2, 1998): p. 58-60.
[31] Gal-Or, B., An old-new European debate on thrust vectoring. International Journal of Turbo and Jet Engines, 1997. 14(4).
[32] Gal-Or, B., Vectored propulsion, supermaneuverability and robot aircraft. Recent Advances in Military Aviation. Vol. I. 1990, Haifa: The Jet Propulsion Laboratory. 275.
[33] Gal-Or, B., Safe jet aircraft. International Journal of turbo and Jet Engines, 1994. 11: p. 1-9.
[34] Gal-Or, B., Thrust vectoring: theory, laboratory, and flight tests. Journal of Propulsion and Power, 1993. 9(1): p. 51-8.
[35] Gillingham, K. and F. Previc, Spatial Orientation in Flight, in Fundamentals of Aerospace Medicine, R. DeHart, Editor. 1996, Williams and Wilkins: Baltimore. p. 309-97.
[36] Pancratz, D., J. Bomar, and J. Raddin, A new source for vestibular illusions in high agility aircraft. Aviat. Space Environ. Med., 1994. 65(December 1994): p. 1130-3.
[37] Banks, R., D. Salisbury, and P. Ceresia, The Canadian Forces airsickness rehabilitation program, 1981-1991. Aviation, Space and Environmental Medicine, 1992. 63: p. 1098-101.
[38] Banks, R., et al., The push-pull effect. Aviat Space Environ Med, 1994. 65: p. 699-704.
[39] von Beckh, H., Human reactions during flight to acceleration preceeded by or followed by weightlessness. Aero Med, 1959. 30: p. 391-409.
[40] CF, The Push-pull Effect (video), . 1996, Canadian Forces Directorate of Flight Safety: Toronto.
[41] Mohler, S., G effects on the pilot during aerobatics, . 1972, FAA.
[42] Kirkham, W., S. Wicks, and D. Lowrey, G incapacitation in aerobatics pilots: a flight hazard, . 1982, FAA.
[43] Deidrichs, R., Adverse effect of negative Gz on subsequent high positive Gz: a need for research and education. Aeromedical and training Digest, 1990(4): p. 36-8.
[44] Lehr, A., et al., Previous exposure to negative Gz reduces relaxed +Gz tolerance (abstract). Aviation, Space and Environmental Medicine, 1992. 63(5): p. 405.
[45] Prior, A., T. Adcock, and G. McCarthy, In-flight arterial blood pressure changes during -Gz to +Gz manoeuvring (abstract). Aviat Space Environ med, 1993. 64(5): p. 428.
[46] Banks, R., et al., The effects of varying time exposure to -Gz on subsequent decreased +Gz physiological tolerance (push-pull effect). Aviat Space Environ Med, 1995. 66: p. 723-7.

[47] Goodman, L. and S. LeSage, Physiological responses to a tilt table simulation of the push-pull effect (abstract). Aviation, Space, and Environmental Medicine, 1998. 69(3): p. 202.

[48] Wright, H. and F. Buick, The +Gz-tolerance limits of the push-pull phenomenon (abstract). Aviation, Space, and Environmental Medicine, 1998. 69(3): p. 202.

[49] Banks, R., Gender difference in +Gz tolerance following -Gz (push-pull effect) (abstract). Aviation, Space, and Environmental Medicine, 1995(66th Annual Scientific Meeting of the Aerospace Medical Association).

[50] Chelette, T. and W. Albery, Does combat edge compromise G protection subsequent to a push-pull effect maneuver? (abstract). Aviation, Space, and Environmental Medicine, 1998. 69(3): p. 202.

[51] Prior, A. Negative to positive Gz acceleration transition. in AGARD Lecture Series No 202. 1995. USA, Germany, UK: AGARD.

[52] Latchman, S. and W. Greenlaw, The incidence of g-loc in the Canadian Forces, . 1996, Operational Research Division Air Command Headquarters: Winnipeg, Manitoba, Canada.

[53] Williams, R., et al., Adverse effects of Gz in civilian aerobatic pilots (abstract). Aviation, Space, and Environmental Medicine, 1998. 69(3): p. 201.

[54] Shamiss, A., L. Chapnik, and N. Yoffe, Physiologic incidents in the Isreali Air Force 1994-1996 (abstract). Aviation, Space, and Environmental Medicine, 1998. 69(3): p. 232.

[55] Michaud, V., T. Lyons, and C. Hansen, Frequency of the "push-pull" effect in USAF fighter operations (abstract). Aviation, Space, and Environmental Medicine, 1998. 69(3): p. 201.

[56] Banks, R. and M. Paul, Death due to push-pull effect. Aviation, Space, and Environmental Medicine, 1996(67th Annual Meeting of the Aerospace Medical Association).

[57] Banks, R. and G. Gray, "Bunt bradycardia": two cases of slowing of heart rate inflight during negative Gz. Aviat Space Environ Med, 1994. 65: p. 330-1.

[58] Burton, R. and J. Whinnery, Biodynamics: Sustained Acceleration, in Fundamentals of Aerospace Medicine, R. DeHart, Editor. 1996, Williams and Wilkins: Baltimore. p. 201-60.

[59] Banks, R., The operational significance of experimental bias in centrifuge acceleration research. Aviation, Space, and Environmental Medicine, 1995(66th Annual Meeting of the Aerospace Medicine Association).

[60] Lambert, E., Effects of positive acceleration on pilots in flight, with a comparison of the responses of pilots and passengers in an airplane and subjects on a human centrifuge. Journal of Aviation Medicine, 1950. 21: p. 195-220.

[61] Lambert, E., Comparison of the protective value of an anti-blackout suit on subjects in an airplane and on the Mayo centrifuge. Journal of Aviation Medicine, 1950. 21: p. 28-37.

[62] Lambert, E., Comparison of the physiologic effects of positive acceleration on a human centrifuge and in an airplane. Journal of Aviation Medicine, 1949. 20: p. 308-335.

[63] Fraser, W., Monitoring the crew (abstract). Aviation, Space, and Environmental Medicine, 1998. 69(3): p. 217.

[64] Fraser, W., Life support systems for the next generation tactical aircraft (abstract). Aviation, Space, and Envrionmental Medicine, 1998. 69(3): p. 236.

[65] Walsh, C., S. Cirovic, and W. Fraser, A cardiovascular simulation including venous valves and anti-g protective measures (abstract). Aviation, Space, and Environmental Medicine, 1998. 69(3): p. 241.

[66] Cirovic, S., C. Walsh, and W. Fraser, The effect of elevating central arterial and venous pressures on Gz tolerance (abstract). Aviation, Space, and Environmental Medicine, 1998. 69(3): p. 241.

[67] Tedor, J., Flight simulation. Aerospace Engineering, 1993(August): p. 21-4.

[68] Scott, W., Better modelling will alter culture of flight testing. Aviation Week and Space Technology, 1998(March 23, 1998): p. 84-6.

4.0 Mathematical Model of the DES.

The mathematical model of the DES is a representation of the geometric, kinematic, and dynamic parameters of the DES that accurately models the response of the centrifuge to operator inputs. To model the DES, it is first necessary to have an understanding of the geometry of the centrifuge and the coordinate frames used to express its motion. This material is described in Section 4.1

The model of the DES can then be separated into two parts. The first part, described in Sections 4.2 - 4.3, describes the "forward" model of the centrifuge. A forward model is one that permits an operator to predict the relevant output, in this case crewmember accelerations, after specifying a set of command inputs. The command inputs for the DES are a time history of arm velocities and fork/cab positions.

The forward model itself can also be subdivided into two parts. The modeling of the centrifuge kinematics, based on the geometry of the DES, is described in Section 4.2. The model of the DES dynamics, which reflect the response and limitations of the motors as well as inertial properties of the centrifuge, is described in Section 4.3. There was no effort to model the transient dynamics of the centrifuge structure in this project.

In addition, Sections 4.4 through 4.6 discuss the "inverse" modeling of the centrifuge. An inverse model is one that permits an operator to specify a set of desired outputs in this case crewmember accelerations, and then compute the necessary command inputs to achieve that output. Sections 4.4 and 4.5 describe the inverse kinematics of the centrifuge. Inverse dynamics are described in Section 4.6.

4.1 DES Geometry and Coordinate Frames.

The geometry of the DES used for the mathematical model is displayed in Figure 4-1. Figure 4-1 is not a scaled drawing, but it does show the sequential gimbals that allow the DES to position a rider with respect to the generated centrifuge acceleration. Some physical dimensions of the centrifuge are shown in Table 4-1. The parameters in Table 4-1 also represent variables in the DES model software, and can be modified to explore the change in DES capabilities if desired.

The point "R" in Figure 4-1 is assumed to be at the geometric center of the cab. The reference frames are all "local" reference frames in the sense that they remain fixed to the portion of the centrifuge or rider that they represent. There are local reference frames for the arm, fork, cab, seat, pilot and accelerometers. Of course, the centrifuge arm coordinate frame is always coincident with the global fixed coordinate frame prior to any movement of the arm.

Figure 4-1: Salient DES Reference Frames and their Respective Orientations

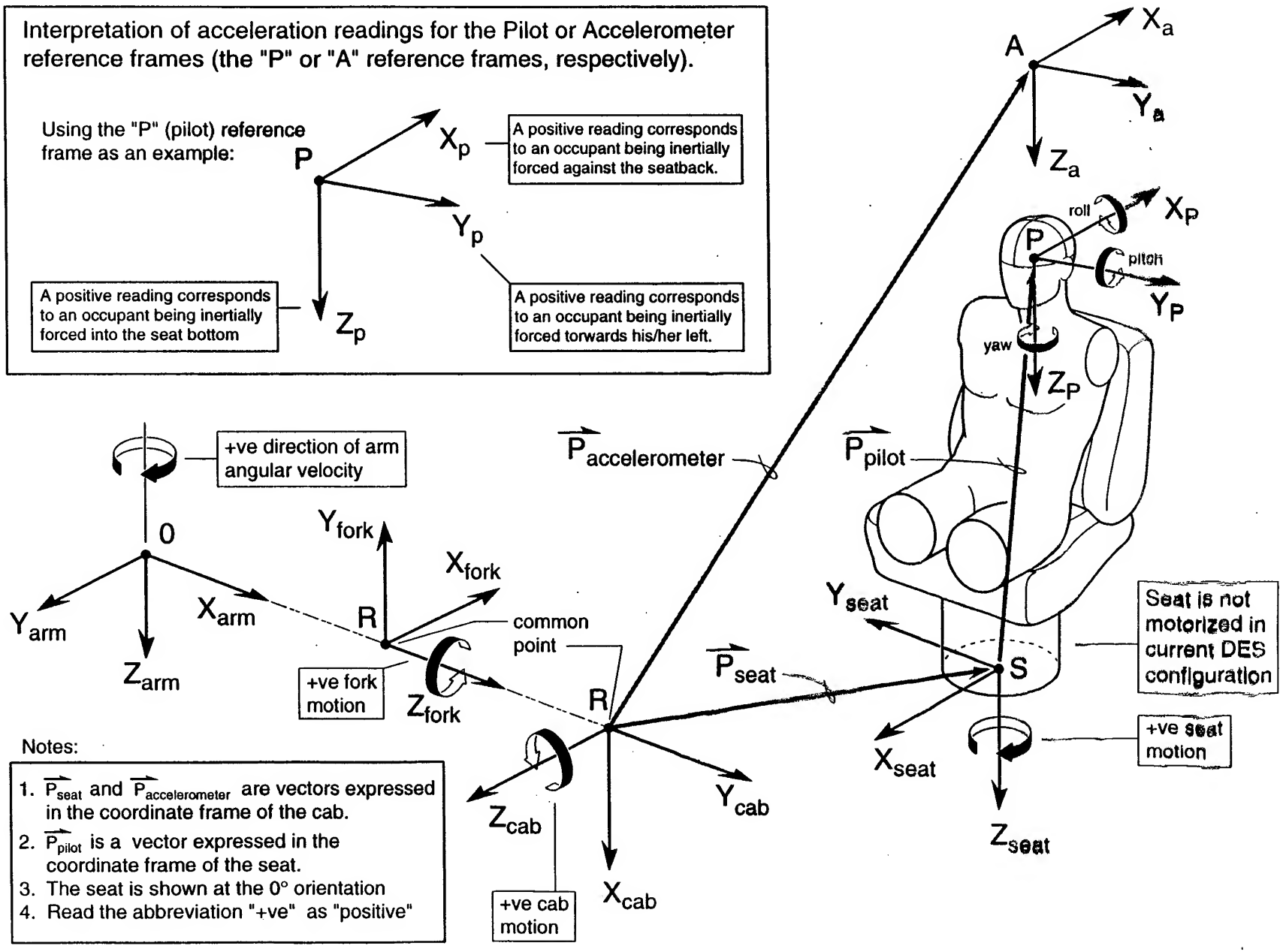

Table 4-1 Relative Positions of Various Key Points and Bodies

Vectors (and their components if applicable)		Distance [ft]
Arm radius $\vec{R}$		19.0
$\vec{P}_{pilot}$	X_{seat}	-0.5
	Y_{seat}	0.0
	Z_{seat}	-0.5
$\vec{P}_{acceleromter}$	X_{cab}	1.0
	Y_{cab}	0.0
	Z_{cab}	-3.0
$\vec{P}_{seat}$	X_{cab}	0.0
	Y_{cab}	0.0
	Z_{cab}	0.0

As indicated by the vector $\vec{P}_{pilot}$, the DES occupant (pilot) reference frame is defined with respect to the seat. When the seat is assigned the [0,0,0] location, the pilot frame is then automatically located at the center of the cab. The pilot reference frame in Table 4-1 is thus offset from the center of the cab by a little over 0.5 ft. (expressed in seat reference frame).

Since the accelerometers are mounted on the wall of the cab, the position of the accelerometers, $\vec{P}_{accelerometer}$, was defined with respect to the cab reference frame. The implication is that the accelerometer readings will not change if the orientation of the seat is modified. The predicted pilot accelerations would change if the seat were oriented differently, however.

The DES software allows a motorized seat to be modeled, although this degree of freedom is not part of the current DES configuration. Each DOF requires a separate coordinate system. Thus, the seat reference frame, whether the seat is movable or not, is defined in terms of one rotational DOF and one static position vector with respect to the cab reference frame. The cab reference frame is embedded within the fork reference frame which itself is placed at a distance R away from the origin of the arm reference frame. The cab, fork, and arm each have one rotational DOF. Thus, the mathematics of the DES software represents either the existing 3-DOF or a theoretical 4-DOF model.

The mathematical relationships between the reference frames, in terms of rotational transformation matrices, are expressed below:

Inertial Frame to Arm Frame:

$$ {}^{A}_{0}R = \begin{bmatrix} C_1 & S_1 & 0 \\ -S_1 & C_1 & 0 \\ 0 & 0 & 1 \end{bmatrix} $$

(a)

Arm Frame to Fork Frame:

$$ {}^{F}_{A}R = \begin{bmatrix} 0 & -C_2 & -S_2 \\ 0 & S_2 & -C_2 \\ 1 & 0 & 0 \end{bmatrix} $$

(b)

Fork Frame to Cab Frame:

$$ {}^{C}_{F}R = \begin{bmatrix} 0 & -C_3 & S_3 \\ 0 & S_3 & C_3 \\ -1 & 0 & 0 \end{bmatrix} $$

(c)

Cab Frame to Seat Frame:

$$ {}^{S}_{C}R = \begin{bmatrix} 0 & -S_4 & C_4 \\ 0 & -C_4 & -S_4 \\ 1 & 0 & 0 \end{bmatrix} $$

(d)

Eqs. 4-1

Where C_i and S_i refers to cos $(\theta_i)$and sin(θ_i) is the angle of the "next" frame with respect to the present frame. Recall that all rotations are done about the respective z-axes of each coordinate frame, as shown in Figure 4-1.

One additional rotational transformation matrix allows the pilot to be assigned a static initial roll/pitch/yaw $(\gamma / \beta / \alpha)$ orientation with respect to the seat reference frame. Figure 4-1 indicates the positive roll/pitch/yaw directions and the equation below represents the corresponding transformation matrix:

Seat Frame to Pilot Frame:

$$ {}^{P}_{S}R = \begin{bmatrix} -C_\alpha C_\beta & -C_\alpha S_\beta S_\gamma - S_\alpha C_\gamma & -C_\alpha S_\beta C_\gamma + S_\alpha S_\gamma \\ S_\alpha C_\beta & S_\alpha S_\beta S_\gamma - C_\alpha C_\gamma & S_\alpha S_\beta C_\gamma + C_\alpha S_\gamma \\ -S_\beta & C_\beta S_\gamma & C_\beta C_\gamma \end{bmatrix} \qquad \text{Eq. 4-2} $$

4.2 DES Forward Kinematics.

Based on the coordinate systems defined in Section 4.1, this section discusses the analysis of the forward kinematics of the centrifuge. Given specified displacements or velocities as a function of time for any or all of the arm, fork, cab, and seat degrees of freedom, the forward kinematics algorithms calculate the linear and angular accelerations and the angular velocities at the pilot position in the pilot reference frame. Using a method outlined by Craig[2], the angular velocity, angular acceleration, and linear acceleration of each "link" or DOF of the centrifuge can be calculated, beginning with the base or fixed-Earth reference frame and working outward to the pilot's position. The following equations describe the transformation of angular velocity, and acceleration, and linear acceleration from one "link" to the next:

$$\dot{\omega}_{i+1} = {}^{i+1}_{i}R\dot{\omega}_i + {}^{i+1}_{i}R\omega_i \times \dot{\theta}_{i+1}\hat{z}_{i+1} + \ddot{\theta}_{i+1}\hat{z}_{i+1} \qquad \text{Eq. 4-3}$$

$$\omega_{i+1} = {}^{i+1}_{i}R\omega_i + \dot{\theta}_{i+1}\hat{z}_{i+1} \qquad \text{Eq. 4-4}$$

$$\dot{\upsilon}_{i+1} = {}^{i+1}_{i}R\left[\dot{\omega}_i \times {}^{i}P_{i+1} + \omega_i \times \left(\omega_i \times {}^{i}P_{i+1}\right) + \dot{\upsilon}_i\right] \qquad \text{Eq. 4-5}$$

The term "link" is used here to reflect the fact that these kinematic equations include not only the relative rotations, but also the relative positions from one body or reference frame to the next. BRC implemented these equations in the DES software, and verified the algorithms with the tests discussed in Section 5.

4.3 DES Forward Dynamics.

A model of the DES dynamics refers to a mathematical model that accounts for the differences between a commanded (input) and an obtained (output) signal. BRC determined from testing that the three existing DOFs of the DES centrifuge (the arm, fork, and cab), each had different dynamics, although the dynamics of the fork and cab were similar enough that the form of the model could be the same.

Section 4.3.1 discusses the model that was developed for the arm dynamics, and Section 4.3.2 discusses the models for the cab and fork dynamics. In general, dynamic models can attempt to model the effects of individual components that make up the DES, or they can be modeled in "lumped parameter" fashion. Because of the difficulty in testing individual subsections of the DES, BRC determined that the centrifuge dynamics could best be modeled with lumped parameters. Using BRC's approach, the Air Force could update the model of the centrifuge dynamics by running some standard acceleration profiles whenever the DES is upgraded or changed.

No dynamics were modeled for the seat since the seat is not a degree of freedom in the current DES configuration.

4.3.1 Model for the Arm Dynamics.

Two different approaches to modeling the arm dynamics were treated in the Phase II project. The first approach investigated a 2nd order transfer function model which gave satisfactory results, but which sometimes differed significantly from the expected output. The second approach was to implement a more detailed algorithm that accounted for a consistent behavior of the observed arm input voltage traces that BRC noted during DES testing. Although this version of the arm dynamics was more accurate, it was also mathematically difficult to apply in some circumstances -- for instance, when a series of small changes in arm angular velocities was going to be commanded.

Figure 4 – 2 Model for the Forward Arm Dynamics

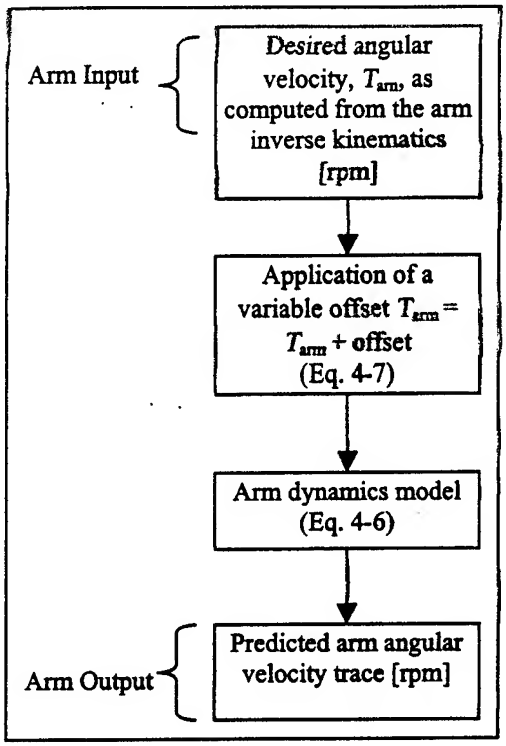

Figure 4-3 The Three Blocks which Form the Arm Dynamics Model

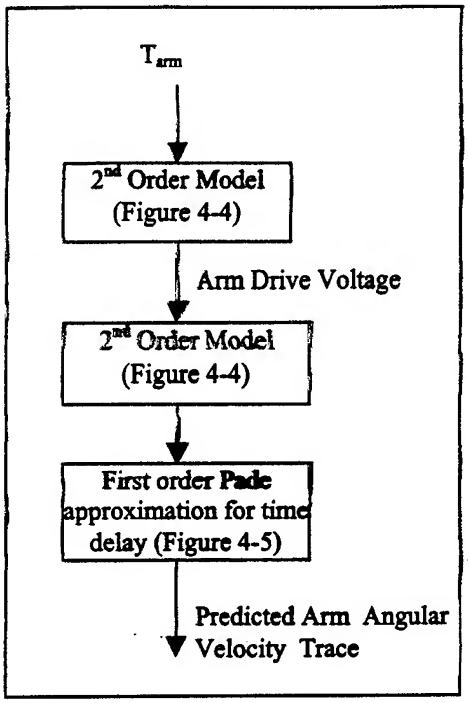

After experimenting with other models, BRC finally arrived at an arm dynamics model that was a 5th order model. The transfer function of this model is given below:

$$T_{arm}(S) = \frac{N_1 s + N_0^2}{D_5 s^5 + D_4 s^4 + D_3 s^3 + D_2 s^2 + D_1 s + D_0} \qquad \text{Eq. 4-6}$$

Equation 4-6 represents several lower order transfer functions that were combined into a single higher order transfer function. The details regarding the succession of lower order transfer functions is given in Figure 4-3, while Figure 4-2 represents the overall model for the arm dynamics. As suggested in Figure 4-3 the modeling of the arm dynamics was based, in part, on the generated arm drive voltage trace which occurred at an intermediate stage within the dynamics. This trace did show dynamic effects, and it was available as an output in all the tests that BRC conducted on the centrifuge. Note that the mathematical expressions shown in Figures 4-4 and 4-5 are called upon in Figure 4-3.

Figure 4-4 Generic 2nd Order Transfer Function Model

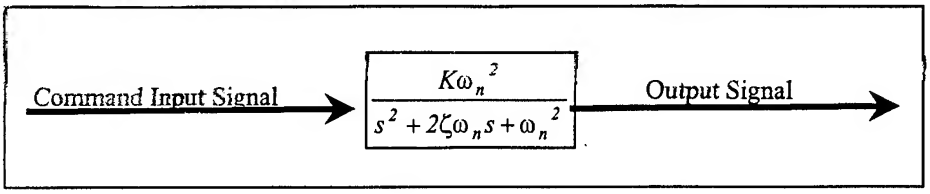

Note also that the N_i and D_i parameters in Equation 4-6 are constants, such that the arm dynamics model is then a constant parameter dynamic model. However, a varying offset was noted to occur between the desired angular velocity as commanded by a DES input file and the obtained arm angular velocity, even in terms of a steady-state error. The offset varied linearly with respect to the angular velocity level (in rpm units) as follows,

$$\text{offset} = -(0.035\ \omega_{\text{command}} + 0.15) \qquad \text{Eq. 4-7}$$

Equation 4-7 signifies that a commanded arm angular velocity level will result in a lower achieved angular velocity (as indicated by the negative sign in Equation 4-7). This equation has been included in the portion of the DES Simulation computer code that assimilates a DES commands file and then runs the forward kinematics and dynamics.

Figure 4-5 Transfer Function Model for the $e^{\tau s}$ Time Delay Using First Order Pade Approximation

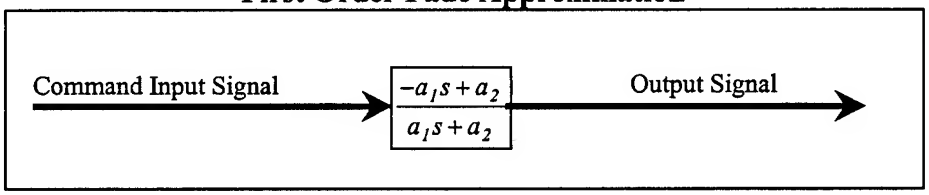

An example is given here to better illustrate the effect of this offset. Assume the recorded arm angular velocity is 18.5 rpm. As suggested by Equation 4-7, the actual achieved arm angular velocity would then be approximately 17.7 rpm, as opposed to the commanded 18.5 rpm.

For reference, Section 5.2.2 gives the values computed for the N_i and D_i parameters appearing in Equation 4-4.

4.3.2 Models for the Fork and Cab Dynamics.

Both the fork and cab dynamics were successfully modeled in the DES Simulation software with a 2nd order model. Both models were, however, complemented with a time delay feature making each of those two dynamic models a four-parameter model. The model natural frequency, ω_n, a damping factor, ζ, a gain K, and a time delay, τ, were the parameters of the models, as shown in Figure 4-6.

The inputs for either the fork or cab DOF are the angular positions. The model input and output are in units of degrees. Section 5.2.2 lists the values, which were arrived at for the four cab and fork parameters listed below.

Figure 4-6 Generic 2nd Order Transfer Function Model with Time Delay

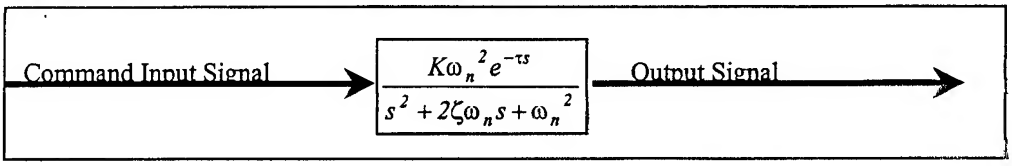

4.3.3 Implementation of the Dynamic Models.

A built-in function exists within Matlab to handle the combination of a transfer function and an input command, to produce an expected output signal. This function is called *lsim.m* and it is used in several locations within the DES Simulation software.

4.4 Modeling the DES Inverse Kinematics.

The complete inverse kinematics algorithm is driven by a set of desired accelerations which are specified by the user of the DES Simulation software. The desired accelerations consist of accelerations as a function of time for the x-, y- and z-directions in the pilot reference frame (Figure 4-1).

The sections, which follow, describe the algorithms used to compute the DES movements necessary to achieve or best approximate the specified desired acceleration. The incorporation of the inverse dynamics algorithm into the general solution process is described in Section 4.6.

Section 4.4.1 describes different approaches used to compute the arm inverse kinematics. Sections 4.4.2 and 4.4.3 clarify the two different solution methods, which were devised to perform the fork, cab, and seat inverse kinematics.

4.4.1 Arm Inverse Kinematics.

The Phase I Report described a solution method for the inverse kinematics of the arm that has been replaced in the Phase II project. Although the initial algorithm remained in use during a fair portion of the Phase II study, it was known that it suffered an important drawback. This initial solution algorithm could not accommodate situations where the desired acceleration magnitude would fall below 1 G. In these situations, the Phase I algorithm became numerically unstable.

To overcome these difficulties, a new algorithm was devised. The algorithm is not based on an analytical differential equation solution, but rather, it is based on a state-space model of the centrifuge. An input, $U(t)$, to a state-space model is solved for is such a way that the output, $A_c(t)$, optimally approximates a desired acceleration, $A_d(t)$. In the form of an equation, we have,

$$\dot{x} = Ax + BU$$
$$Y = Cx + D \qquad \text{Eq. 4-8}$$

where we seek $U(t)$ such that $A_d(t)^2 - A_c(t)^2$ is optimally minimized at any time t.

In terms of the DES variables, Equation 4-1 is rewritten with a small amount of damping (a value of -25) as,

$$\begin{Bmatrix} \alpha \\ \dot{\alpha} \end{Bmatrix} = \begin{bmatrix} 0 & 1 \\ 1 & -25 \end{bmatrix} \begin{Bmatrix} \omega \\ \alpha \end{Bmatrix} + \begin{bmatrix} 0 \\ 1 \end{bmatrix} U \qquad \text{Eq. 4-9}$$

with a non-linear C matrix and a one-dimensional D matrix yielding an output equation of the form,

$$A_c = \begin{bmatrix} r^2\omega^3 & r^2\alpha \end{bmatrix} \begin{Bmatrix} \omega \\ \alpha \end{Bmatrix} + 32.2^2 \qquad \text{Eq. 4-10}$$

In Equations 4-9 and 4-10, ω is the arm angular velocity, and α is the arm angular acceleration.

During the running solution process, the state-space equation given above is discretized at every time step as,

$$x_{i+1} = \Phi x_i + \Pi U_i$$
$$A_c = C x_{i+1} + 32.2^2 \qquad \text{Eq. 4-11}$$

where, once again, U_i is chosen such that $A_d(t)^2_{i+1} - A_c(t)_{i+1}$ is minimized. The matrices Φ and Π in Equation 4-11 are the discrete time equivalents to the A and B matrices of Equation 4-8[1].

Optimal U_i values are arrived at by using a Matlab optimization toolbox subroutine. However, it is not the actual value of U_i that is of interest here, but rather, it is the values of ω_i and α_i that are retained, once an optimal U_i is found. The inverse kinematics for the are thus solved for, once pairs of ω_i and α_i are chosen for the full simulation time span.

As an example, the solution to an arbitrarily concocted profile is given in Figure 4-7 in terms of a resultant acceleration trace. Corresponding angular velocities and accelerations ω_i and α_i values) are shown in Figure 4-8.

This method was found to be robust and to execute reasonably quickly. In fact, the solution method described is also a promising tool to accommodate a potential "man-in-the-loop" situation, where a centrifuge occupant controls the centrifuge during operation.

Figure 4-7 Sample Solution as Obtained from the Arm Solution Algorithm

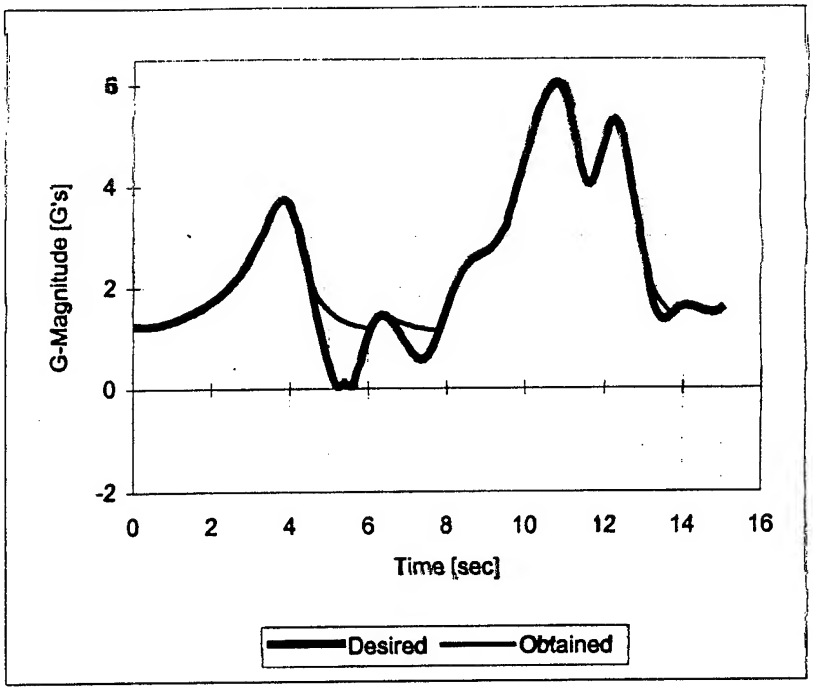

Figure 4-8 Angular Velocity and Accelerations Solution for the Arm Algorithm

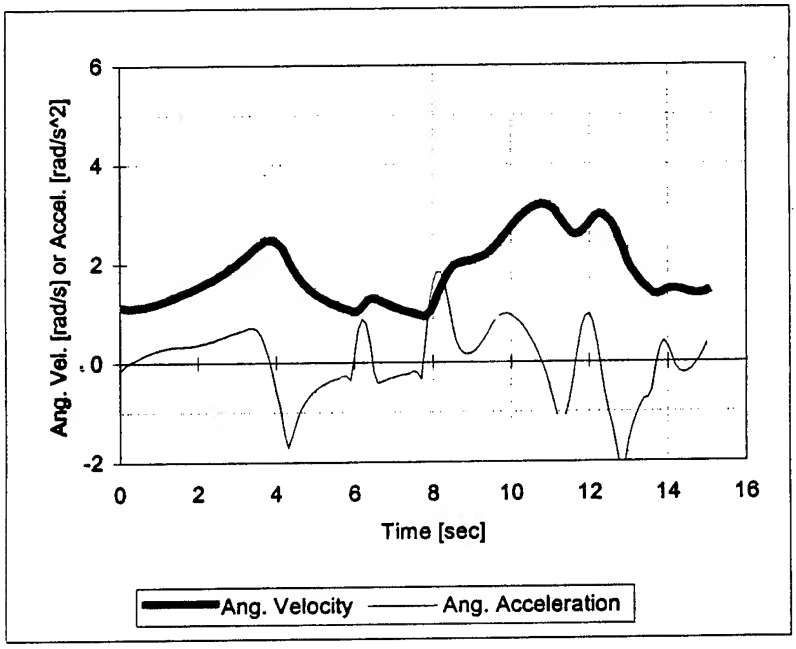

4.4.2 Fork, Cab and Seat Inverse Kinematics – "Pointing Method."

After computing the angular velocity and angular acceleration of the arm required to achieve the desired acceleration magnitude, the next step of the inverse problem is to determine the optimal fork, cab and/or seat angles. These angles would minimize the difference between the desired pilot translational acceleration and the acceleration resulting from the movements of the DES. BRC actually developed two methods, each of which has advantages. The first method labeled as, the "Pointing Method," is described in this section.

Using the computed arm angular velocity and angular acceleration, the acceleration at the end of the arm is given by:

$$A_c = -\left(\dot{\theta}_1^{\,2} R\right)\vec{x} + \left(\ddot{\theta}_1 R\right)\vec{y} + G\vec{z} \qquad \text{Eq. 4-12}$$

Equation 4-12 is consistent with the arm coordinate frame shown in Figure 4-1. The vector A_c will be called the centrifuge acceleration, and it is the acceleration due only to the movements of the arm and gravity.

As previously stated, the goal of the optimization problem is to determine the fork, cab, and/or seat angles which yield the best approximation to the specified pilot acceleration. Referring to Figure 4-9, which shows a simplified representation of the fork and cab geometry, the specified pilot acceleration (i.e., the desired acceleration), A_d, acts at the pilot position defined by $\vec{P}_{pilot}$. However, this algorithm does not account for an offset away from the cab centroid. Thus, the Pointing Method solution specifies desired accelerations at the center of the cab. The Pointing Method minimizes the differences between the desired acceleration component and the centrifuge acceleration component by minimizing the angle between these two vectors according to a scheme expressed as,

$$\phi = cos^{-1}\left(l_c l_d + m_c m_d + n_c n_d\right) \qquad \text{Eq. 4-13}$$

where l_c, m_c, and n_c, and l_d, m_d, and n_d represent the direction cosines of A_c and A_d respectively. Equation 4-13 is the objective function to be minimized. In order to use this equation, A_c and A_d must first be written with respect to the same reference frame. This is accomplished by the following transformation:

$$^0A_d = {}^0_pR\,(A_d)_{pilot} \qquad \text{Eq. 4-14}$$

where,

$${}^0_pR = ({}^0_AR)({}^A_FR)({}^F_cR)({}^c_sR)({}^s_pR) \qquad \text{Eq. 4-15}$$

The analytical expressions for the rotational transformation matrices appearing in Equation 4-15 are given in Section 4.1.

As indicated by Equation 4-13, ϕ is a function of the fork, cab and seat angles only. Namely, Equation 4-16 is of the form,

$$\phi = f(\theta_2, \theta_3, \theta_4) \qquad \text{Eq. 4-16}$$

There is no dependence on any translational offset position of the desired acceleration vector. This optimization method purely varies the fork, cab and seat angles until the minimum value of ϕ is attained, effectively pointing the desired acceleration vector in the direction closest to the centrifuge acceleration vector.

A Matlab optimization tool called *constr.m* is used in the file *invkin.m* to minimize the objective function shown in Equation 4-13.

4.4.3. Fork, Cab and Seat Inverse Kinematics – "Weighted Solution Method."

The second method for inverse fork and cab kinematics is the "Weighted Solution Method." This method solves for the DES fork, cab, and seat positions required to achieve a desired acceleration for the DES pilot after allowing the user to specify the required fidelity of the acceleration components by assigning relative weights. This method is different from the pointing method in that it is possible to specify one component as being "more important" than the other components. The solution algorithm is based on non-linear programming concepts and it is slower than the Pointing Method. Applied to the DES, the error in matching one component of the desired pilot accelerations can be constrained to be either more or less than errors associated with the other components; this relative constraining is done by assigning penalizing weights to the objective equations.

An example of the application of the Weighted Method is presented in Table 4 -2. The table shows the weights used to simulate a Cobra maneuver. In general, it is the relative values of the weights and not their actual value that affects the simulation. It typically takes one order of magnitude difference in weights to create noticeably different results. Note that some profiles will occasionally not change even if weights on a specific component are increased. This signifies that a best solution was already achieved, and no better solution exists or can be found. Results of the example simulation are shown in Figures 4-9 through 4-14. Three different solutions of the Cobra maneuver are given, reflecting different combinations of weighting factors shown in Table 4-2. The figures display resulting accelerations (Figures 4-9 through 4-11) and fork and cab angle time histories corresponding to each of the three simulations (Figures 4-12 through 4-14). In this example, the solutions are optimal with respect to accelerations sensed at the central location of the DES cab.

Table 4-2 Sample Weights for a Cobra Maneuver

Run Type	Weight on x-accels	Weight on y-accels	Weight on z-accels
Emphasis placed on x-accelerations	25	1	5
Emphasis placed on z-accelerations	5	1	25
Equal trade-offs between x- and z-accelerations	15	1	5

The Weighted Method is also capable of accounting for an offset that might exist between the pilot and the cab center. This is because the optimization process uses the actual kinematic equations, as opposed to the "Pointing" Method, which essentially solves a geometric problem. The DES Simulation software allows the user to enable or disable the option of accounting for a possible offset. When disabled, the software executes faster. BRC also attempted to include fork and cab rate limitations into this algorithm, but the method became unstable. For this reason, the rate limitations are applied later in the simulation (see Section 4.5).

In summary, the Weighted Solution Method optimizations scheme uses a simplified forward kinematics expression

$$A_c = (R, \dot{\theta}_1, \ddot{\theta}_2, \theta_2, \theta_3, \theta_4, \vec{P}_{pilot}) \qquad \text{Eq. 4-17}$$

in which the rate of θ_2, θ_3, and θ_4 have been omitted due to the instability they cause during the optimization process.

Next, the weighted optimization examines computed accelerations, assigns user-defined weights, and then minimizes the components equations

$$\begin{aligned} T_x &= abs(A_d - A_p)_{x\text{-components}} \\ Ty &= abs(A_d - A_p)_{y\text{-components}} \\ Tz &= abs(A_d - A_p)_{z\text{-components}} \end{aligned} \qquad \text{Eqs. 4-18}$$

by varying θ_2, θ_3, and θ_4 for each time step. The optimization algorithm that converges to an optimal solution for the formulation given above is performed by the *attgoal.m* subroutine provides with Matlab. The call to this subroutine is made in the file *weighted.m*.

Figure 4-9

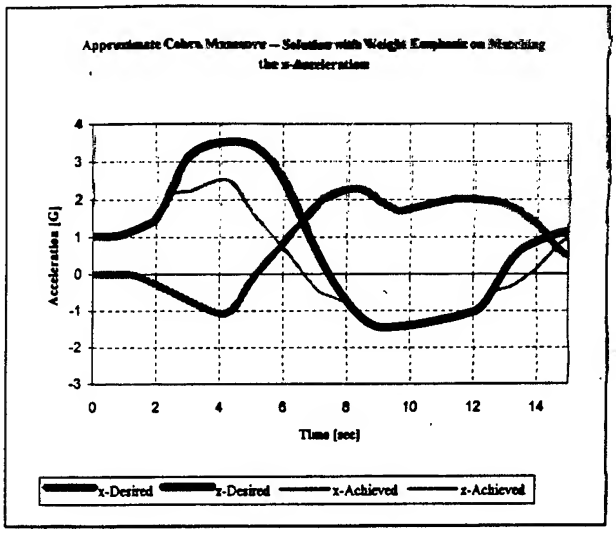

Figure 4-10

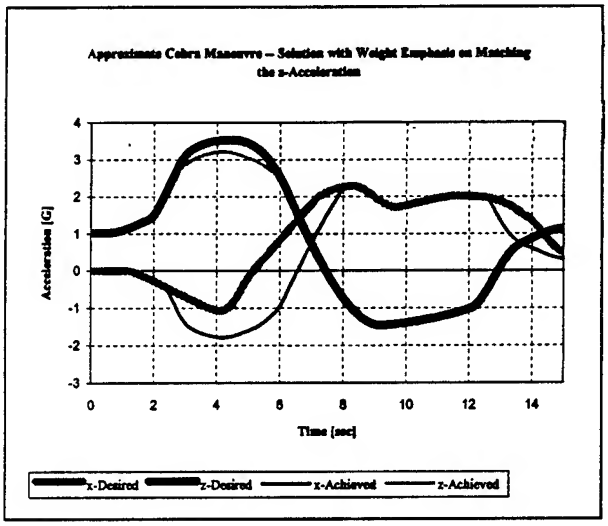

Figure 4-11

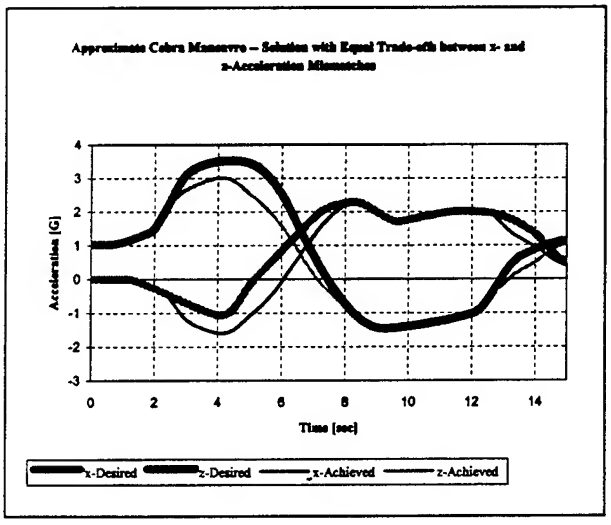

Figure 4-12

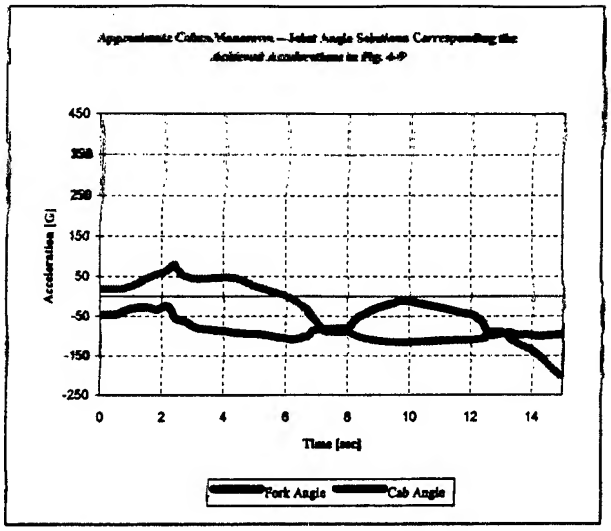

Figure 4-13

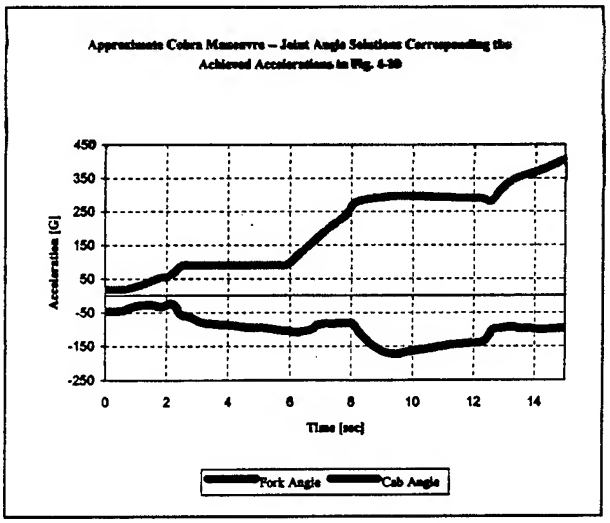

Figure 4-14

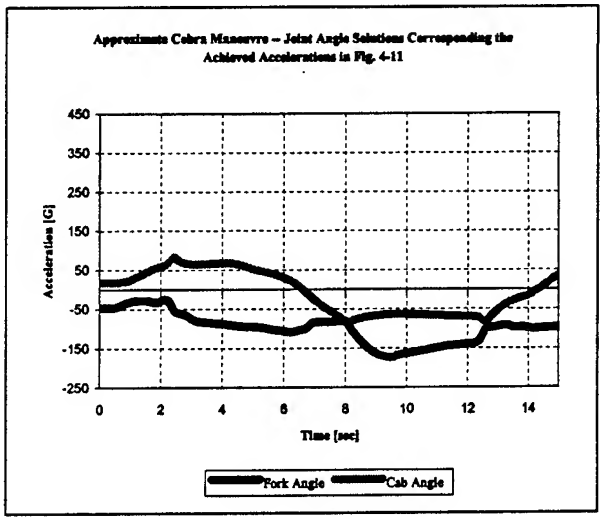

4.5 Application of the DOF Physical Limits – Overview.

The terminology "physical limits" refers to minimum or maximum angular position, velocity or acceleration limits for any of the DES degrees of freedom. Some of these limitations are mechanical in nature, while the DES Controller software imposes others.

The limits for the DES are applied before the application of the dynamic models. The primary reason for this is that the dynamic models implemented in the DES Simulation software always act as filters, mitigating excessive movements. But these dynamics will not necessarily keep the DES motions within the necessary physical limits. Thus, it is necessary to apply the algorithm discussed in Section 4.5.1 to keep the solutions realistic. Also, there are cases, as discussed in Section 4.5.2, where the application of limits prior to the dynamics can be beneficial with regard to the achievement of a good fidelity between desired and achieved accelerations.

Section 4.5.2 describes an algorithm that applies limits by extending the local time span of a profile by a fractional amount of the total simulation time, to achieve a challenging centrifuge profile.

Section 4.5.3 discusses another limitation that needed to be modeled, namely the limitation of the fork and cab from being rotated more than +/- 180°. This limitation is called the fork or cab handicap.

4.5.1 Application of the DOF Physical Limitations without Time Extension.

This algorithm modifies a signal that would typically be the outcome of an inverse kinematics operation. The signal could be an angular velocity or angular acceleration of any of the four-degrees of freedom that were modeled.

Conceptually, the operation is straightforward in that the algorithm simply inspects the given trace, and "clips" the areas that are more than a specified limitation. Since the clipped traces are generally angular velocity or acceleration traces, clipping these values results in the angular positions being modified. When the fork and cab positions are changed in this way, it will change the translational fidelity of the simulation. Thus, this method generally decreases the fidelity between the achieved and desired acceleration signals. However, if the limitations were not exceeded by a large amount, then the decrease in the fidelity is often not dramatic. Figures 4-15 and 4-16 illustrate the application of this method to model arm acceleration limitations. The same algorithm can be applied to model fork, cab, and seat velocity or acceleration limitations.

Figure 4-15 Application of a Limitation without Extending Time

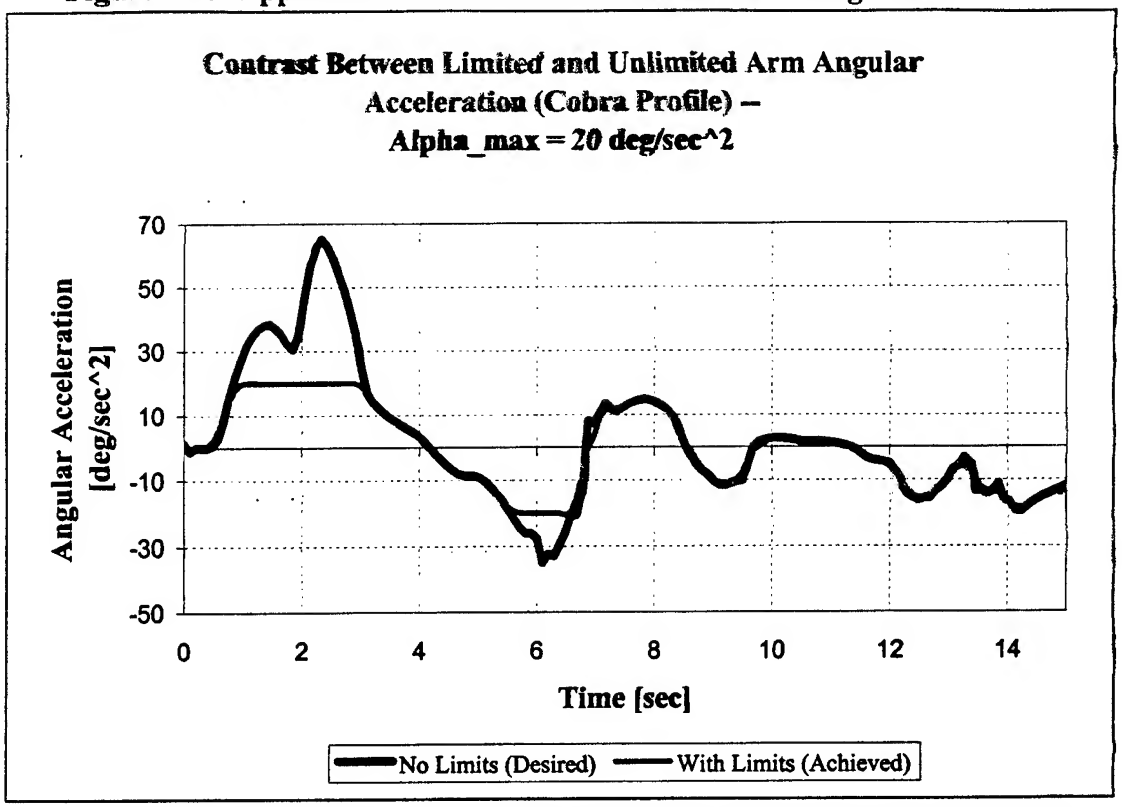

Figure 4-16 Achieved G-Levels Before and After the Limitation Algorithm

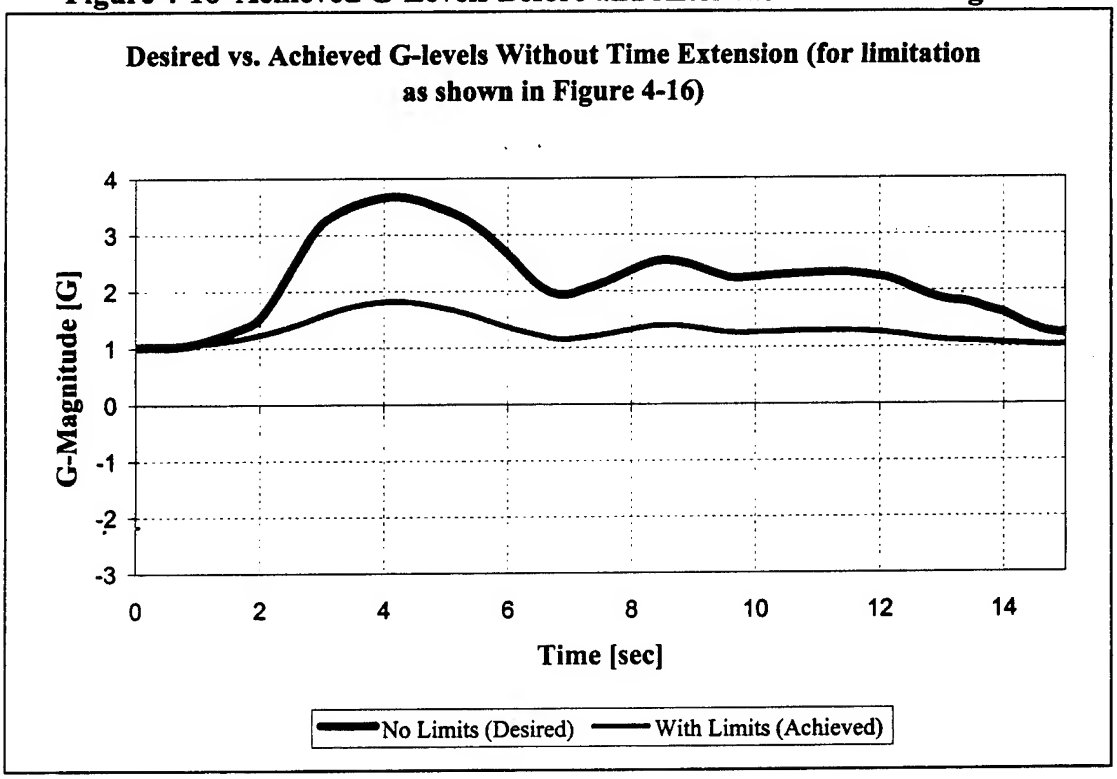

4.5.2 Application of the DOF Physical Limitations with Time Extension.

As in the algorithm of Section 4.5.1, this algorithm modifies a signal that would typical be the outcome of an inverse kinematics operation. The signal could be an angular velocity or angular acceleration of any of the four-degrees of freedom that were modeled.

This algorithm does not clip signal values to a certain level - rather it extends the time that it takes to achieve certain signal values as necessary to meet the limits of the DES. The distortion of time is applied locally, so that only in select areas of a simulation would the centrifuge rider experience accelerations or velocities that have been modified. The outcomes of this method are (1) it applies the centrifuge limits, (2) the fidelity between obtained and desired accelerations are not compromised, and (3) the desired accelerations had to be extended in time in the areas where the profile requirements exceeded centrifuge capabilities.

Figures 4-17 and 4-18 illustrate one instance of the application method.

4.5.3 The Fork and Cab "Handicap" – A Displacement Limitation Imposed by the DES Controller.

This limitation algorithm is actually applied during the solution process of the inverse kinematics problem, as opposed to the two other methods (Section 4.5.1 and 4.5.2) which are applied after the inverse kinematics.

The angular displacement limit is imposed by the current DES Controller software, which does not allow either the fork or cab to exceed 180° total motion. If controlled in the "manual" mode, the fork and cab actually go in a full circle, without any displacement limits, but the controller is usually not in the manual mode during the execution of a profile.

Basically, this limitation is modeled in the inverse kinematics portion of the DES Simulation software by assessing the proximity of a cab or fork angle to the displacement limitation, and by restricting the available window of new angular solutions to the specified displacement limits, if necessary. Namely, if an angle is currently at 45°, the inverse kinematics algorithm will search for a new solution, between –45° and 135° (the optimizer within the inverse kinematics searches up to 90° to the "left" and up to 90° to the "right" of a current angular position). If the current angle is 170°, then the search will span from 80° to 180°. By contrast, if the handicap is not applied (it can be turned off in the DES Simulator software) the same 170° position will trigger a search for an optimal new angle between 80° and 260°.

Another mechanical handicap exists for the fork. This handicap imposes a stand-still on the fork for situations where the radial G-loading exceeds 4G. Again, this limitation is modeled during the inverse kinematics in the sense that, above 4G, the inverse kinematics solves only for new cab (and seat) angles, keeping the fork at its current position.

Figure 4-17 Application of a Limitation by Extending the Time Span

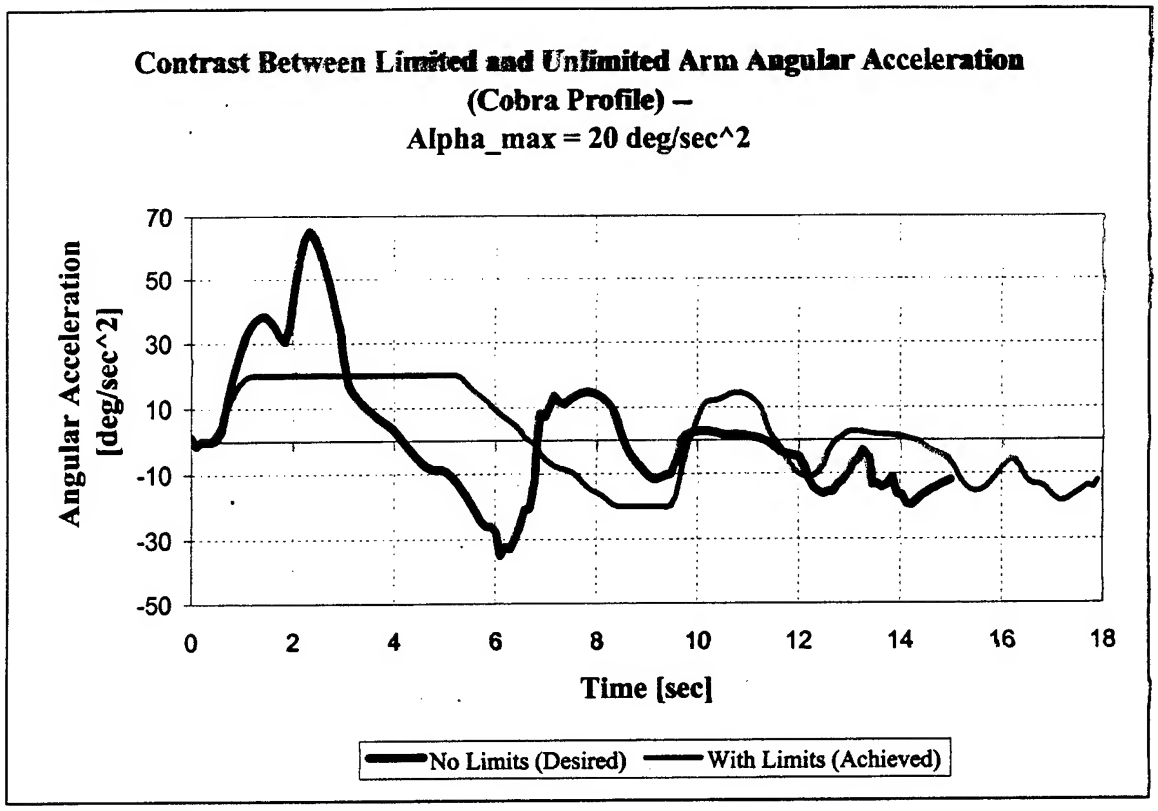

Figure 4-18 Achieved G-Levels Before and After the Limitation Algorithm

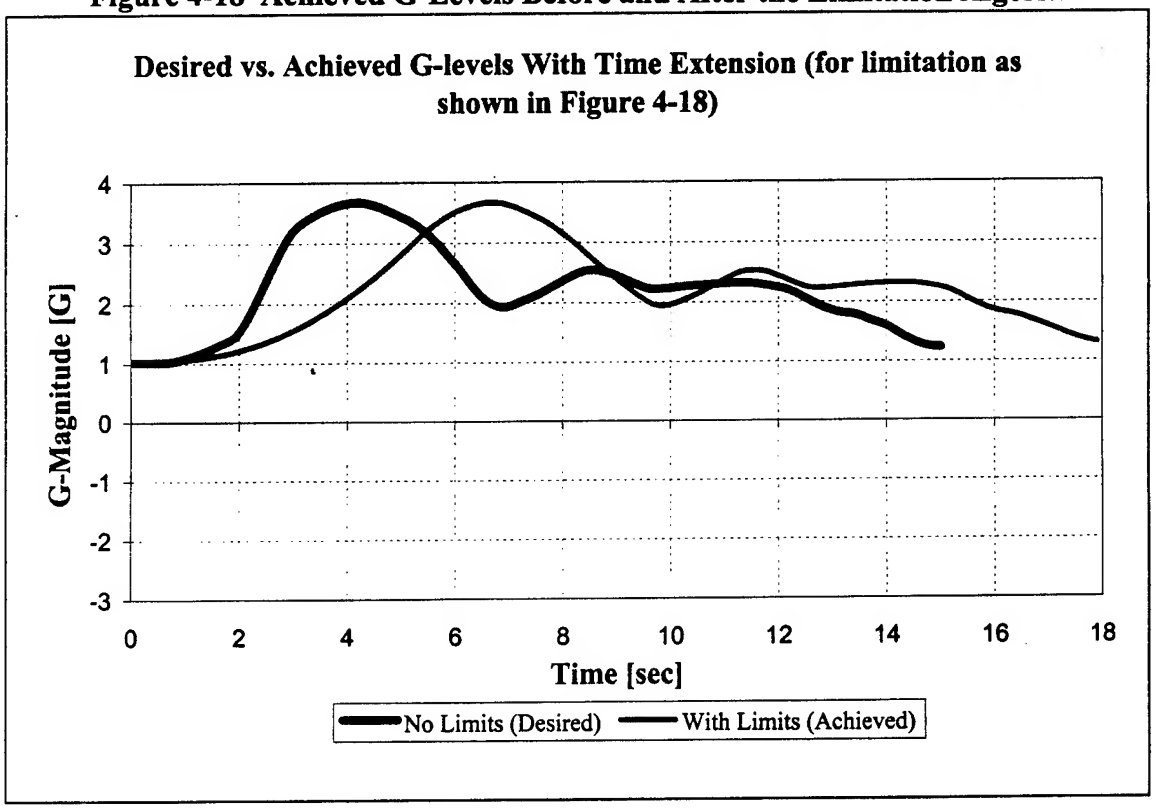

4.6. Inverse Dynamics – Overview.

The algorithm used for the inverse dynamics of the arm (Section 4.6.1) is more complicated than the algorithms used for inverse dynamics of the fork and cab (Section 4.6.2). The reason for this is that the arm command signal is solved before the computation of the fork, cab and seat inverse kinematics. As explained in Section 4.6.1, the primary effects of this requirement is that the arm command has to be shifted in time so that the predicted arm output is best synchronized with the resultant of the desired acceleration traces which were specified by the user.

Since the seat is not an actual DOF in the current DES configuration, there are no forward or inverse dynamics for the seat DOF.

4.6.1 Arm Inverse Dynamics.

The arm inverse kinematics (Section 4.4.1) is succeeded directly by the arm inverse dynamics. But, the arm inverse dynamics precede any of the operations that solve for the fork, cab and seat movements. The reason for this is that the solutions for the fork, cab and seat need to be based on the achievable behavior of the arm (i.e., the achievable G-level).

The primary consequence of this requirement is that the inverse dynamics algorithm for the arm is more complicated than the same algorithm for the fork and cab.

The input to the arm inverse dynamics algorithm is always going to be the optimal arm angular velocity trace, ω_{arm}. The word "optimal" refers to the fact that this trace will originate from the arm inverse kinematics optimization process (Section 4.4.1). Additionally, the ω_{arm} trace may be subjected to the application of the physical arm limitations (Section 4.5) prior to the computation of the inverse dynamics.

Once an ω_{arm} signal is ready, it is run through the generic inverse dynamics algorithm that is discussed in Section 4.6.3. This algorithm requires a dynamics model to be expressed in terms of its state space equations. For reasons discussed further below, the time delay model was not included in the direct inverse dynamics calculations for the arm. So, instead of running the inverse dynamics algorithm discussed in 4.6.3 a single time on the 5^{th} order arm dynamics model (Section 4.3.1), the said algorithm was rather called upon successively to model the inverse dynamics of the 2^{nd} order arm "sub-models".

After producing an arm input command according to the method stated above, the DES Simulation software then feeds this trace back into the arm forward dynamics algorithm to inspect the output trace. Generally speaking, the output trace will have satisfactory magnitude characteristics, but is will be out of phase with the original desired acceleration traces. So, an optimization algorithm had to be created to shift the arm command in time, such the output of this command generates G-levels which are synchronized with respect to the magnitude of the desired accelerations trace.

To some extent, the known delay value characteristic of the arm dynamics could have been used. However, it was noted that in the case of challenging profiles (i.e., difficult to achieve), it was

best to use the cross-correlation algorithm discussed above, rather than blindly applying the known delay value.

An example of the "re-synchronization" of the arm command with the resultant of a set of desired traces is given in Figure 4-19.

Figure 4-19 Illustration of the Post-Dynamics Curve Manipulation

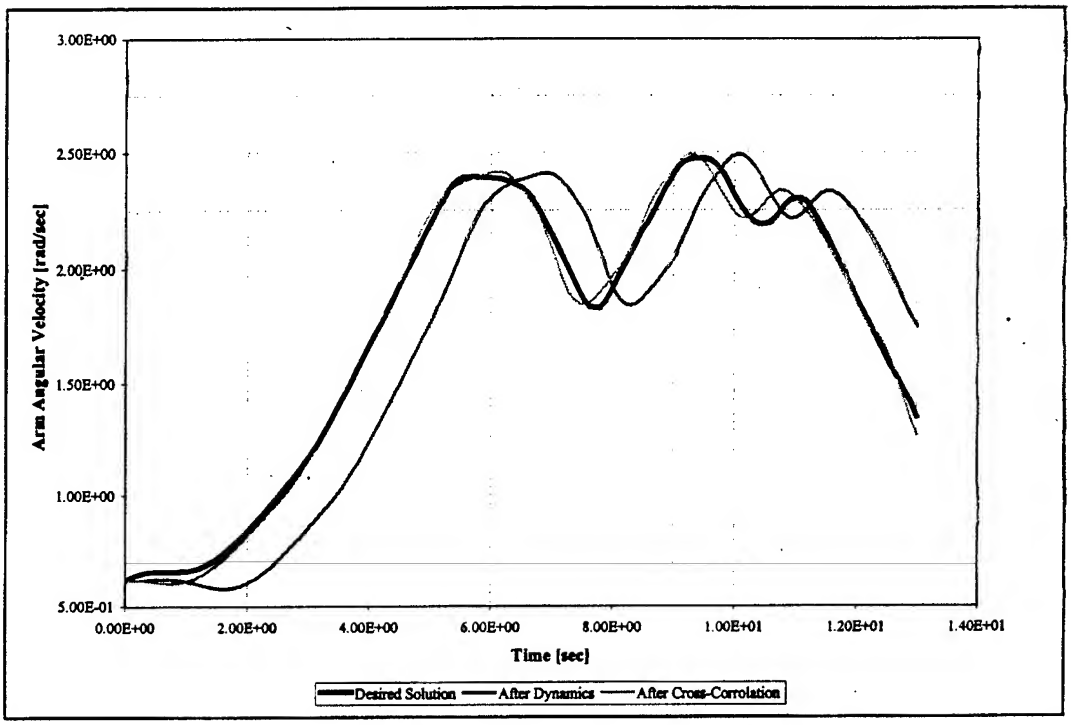

Finally, the inverse dynamics includes a necessary adjustment related to the "offset" which was already described in Section 4.3.1. Namely, a "sister" equation to Equation 4-15 had to be incorporated into the arm inverse dynamics portion of the code. In the case where a desired angular velocity is being specified (as is being done in this section), the desired angular velocity then needs to be incremented by an offset to accommodate the behavior described in Section 4.3.1. Equation 4-19 represents this offset (ω is in rpm units),

$$\text{Offset} = (0.0363\ T_{desired} + 0.17) \qquad \text{Eq. 4-19}$$

An example is given here to better illustrate the effect of this offset. Let the desired angular velocity to produce a certain G-loading be 18.8 rpm. According to Equation 4-16 (and according to experimental observation), it would then be necessary to command an rpm level of 19.6 rpm to actually reach 18.8 rpm.

4.6.2 Fork and Cab Inverse Dynamics.

It was possible to model the fork and the cab dynamics with a 2nd order model, as discussed in Section 4.3.2. Therefore, the inverse dynamics for either the fork or cab yielded a command signal that was computed with the method discussed in Section 4.6.3.

As stated earlier, since the seat is not an existing degree of freedom in the current DES configuration, there are no forward or inverse dynamics for the seat DOF.

4.6.3 Inverse Dynamics for a 2nd-Order System.

This algorithm was used for the arm, fork, and cab inverse dynamic models. It uses the utility available in Matlab, which directly transforms a transfer function into a state-space dynamic model. The Matlab utility in question is called *tf2ss.m*.

As stated in Section 4.3, BRC has created transfer function models for the dynamics of the three DES degrees of freedom. So, applying *tf2ss.m* to any of three models would yield or state-space equivalent model of the following general form,

$$\begin{aligned} \dot{x} &= Ax + BU \\ y &= Cx + D \end{aligned} \qquad \text{Eq. 4-20}$$

Using a dummy matrix,

$$P = [0 \;\; 1]$$

to accommodate the fact that non-square matrices cannot directly be inverted, the sought input, U, given an available output , y, can be obtained as follows,

$$U(t) = \left[P * A^{-1} * B\right]^{-1} * P * \left[A^{-1} * \dot{x} - x\right] \qquad \text{Eq. 4-21}$$

Give a simulation with k data points, the x matrix, in Equation 4-21 would be of a size k by 2. In the DES Simulation software, we set the second column of the x matrix equal to y,

$$x_2(t) = y(t) \qquad \text{Eq. 4-22}$$

and the first column is set as follows,

$$x_1(t) = 0 \qquad \text{Eq. 4-23}$$

because the C matrix is always written as,

$$C = [0 \quad 1] \qquad \text{Eq. 4-24}$$

These mathematics were initially implemented for the 5th order dynamic model of the arm, but the method is now used only for 2nd order models. The method has always produced input signals that return the original desired output upon the re-application of the forward dynamics.

4.7 References.

[1] Meirovitch, L., "Elements of Vibration Analysis", McGraw-Hill Book Company, pp 491-493.

5.0 DES Testing and Validation of the DES Modeling.

The main purpose of this section is to correlate the DES as it exists, with the theoretical and "customs" models that were created and presented throughout Section 4.

Section 5.1 gives an overview of the tests that BRC conducted at WPAFB in collaboration with Veridian. These tests were carried out to help BRC better understand the operation and general behavior of the DES as a machine. Section 5.2 describes the approach taken by BRC regarding how the data from the tests were used. Considering the combination of all the modeling algorithms (kinematic and dynamic models), Section 5.3 progresses to the validation process. It contrasts recorded with predicted output results in terms of DOF movements, and the accelerations generated at the accelerometer location.

5.1 Overview of DES Tests.

BRC and Veridian conducted a number of tests on the centrifuge to help determine dynamic parameters and to generally validate the mathematical model of the DES.

First set of tests: In June 1996, approximately 40 tests were conducted which consisted of a series of step functions. These functions were input as commands for the arm, fork, and cab. The focus was to study the arm. A BRC engineer was on-site.

Second set of tests: In October 1996, approximately 100 tests were run primarily to study the fork and cab. The movements of the fork and cab were studied at different G-levels and for different commanded inputs. These inputs were generally still in the form of step functions.

Third set of tests: The next set of tests (June 1997) focussed on commands which were not step functions, but were gradual commands, within the capabilities of the arm, fork and cab. This set of tests totaled approximately 50 test runs. A BRC engineer was on-site for these tests

Fourth set of tests: After June 1997, there were a number of repairs that were performed on the fork controls and the cab motors were replaced. Therefore, Veridian reran about half the runs from the third set of tests (approximately 25 runs, in January 1998).

Fifth set of tests: This set included about 20 runs that were performed in June 1998. The DES Simulation software at its then-current state was used to generate profiles, and to cross-correlate different parameters between the actual DES, and the software. BRC engineers were on-site.

No test grids are currently available for the 4^{th} and 5^{th} testing sessions. However, copies of the test grids for the 1^{st} through 3^{rd} set of tests are available in Appendix A.

5.2 Study of Dynamic and Other Miscellaneous DES Parameters.

As indicated in Section 5.1, tests run by BRC on the DES centrifuge were conducted to study the dynamics of each of the three centrifuge degrees of freedom.

The input signals for the degrees of freedom were of many styles to capture the different behaviors of the centrifuge. An iterative optimization process was applied to the resulting data to arrive at reasonable parameters for each of the chosen dynamic models.

Sections 4.3.1 and 4.3.2 explain how and which dynamic models were chosen for each of the DES DOFs. By contrast, Section 5.2.1 explains the iterative optimization process that was used for any of the DOF models to obtain the parameters corresponding to each DOF model. The arm model became a seven-parameter model, and the fork and cab were each modeled with a four-parameter model.

Section 5.2.2 gives values for the parameters of each dynamic model. It describes a number of DES specific characteristics, which were, for the most part, also incorporated into the DES Simulation software (DOF limits, DES input file format, etc.).

5.2.1 The Optimization Algorithm to Estimate Dynamic Model Parameters.

The method of analysis that is described was applied a number of times to each of the DES gimbals. It was applied at least as often as the number of different dynamic models that were chosen (and rejected or, finally, accepted) for the analysis and modeling of a given gimbal.

Figure 5-1 in conjunction with Figure 5-2 illustrates the iterative process required for minimizing the error associated with a given prospective dynamic model. A minimized error was of course not necessarily the end of the design of a dynamic model. The very end of the modeling process is not shown in Figure 5-1. It would consist of a visual inspection of the performance of a given model, i.e., the fact that the error was minimized in one optimization run was not necessarily an indication that the visual results (plot of the responses) output by a model were satisfactory. The latter explains why models of different form were created by iteration, forcing the process shown in Figures 5-1 and Chart 5-2 to be repeated multiple times.

Figure 5-1 Generic Process of an *M*-Parameter Dynamic Model

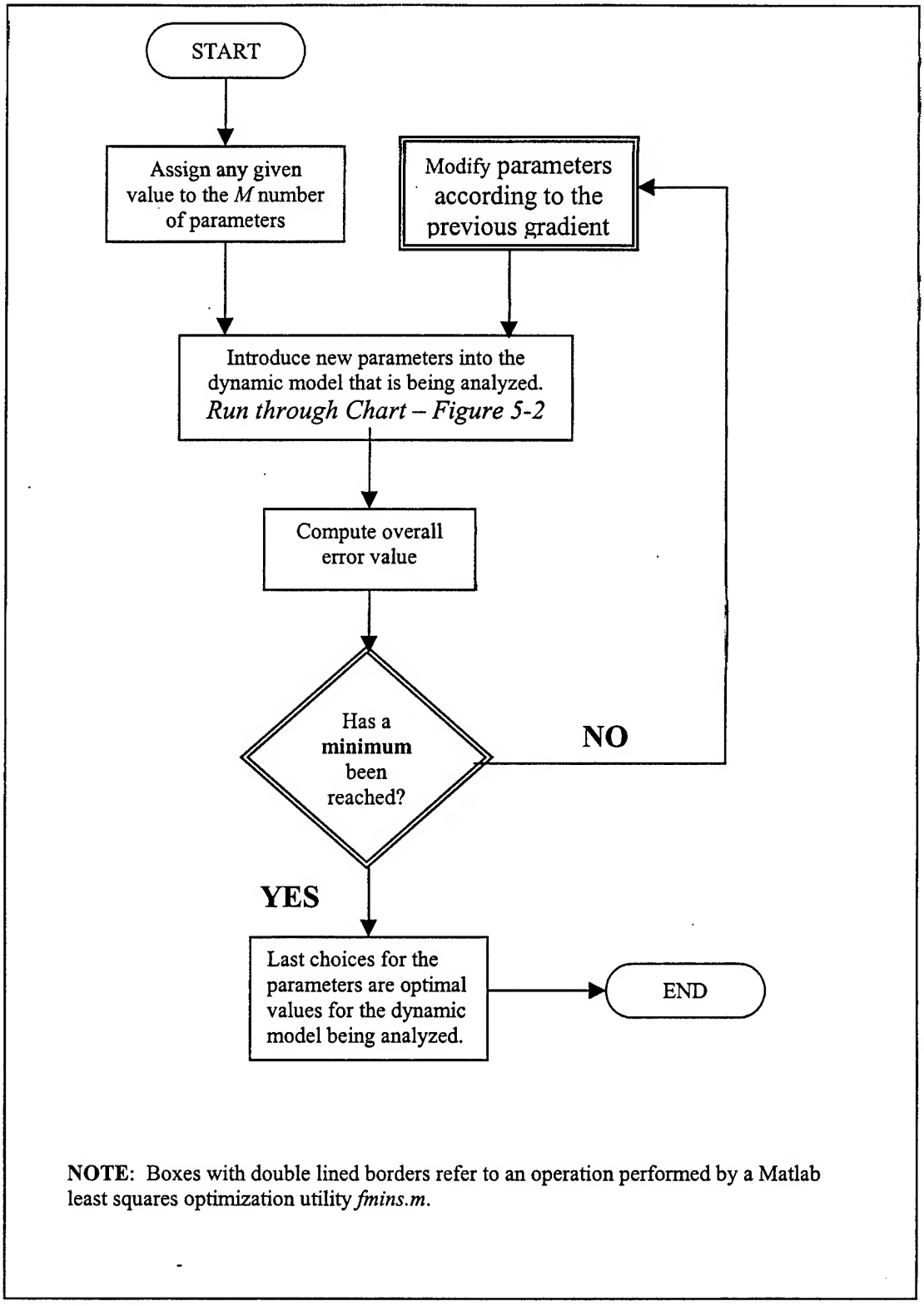

NOTE: Boxes with double lined borders refer to an operation performed by a Matlab least squares optimization utility *fmins.m*.

Figure 5-2 Application of *N*-Sources of Test Data to the Optimization of One Dynamic Model

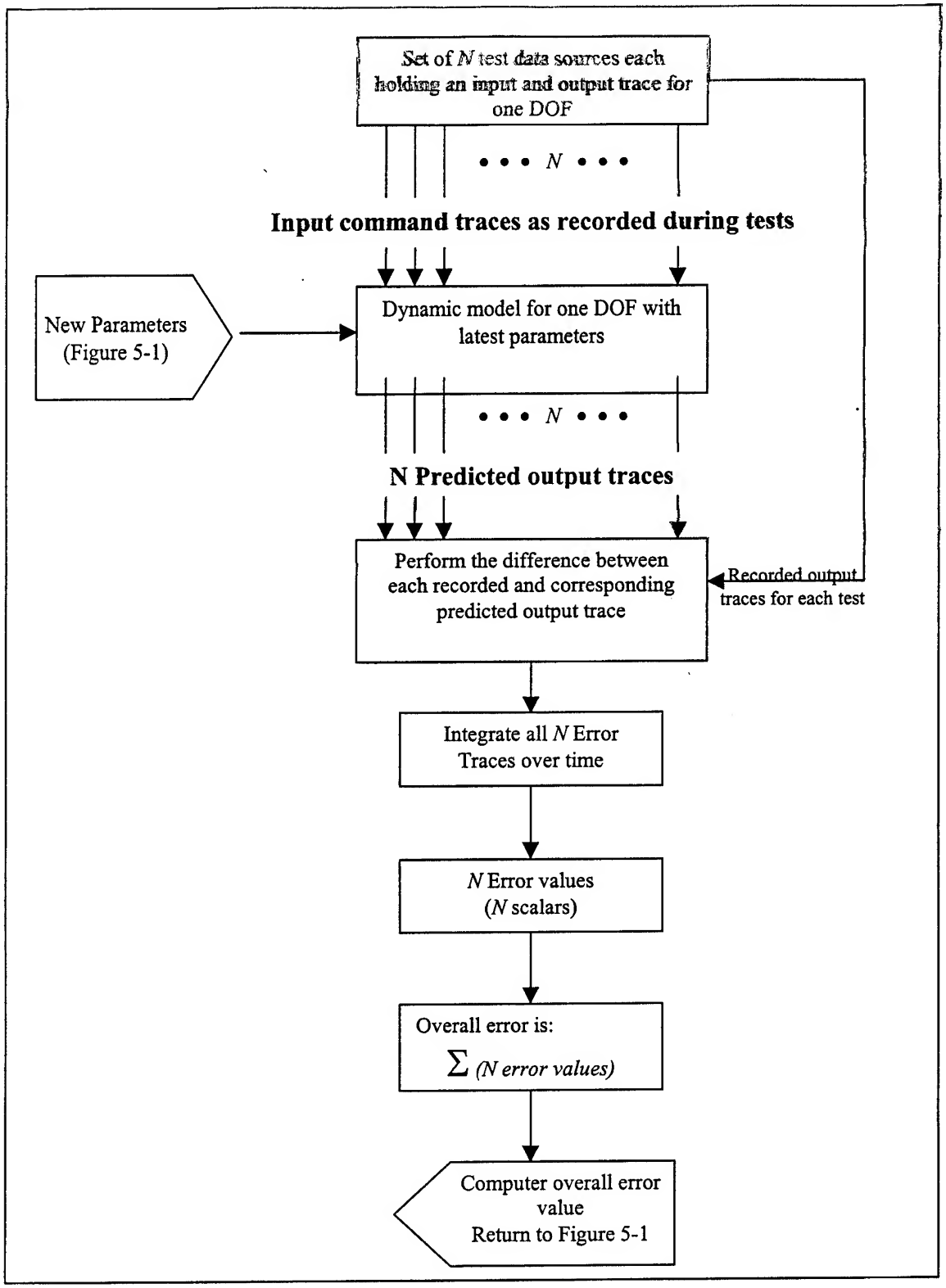

5.2.2 Resulting Values for All Dynamic Modeling Parameters and Limitations.

A. Parameters for the Dynamic Models:

The theoretical models for the dynamics of the DES DOFs are covered in Sections 4.3.1 and 4.3.2. This section now gives the values, which were assigned to the parameters of each model. These values were arrived at by following the methodology described in Section 5.2.1.

Arm Dynamics Parameters:

Numerator	*Denominator*
$N_1 = -1.04E+03$	$D_5 = 3.47E-01$
$N_0 = 2.80E+03$	$D_4 = 8.74E+01$
	$D_3 = 2.27E+03$
	$D_2 = 8.62E+03$
	$D_1 = 9.46E+03$
	$D_0 = 2.80E+03$

(variables appear in Eqs. 4-6)

Fork Dynamics Parameters:

$$\omega_n = 3.39\times10^{0}$$
$$\xi = 6.30\times10^{-1}$$
$$\kappa = 1.02\times10^{0}$$
$$\tau = 1.42\times10^{-1}$$

(variables appear in Figure 4-5)

Cab Dynamics Parameters:

$$\omega_n = 2.36\times10^{2}$$
$$\xi = 1.00\times10^{1}$$
$$\kappa = 9.70\times10^{-1}$$
$$\tau = 4.00\times10^{-2}$$

(variables appear in Figure 4-5)

Dynamic models may vary in form upon changes in any of the DES drive systems. A practical GUI to modify dynamic parameters would therefore have been superfluous. Hence, the mentioned values above are hard-coded in the DES Simulation software. However, in view of possible upgrades, BRC will train DES technicians on the manner in which the software code could be modified to accommodate new dynamic models and parameters.

B. Motor Capability Limits:

The DES Simulation software runs based on a number of user-defined dynamic parameters. These parameters are not dynamic model parameters as discussed above, but they are representative of some of the important motor limitations; namely, that they are the angular velocity and angular acceleration limitations. The values for these limitations are easily adjustable in a user-friendly GUI environment. Also, refer to Section 4.5 to learn more about the manner in which these limitations are applied. Table 5-1 gives a listing of the current DES limitations. These are, however the run-time limitations for the centrifuge as controlled by the Primary Controller. The Conclusions in Section 6 and Section 8.8 elaborate somewhat more on the actual physical DES capabilites, which are better than those listed in Table 5-1.

Table 5-1 DES Kinematic Limits

	ω_{max} [deg/sec]	α_{max} [deg/sec^2]
Arm	270	15.5
Fork	60	70
Cab	50	80

Note that, in addition to these rate limitations, the fork and cab also suffer from displacement limitations. The nature of those limitations is discussed in Section 4.5.3.

An important note to make here is that none of the limitations are modeled in the forward simulation portion of the DES Simulation software – the dynamics are, however, modeled in the forward simulation. The reason for this is as follows. As far as the rates are concerned, it is assumed in the forward simulation that a user will detect excessive rates upon the creation of a profile. The same assumption is made for possible excessive displacements. The third limitation that is discussed in Section 4.5.3 (i.e., 4 G lock-up of the fork) is not modeled either, in the forward simulation. The DES technicians are already equipped with a forward simulator, which raises warning flags if a given profile is not achievable. Attempts were made to include these

limitations in the forward simulation of the DES Simulation software, but the time available was not sufficient to overcome the analytical and coding difficulties. It should be emphasized, however, that the inverse simulation does account for all limitations, such that the commands created by an inverse simulation should always fall within the capabilities of the DES motors.

5.3 Validation of the DES Simulation Software.

This section reports on the successful match between test and simulated data. This success indicates that the DES Simulation software is equipped with a forward kinematics model and appropriate dynamic models that, in combination, provide a good representation of the DES.

The results shown here are based on data collected during BRC's 5th round of tests. More specifically, the DES Simulation software is compared against two tests; however, BRC cross-checked its software in-house against many other tests to confirm the validity of the models.

Test #08 is used to show the match between recorded and simulated angular velocity traces. Many changing slopes and levels characterized the angular velocity in this test. By contrast, Test #19 does not exhibit a particularly great number of changes in the arm angular velocity, but the fork and cab in Test #19 go through many different movements. The great variety in their movements in turn yielded acceleration traces which could not serendipituously be matched by the DES Simulation software.

An important note is that all of the profiles that were run during the 5th round of tests were profiles generated by the DES Simulation software. A truncated view of the file created by the DES Simulation software for Test #19 is given in Table 5-2. The graphical profile editor segment of the software was used to create these profiles (see the User's Manual to get acquainted with the Graphical Profile Editor). Therefore, the commands that ran the actual centrifuge were the same commands that ran the models (the models for Test #08 and #19). Results are shown in Figures 5-3 and 5-4.

The transient mismatch in Figure 5-3 around the 75-second time region shows an error in the model for cases where a high G-onset rate is applied. This mismatch only occurs when the DES is modeled in the forward direction. In the inverse direction, all limitations have successfully been implemented such that resulting commands will produce predicted results, without a mismatch.

Table 5-2 Input – Test #19

149	2			
1	0.6000	1.00	0.00	0.00
2	0.6000	1.00	-0.57	0.51
3	0.6000	1.00	-2.03	1.80
4	0.6000	1.00	-4.11	3.63
5	0.6000	1.00	-6.63	5.84
6	0.6000	1.00	-9.47	8.32
7	0.6000	1.01	-12.52	10.99
8	0.6000	1.01	-15.71	13.75
9	0.6000	1.02	-18.96	16.56
10	0.6000	1.03	-22.20	19.34
11	0.6000	1.06	-25.37	22.04
12	0.6000	1.09	-28.39	24.59
13	0.6000	1.14	-31.19	26.89
14	0.6000	1.21	-33.64	28.85
15	0.6000	1.30	-35.63	30.32
16	0.6000	1.40	-36.96	31.09
17	0.6000	1.53	-37.34	32.37
18	0.6000	1.67	-36.28	37.37
19	0.6000	1.82	-33.89	44.98
20	0.6000	1.97	-30.47	54.33
21	0.6000	2.13	-26.21	64.81
22	0.6000	2.28	-21.27	75.98
23	0.6000	2.43	-15.78	87.45
24	0.6000	2.55	-9.85	98.87
25	0.6000	2.63	-3.57	109.90
26	0.6000	2.68	2.99	120.13
27	0.6000	2.68	9.76	129.09
28	0.6000	2.68	16.67	136.12
29	0.6000	2.68	23.67	140.24
30	0.6000	2.68	30.68	139.90
31	0.6000	2.68	37.67	134.75
32	0.6000	2.69	44.57	126.10
33	0.6000	2.69	51.32	115.11
34	0.6000	2.69	57.85	102.75
35	0.6000	2.70	64.10	89.88
36	0.6000	2.70	69.99	77.27
37	0.6000	2.70	75.42	65.61
38	0.6000	2.71	80.28	55.56
,	,	,	,	,
,	,	,	,	,
,	,	,	,	,
,	,	,	,	,
,	,	,	,	,
,	,	,	,	,
,	,	,	,	,
139	0.6000	1.01	-10.95	-25.02
140	0.6000	1.01	-9.62	-22.28
141	0.6000	1.00	-8.33	-19.52
142	0.6000	1.00	-7.07	-16.79
143	0.6000	1.00	-5.86	-14.10
144	0.6000	1.00	-4.72	-11.50
145	0.6000	1.00	-3.66	-9.02
146	0.6000	1.00	-2.68	-6.71
147	0.6000	1.00	-1.82	-4.62
148	0.6000	1.00	-1.09	-2.81
149	0.6000	1.00	-0.52	-1.36
(1)	(2)	(3)	(4)	(5)

(1) Line Counter
(2) Delta-t [sec]
(3) Desired G-level [G's]
(4) Cab Angle Position Command [deg]
(5) Fork Angle Position Command [deg]

← Refer to Legends

Figure 5-3 Correlation between Recorded and Simulated Arm Angular Velocity

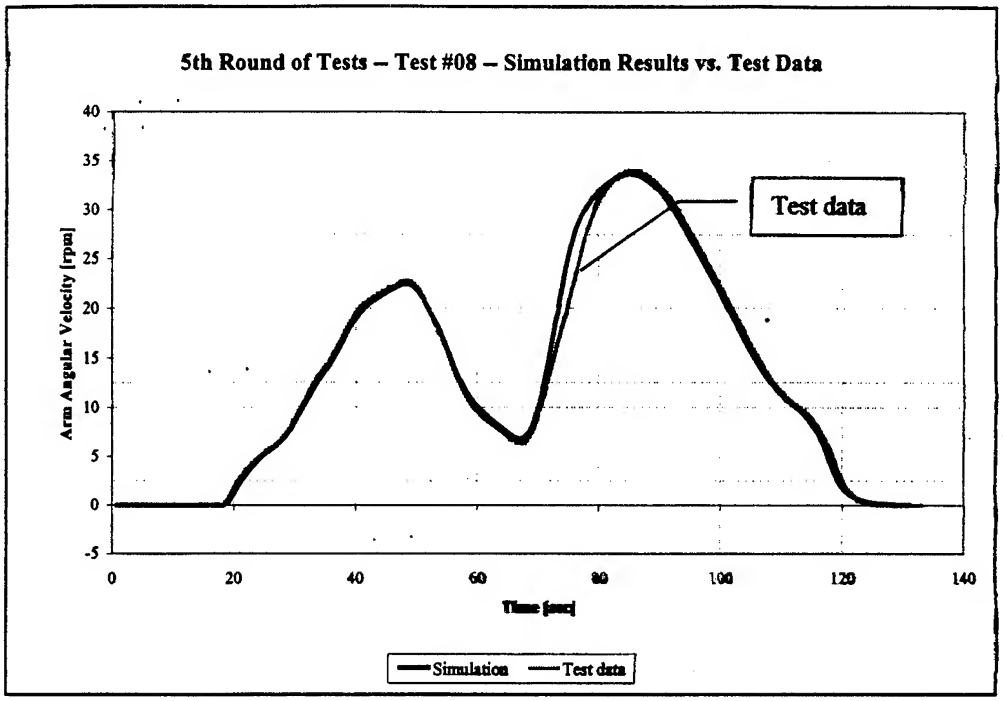

Figure 5-4 Correlation between Recorded and Simulated Arm Angular Velocity

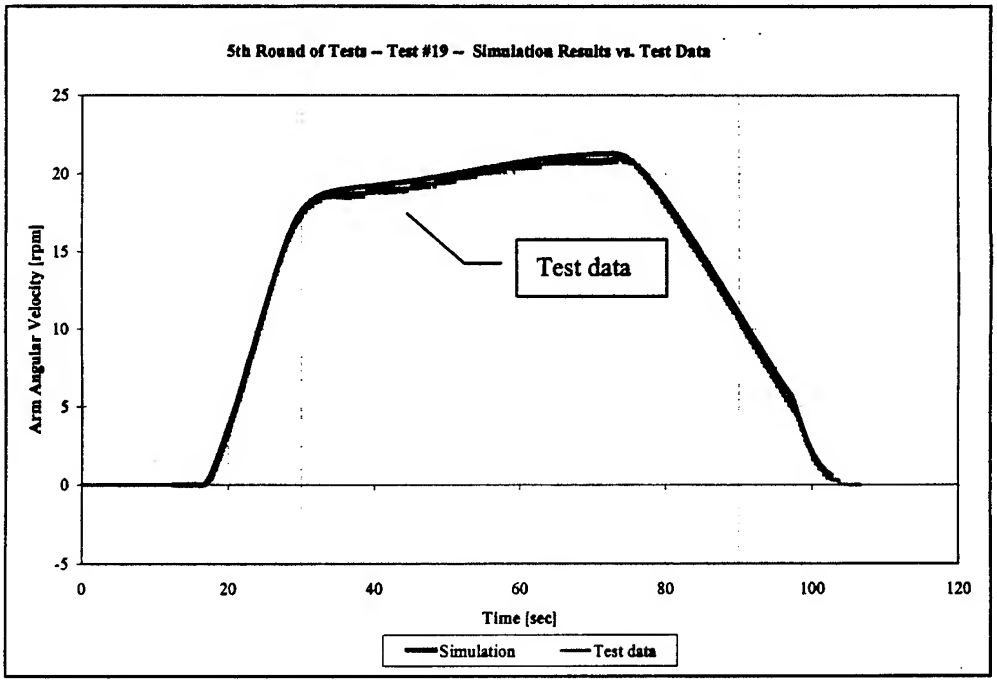

Figure 5-5 Correlation between Recorded and Simulated Cab Position

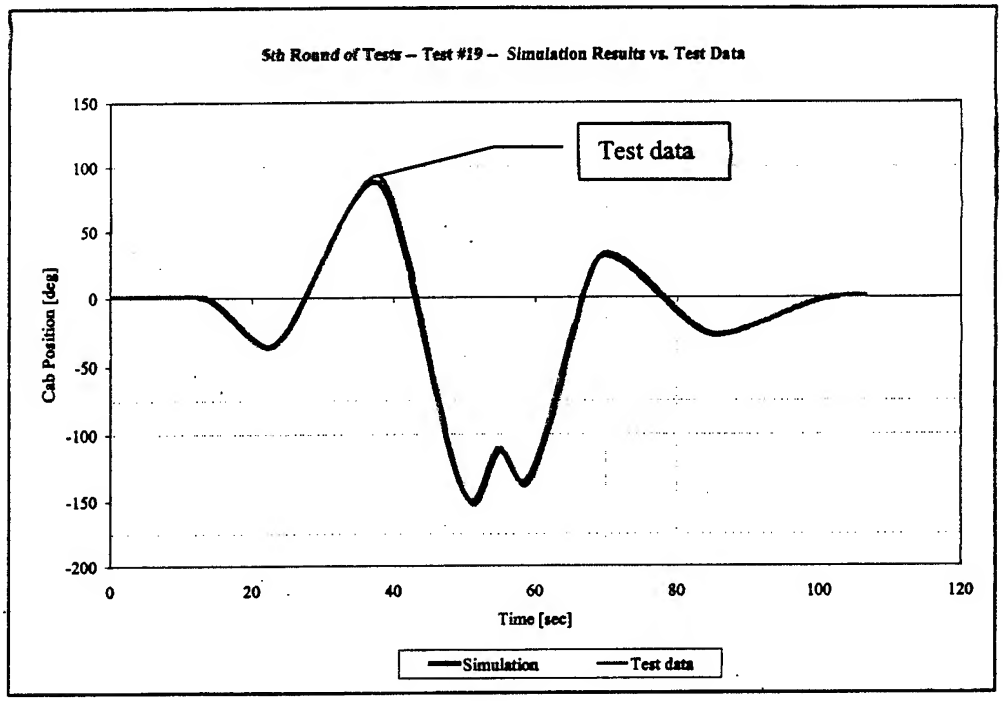

Figure 5-6 Correlation between Recorded and Simulated Fork Position

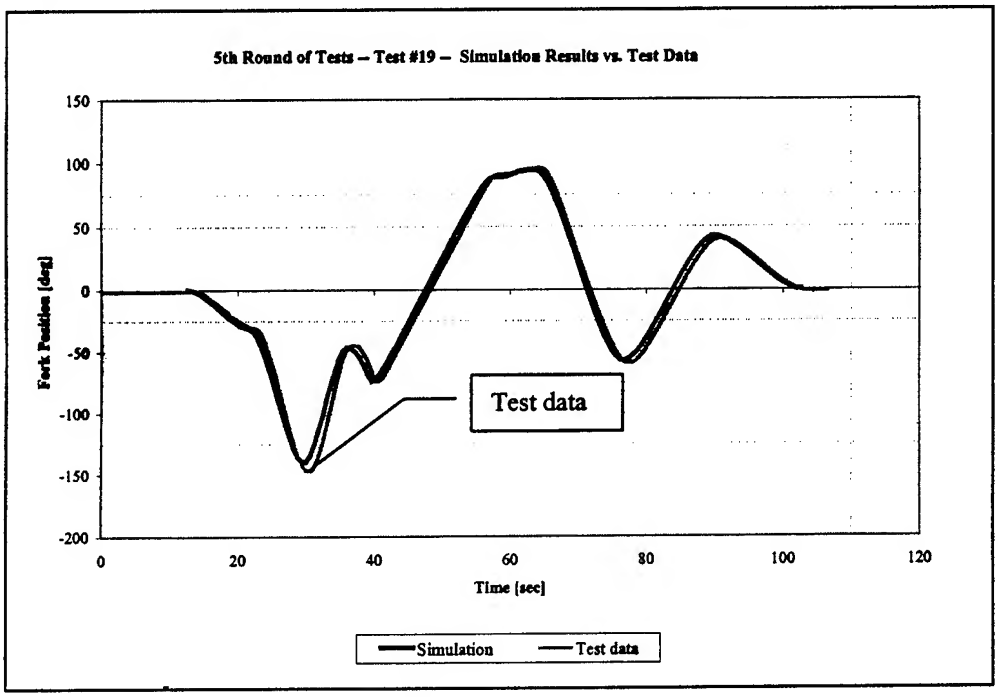

Figure 5-7 Correlation between Recorded and Simulated x-acceleration

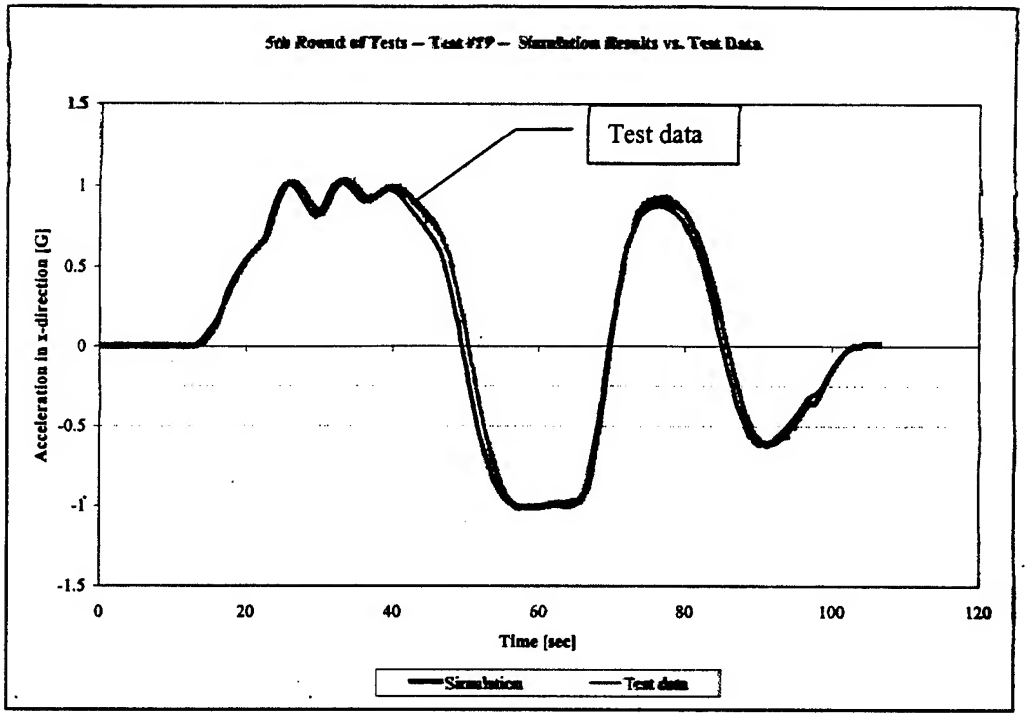

Figure 5-8 Correlation between Recorded and Simulated y-acceleration

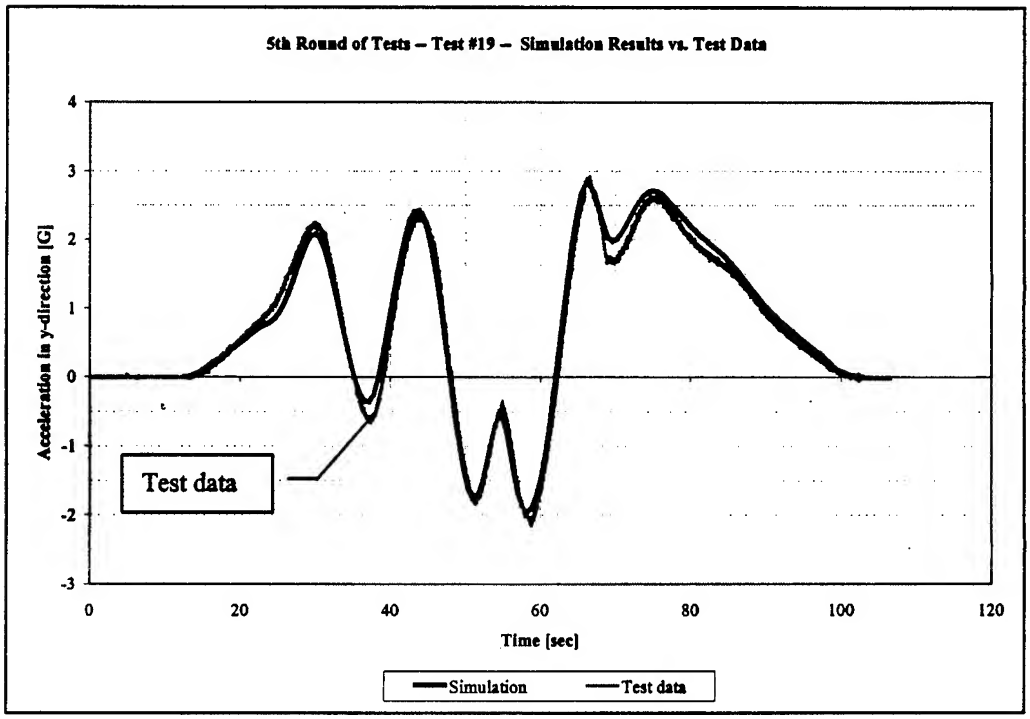

Figure 5-9 Correlation between Recorded and Simulated z-acceleration

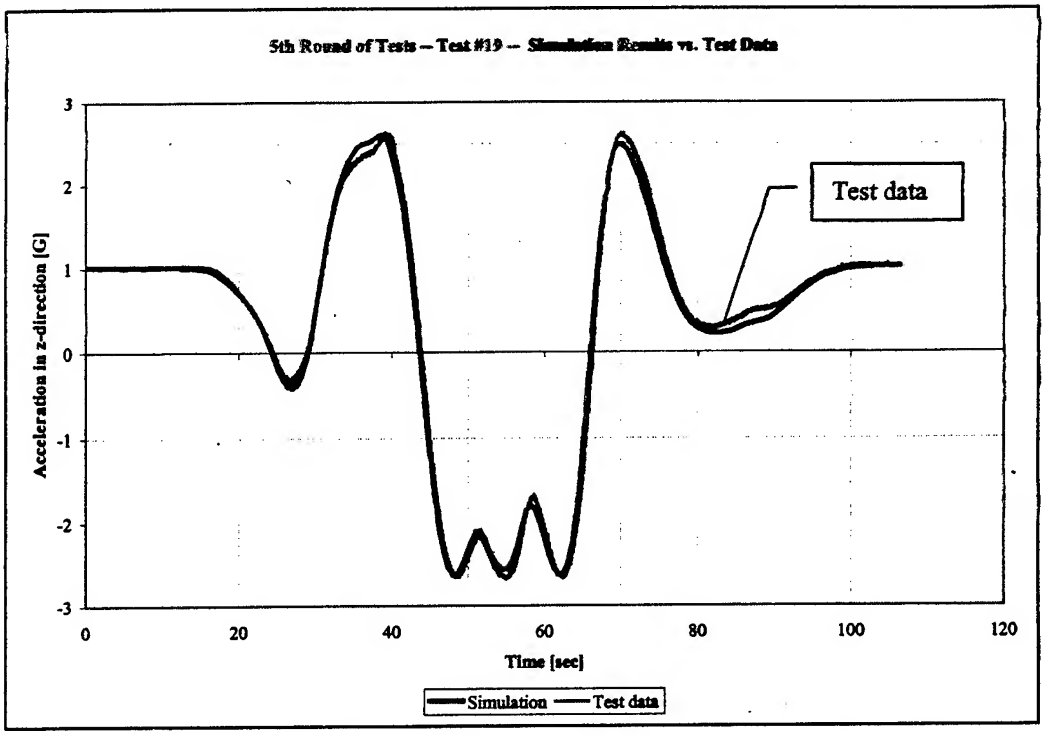

6.0 Rollover Simulation Using the DES.

As a commercial application for the Dynamic Environment Simulator (DES), it is proposed to use the DES to simulate vehicle rollover occupant kinematics. Rollover data to achieve the simulations discussed herein were taken from the literature[12]. This section discusses the characteristics and source of rollover data, the equations used to develop the rollover simulations, and the results of the simulations.

6.1. Introduction to Rollovers.

Figure 6-1 Section Format

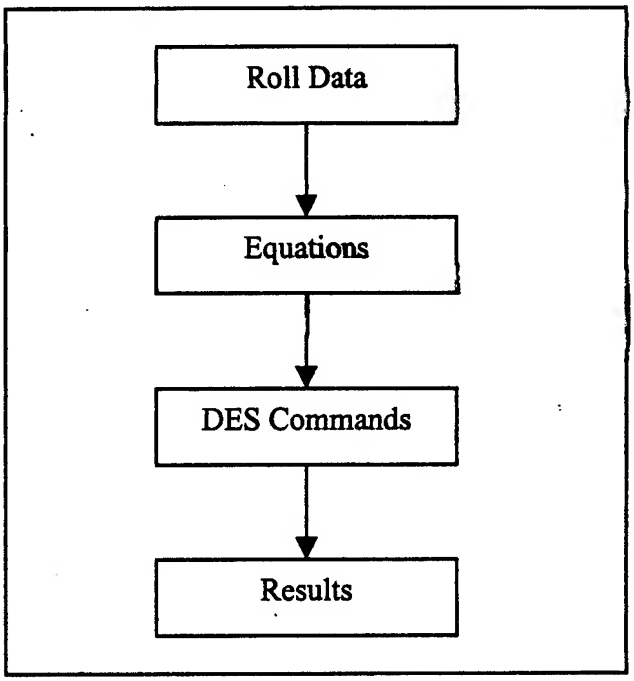

There are not many tools available to help vehicle designers and safety experts understand vehicle rollover dynamics. The DES could become a promising tool to (1) study the movements of occupants with respect to the vehicle's interior and restraint systems, and (2) to examine the effects of various engineering changes to a vehicle's interior environment for improving safety.

To achieve the necessary inertial accelerations on the occupant, data from experimental rollover events was used to develop several "desired" acceleration profiles. The angular velocities of the test vehicles over time were used to compute typical accelerations on both the driver and passenger for each roll event. Using DES Simulation software, sets of theoretical DES gimbal movements to approxiamate desired accelerations were developed. None of the DES dynamic limitations were applied for this feasibility study, and the seat was locked at 0° orientation (see Figure 4-1) for most simulations.

Through the development of the simulation data, it became apparent that simulating an entire roll sequence would be impractical for the DES and of low scientific merit. It was recognized that rollover simulations should be modeled in a piecewise fashion. Of particular interest in this

study were the first 180° of a rollover. During a rollover, the vehicle begins to tip after sliding laterally – the wheels lift off the ground on one side. This is called the roll onset. At this time, the orientation of the vehicle is slightly over 0° (horizontal with respect to the ground). After the roll onset, the entire vehicle becomes airborne. Typically, the vehicle remains airborne as it rotates until it is at approximately 180°. At this point, it is possible for a protruding segment of the vehicle to strike the ground. This strike point was used as the reference point at which to divide the roll event (i.e., +/- 180°).

6.2 Rollover Data.

In order to create a set of theoretical DES gimbal movements, various data had to be calculated based on the published angular velocity information. Two different roll events were examined. Roll one was a soil-tripped roll. Roll two was a curb-tripped roll. Data for the vehicle motion, occupant behavior, and finally the DES gimbal movements were determined for each set of data.

The rotational position of the vehicle and the angular acceleration were determined from the given angular velocity. Differentiation of the angular velocity over time yielded the angular acceleration. Integration of the angular velocity over time yielded the roll angle. The roll angle versus time and the angular velocity versus time for each of the two roll events is shown in Figures 6-2 through 6-5. For roll one, the data was truncated after one roll was completed. As shown in the angular velocity plot, the vehicle continuied to roll after 1.8 seconds. By contrast, the data for roll two ended prior to the completion of one full roll.

Figure 6-2 Orientation of Vehicle During Roll One

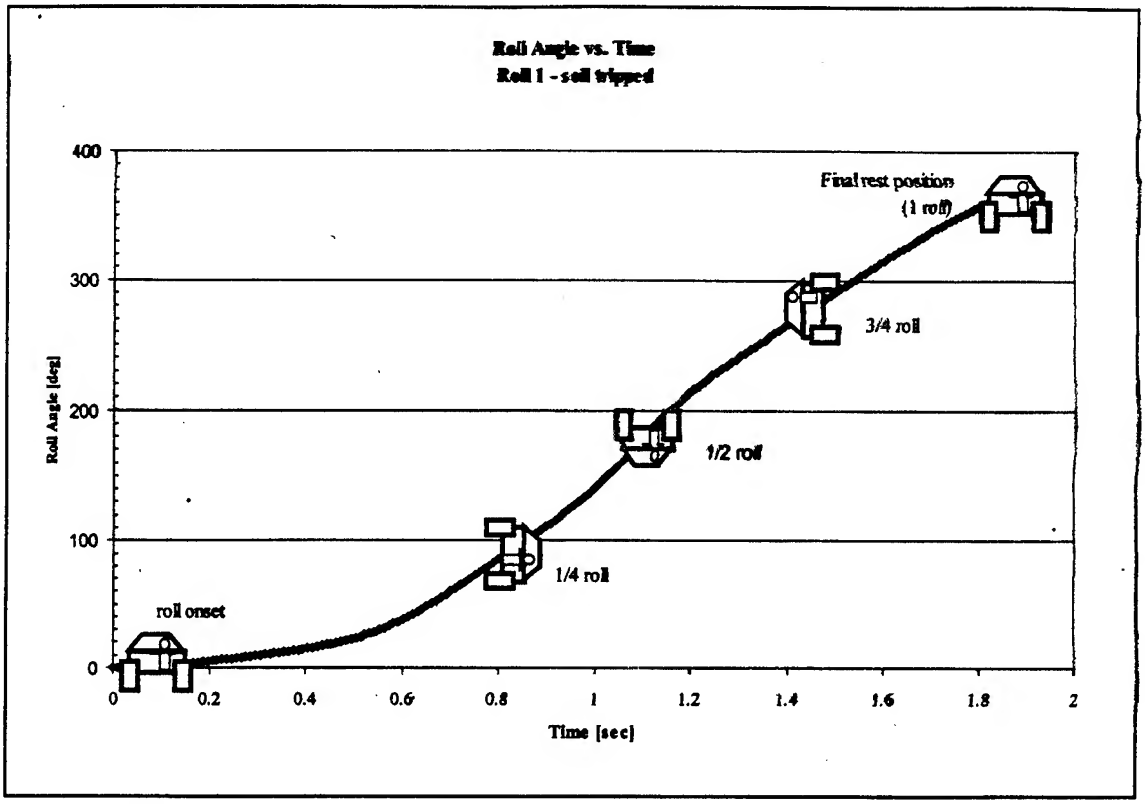

Figure 6-3 Angular Velocity of Vehicle During Roll One

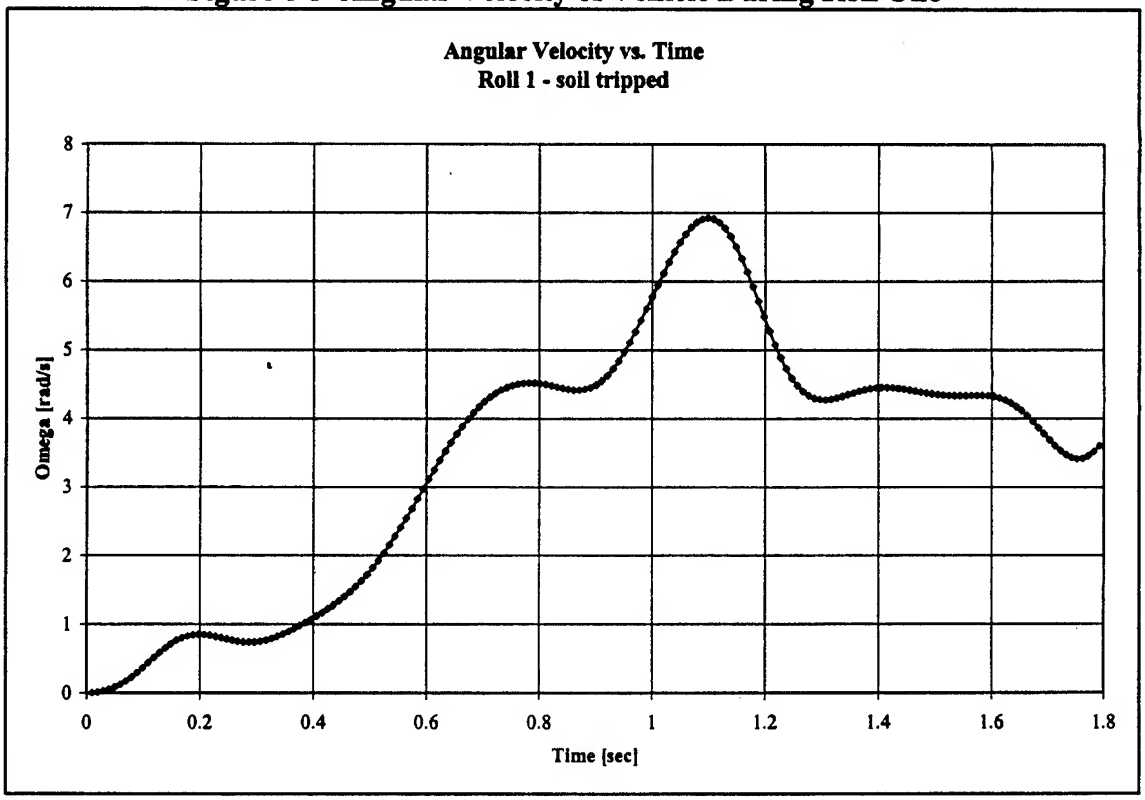

Figure 6-4 Orientation of Vehicle During Roll Two

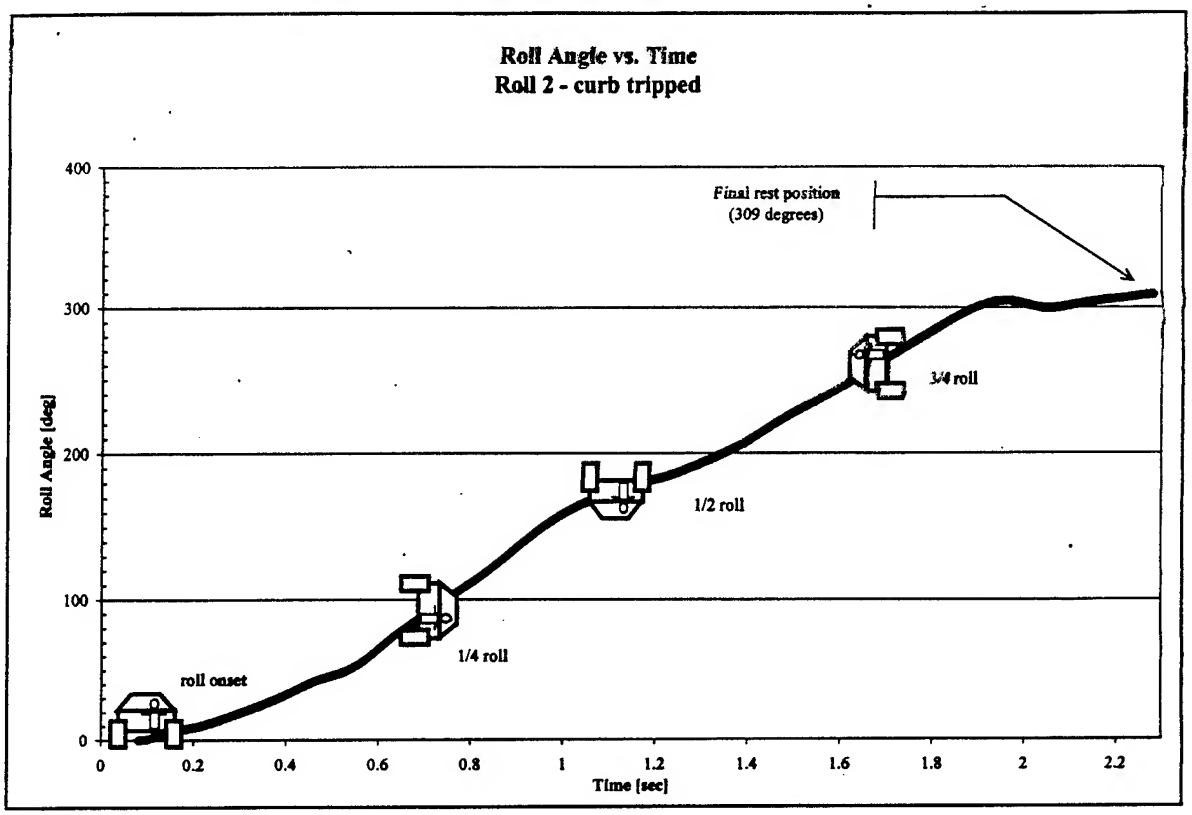

Figure 6-5 Angular Velocity of Vehicle During Roll Two

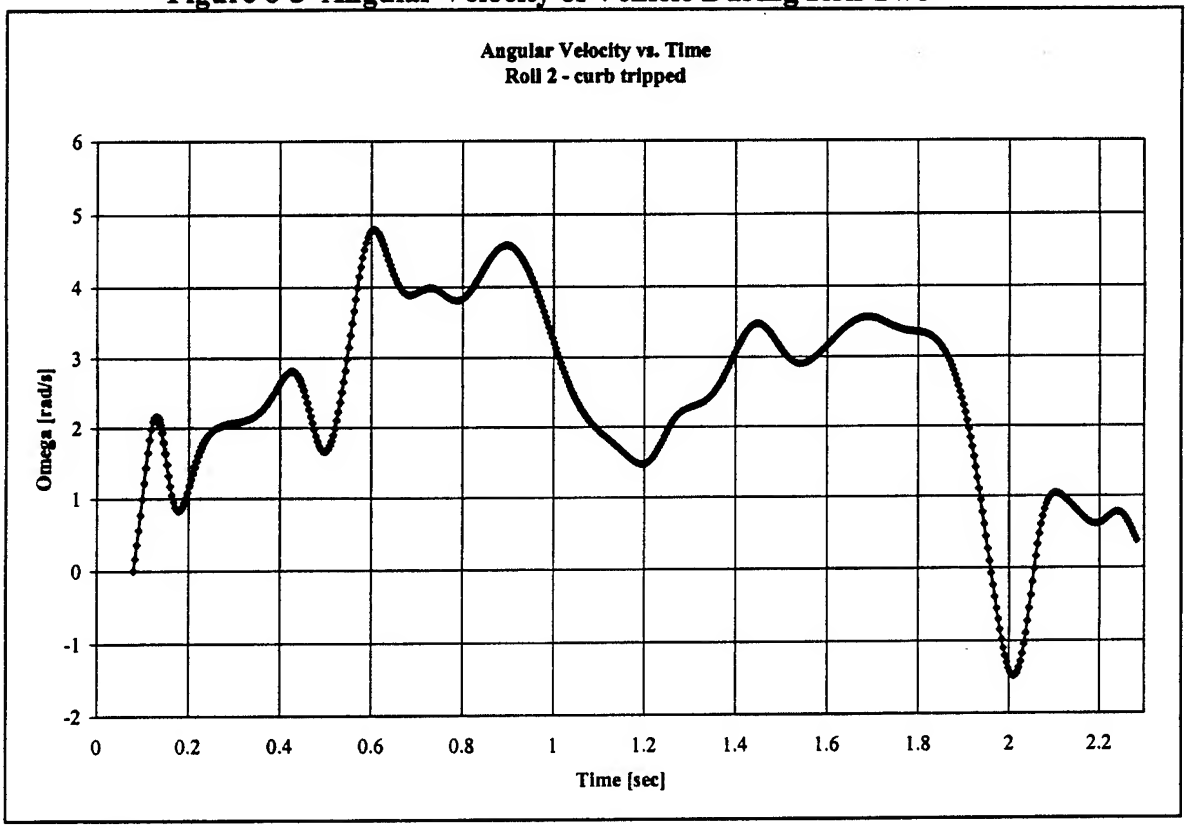

6.3 Fundamental Equations.

To simulate the rollover event, various kinematic quantities had to be calculated for the occupants. Given an angular velocity as a function of time, the inertial accelerations on each occupant could be determined. Accelerations on the occupants in the driver and passenger seating positions were studied.

Given an assumed horizontal distance from the vehicle CG to the occupant (2.5 ft. in this study), and given the angular velocity and angular acceleration, it was possible to calculate the inertial accelerations on the *driver in global coordinates* as follows:

$$\ddot{Y}_{driver} = -r\omega^2\cos\theta - r\alpha\sin\theta - f_{drag} \qquad \text{Eqs. 6-1}$$

$$\ddot{Z}_{driver} = r\omega^2\sin\theta - r\alpha\cos\theta + g$$

where:

f_{drag} [=] force opposing the sideways vehicle motion
r [=] distance from vehicle CG to occupant
ω [=] angular velocity of vehicle
α [=] angular acceleration of vehicle
θ [=] angular position of vehicle

Since the roll event was assumed to be a "pure" roll close to the x-axis of the vehicle, the desired forward (x-axis) component of acceleration was zero.

Once the accelerations were determined in global coordinates, they were transformed to local vehicle coordinates. These results were converted to units of G to be useable by the DES software.

Since the orientation of the passenger is different from the driver with respect to the vehicle CG, the kinematics of the passenger were also analyzed. The inertial accelerations on *the passenger in global coordinates* were calculated as follows:

$$\ddot{Y}_{passenger} = r\omega^2\cos\theta + r\alpha\sin\theta - f_{drag} \qquad \text{Eqs. 6-2}$$

$$\ddot{Z}_{passenger} = -r\omega^2\sin\theta + r\alpha\cos\theta + g$$

where, the variables have the same definitions as given above.

Again, the accelerations were transformed to local vehicle coordinates and then converted to units of G.

It should be noted that the term f_{drag} (the drag factor) was used to account for the lateral vehicle deceleration and the deceleration is due to the exchange of energy from kinetic to rotational energy.

6.4 Using the DES Simulations Software.

To some extent, the reader may want to familiarize him- or herself wth the DES Simulation software to better relate to and understand some of the issues discussed in the remainder of this section.

6.4.1 Occupant Data.

During a simulation of a rollover event, it is important to address the behavior of the occupant with respect to the vehicle interior. The DES simulation of the vehicle rollover imparts the inertial accelerations experienced by an occupant during the event. Understanding the coordinate systems used by the DES is of critical importance to the study of the movement of the occupant. The coordinate system of interest herein is shown in Figure 4-1 under the label "Pilot" reference frame.

As described previously, the inertial accelerations on the occupant were calculated. These were the accelerations experienced by the passenger or driver during the rollover event. Figure 6-6 is a schematic showing the forces due to acceleration acting on the passenger at a roll orientation of approximately 30° with respect to horizontal. Figure 6-6 is a rear view of a passenger-side leading roll event.

6.4.2 DES Data.

The accelerations generated by the DES are achieved by the motion of the centrifuge. The motions of the individual gimbals are determined using the inverse kinematics solving feature of the DES simulation software. The desired acceleration profiles are shown in Figures 6-7 through 6-10.

In order to determine the required motions of the centrifuge, the desired acceleration performance was entered into the simulation software via the Graphical Profile Editor. The desired accelerations traces as derived from the published data can be noisy and irregular with respect to the centrifuge performance, so the desired acceleration traces were 'stylized' to smooth these irregularities. Also, short-duration, high-G acceleration pulses were moderated to facilitate solutions.

Figure 6-6 Forces Acting on Passenger at 30 Degree Roll Angle

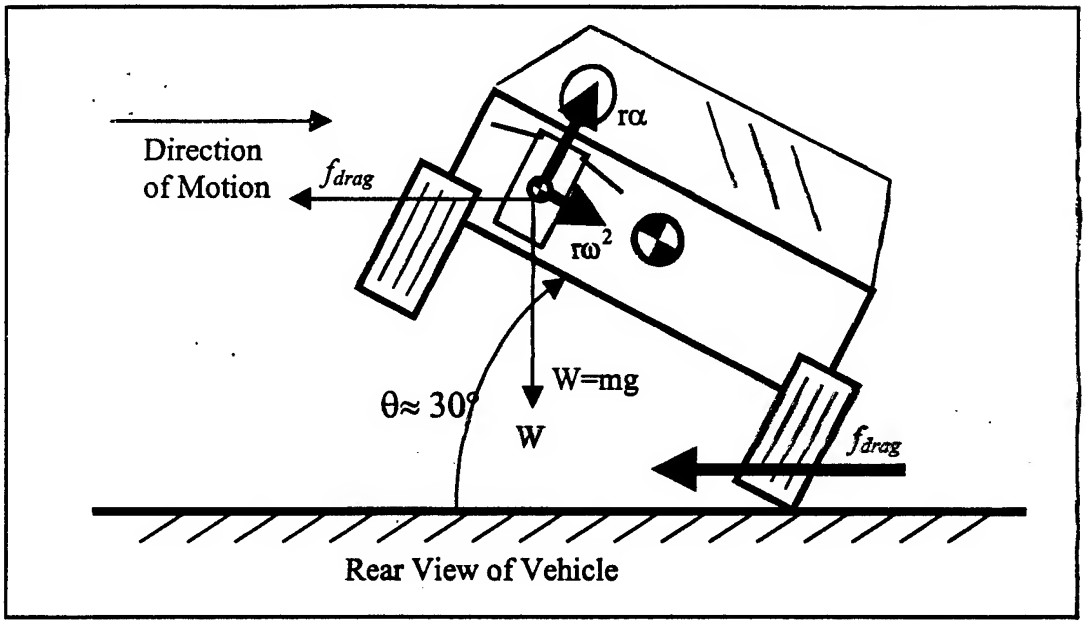

6.5 Results of Simulations.

Once the desired acceleration curves were entered, the DES simulation software solves the required centrifuge movements. Initially, two complete rollover events were analyzed to provide a range of possible simulation conditions. Results were determined without kinematic and dynamic limits applied to examine the feasibility of simulating a rollover. After attempting to model a complete roll, a smaller segment of the rollover was modeled in order to reduce complexities and provide more meaningful results. The results of the latter simulations are discussed in the following sections.

6.5.1 Factors Affecting Results.

When creating DES gimbal movements from a desired acceleration profile, several factors affect the input traces generated. The way a curve is 'stylized' or traced in the Graphical Profile Editor, affects the results. By smoothing the desired response, or by lowering the desired magnitude peaks, the DES response can be optimized.

Also, the method of solution selected (whether the pointing method or the weighted method) affects the results. Further, if the weighted method is selected, then each of the weights for the three acceleration components can be varied. This allows the user to specify which acceleration components are more important to match.

The simulation software allows the seat to be either fixed at any angle or unlocked to move as a motorized DOF.

Finally, the time span of simulation profile can be manually increased in the Graphical Profile Editor, or the solution software can automatically extend the time scale so that the DES Simulation software eventually creates more realistics performance demands for the arm and gimbal movements.

6.5.2 Results of a Piecewise Rollover Modeling Effort.

Two different roll events were analyzed. The results of simulating each roll are presented here. As mentioned earlier, roll one was a soil tripped roll event and roll two was a curb tripped event. When solving the inverse kinematic solution, the following parameters were controlled:

1) The seat was locked at 0°.
2) The weighted method of solving the inverse kinematic solution was used. Equal weights were used for each component.
3) The roll event time was stretched by 50%. An additional 1 second was added to the start of the profile to stimulate a steady-state operating condition before the simulation.
4) For roll one, the y-acceleration directions given in Figures 6-7 and 6-8 were reversed (again, to facilitate more achievable solution traces).
5) To facilitate the solution process, the desired x-acceleration was characterized by a curve rising from 0 to 1 G (as opposed to having a 0 G acceleration trace).

Data from each roll event was truncated after 180°, which was at $t = 1.1$ seconds for roll one, and $t = 1.2$ seconds for roll two. A lead-in period of 1 second was necessary to run the simulation software, which explains the time shift of 1 second in the plots that follow ($t = 1.1$ sec becomes 2.1 sec, and $t = 1.2$ sec becomes 2.2 sec).

The piecewise modeling was completed on both roll one and roll two. Again, the results were determined without amy limits applied onto the DOFs during or after the solution, and the desired accelerations were all stylized, or smoothened prior to running the DES Simulation software.

The results for roll one are shown in the following Figures 6-11 through 6-16.

Figures 6-11 through 6-13 — half roll desired vs. actual accelerations (driver)
x, y, z components
Figures 6-14 through 6-16 — half roll desired vs. actual accelerations (passenger)
x, y, z components

The results for roll two are shown in the following Figures 6-17 through 6-22.

Figures 6-17 through 6-19 — half roll desired vs. actual accelerations (driver)
x, y, z components
Figures 6-20 through 6-22 — half roll desired vs. actual accelerations (passenger)
x, y, z components

The figures for roll one demonstrate close agreement between the desired and achieved accelerations. The figures for roll two show some discrepancy between the desired and achieved accelerations. As stated earlier, roll two was a curb tripped roll. This type of roll would be expected to generate higher initial rates of angular accelerations. One of the limiting factors in creating a simulation with the DES is the difficulty of achieving large changes in occupant inertial accelerations over a short period of time.

6.5.3 Additional Modeling Effort Using the DES Simulation Software to Reduce Required Gimbal Rates.

This section describes the process of recomputing the forward kinematics after stylizing an initial set of solutions obtained for the gimbal movements. Both operations can be achieved with the DES Simulation software. The purpose of this approach is to reduce the demands on the gimbal movements without excessively sacrificing acceleration fidelities.

As shown by the "raw" curves in Figure 6-25, fork and cab movements were occasionally required to shift from one angular position to another rather quickly (note the time scale in Figure 6-25). The "raw" curves are solutions for the desired accelerations shown in Figure 6-23. Now, contrast Figure 6-23 with Figure 6-24, whose traces were obtained from the stylized cab

and fork movements shown in Figure 6-25. Accelerations in the y- and z-directions are still comparable in both graphs, which is the objective (matching x-accelerations was not considered most relevant in this feasibility study). At the same time, the most abrupt cab and fork movements were eliminated.

However, the required rates shown in Figures 6-27 and 6-28 are still quite high. Although the DES Simulation software could be used to render the profiles more achievable, BRC believes that the DES centrifuge capabilities will need to match, or exceed, the capability requirements listed in the Conclusions of this section in order to become a useful tool for rollover analyses and simulations.

Figure 6-26 illustrates the demands that would be placed on the arm performance requirements, after stylizing of the arm angular velocity curve.

The performance requirements given in the Conclusions of this section reflect expectations that a comprehensive rollover study, with many simulation iterations (a task outside of the scope of this project) would at best lead to those requirements stated in the Conclusions. Also, refer to the conclusions for a comparison with current capabilities.

Figure 6-7 Inertial Acceleration as Computed from Equations 6-1 for Roll One

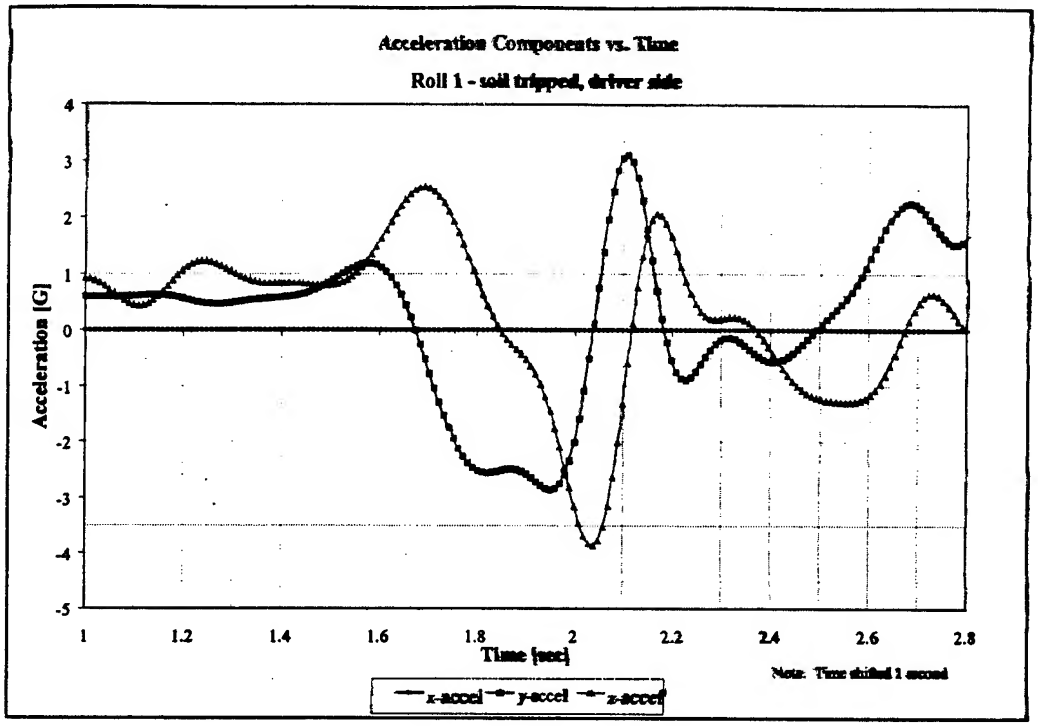

Figure 6-8 Inertial Acceleration as Computed from Equations 6-2 for Roll One

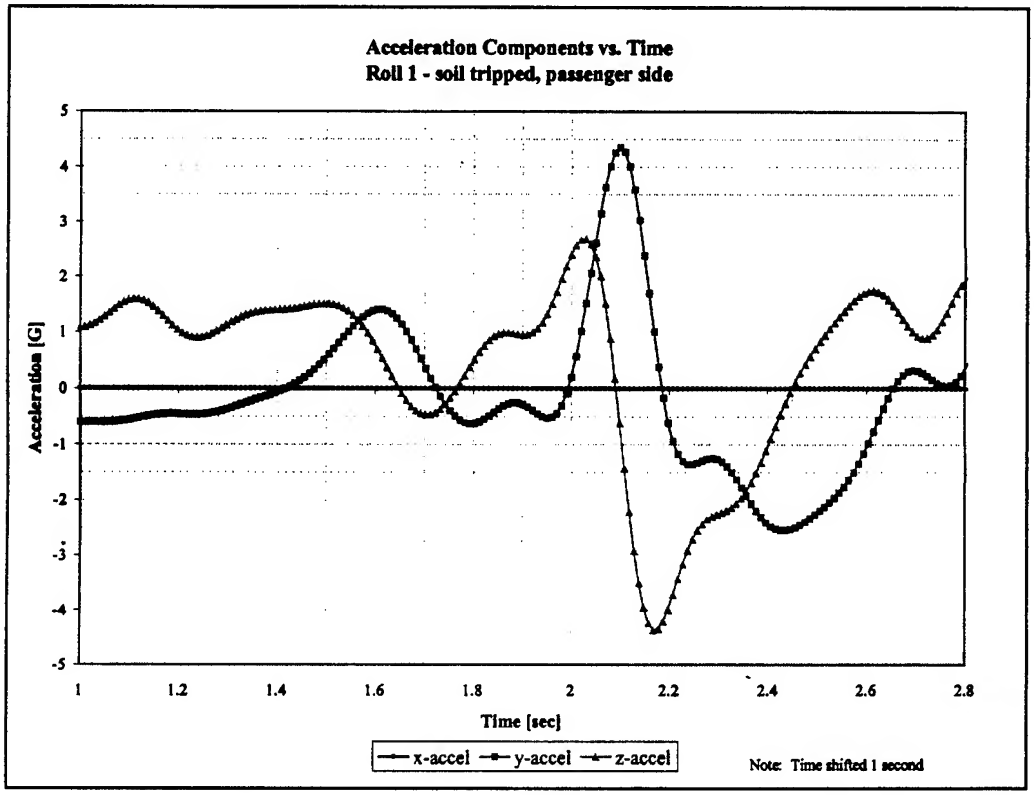

Figure 6-9 Inertial Accelerations as Computed from Equation 6-1 for Roll Two

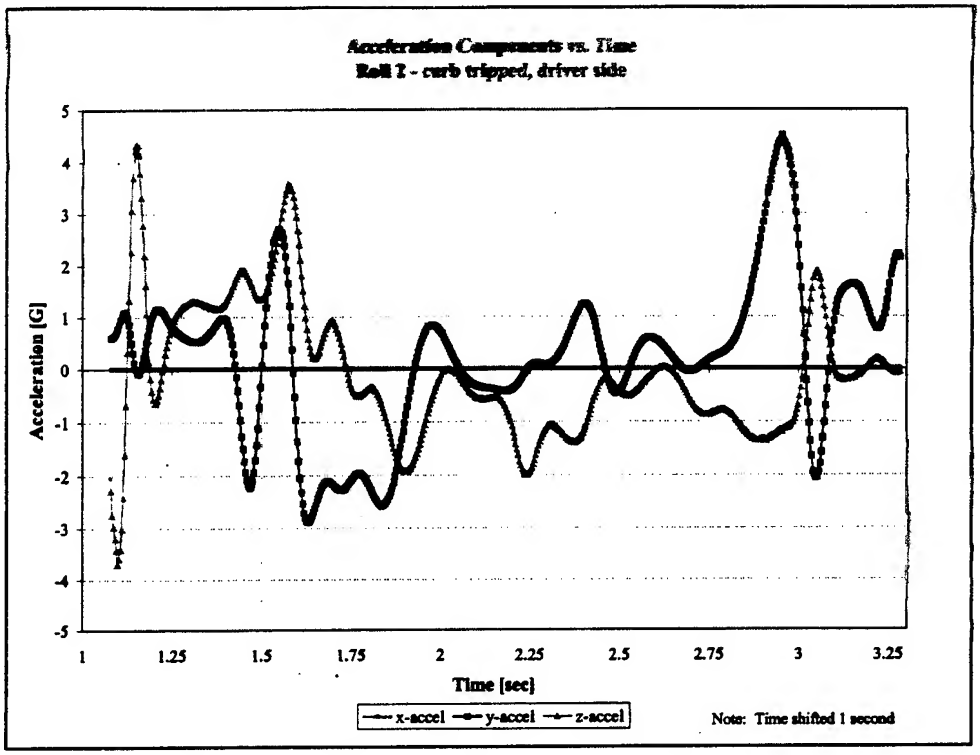

Figure 6-10 Inertial Accelerations as Computed from Equations 6-2 for Roll Two

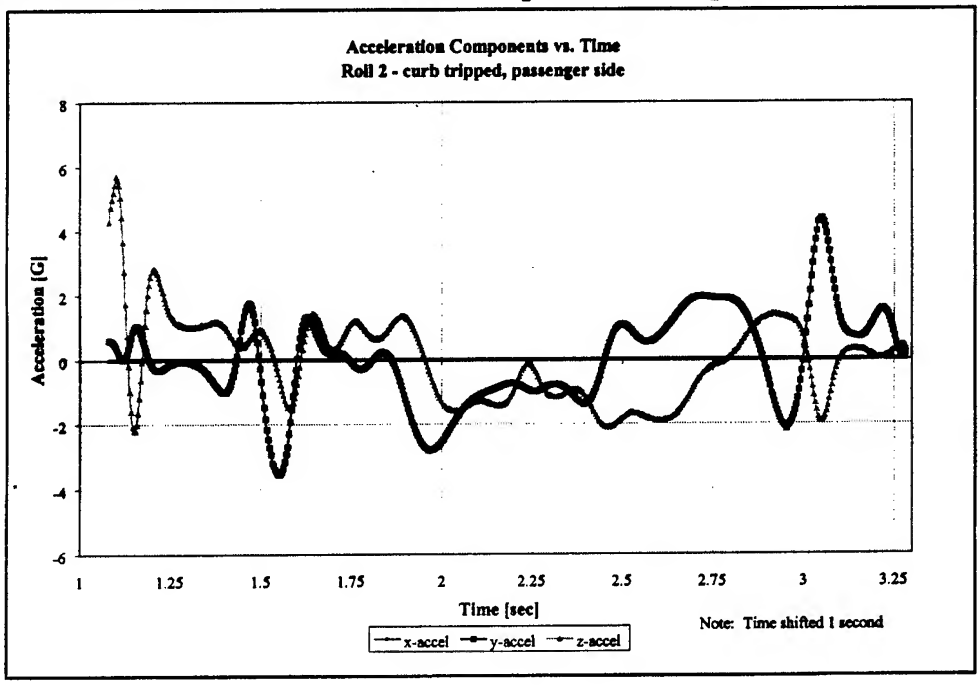

Figure 6-11 Half Roll Accelerations on Driver (x-component) for Roll One

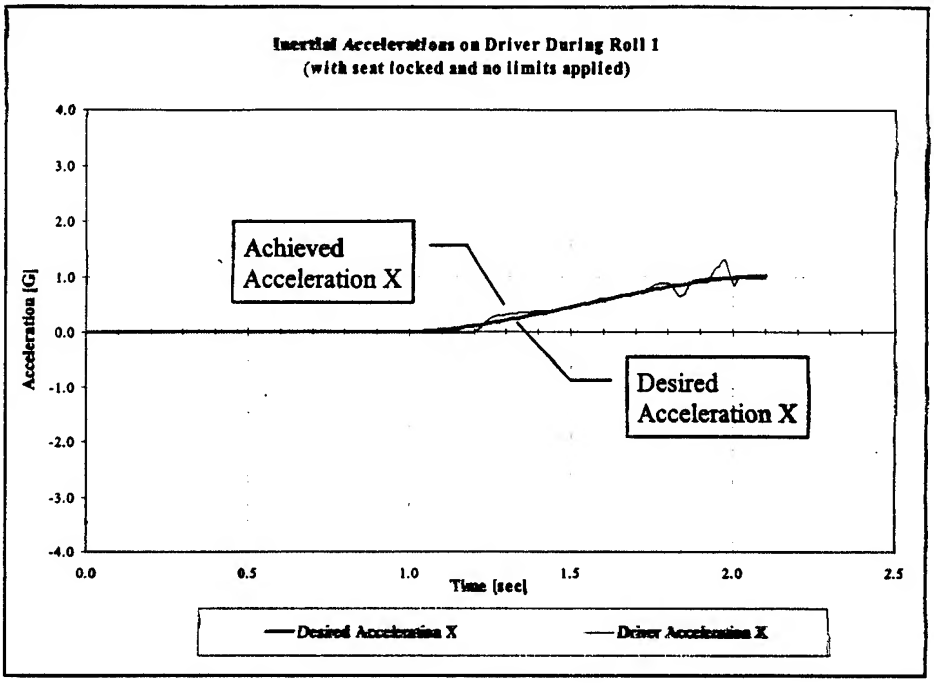

Figure 6-12 Half Roll Accelerations on Driver (y-component) for Roll One

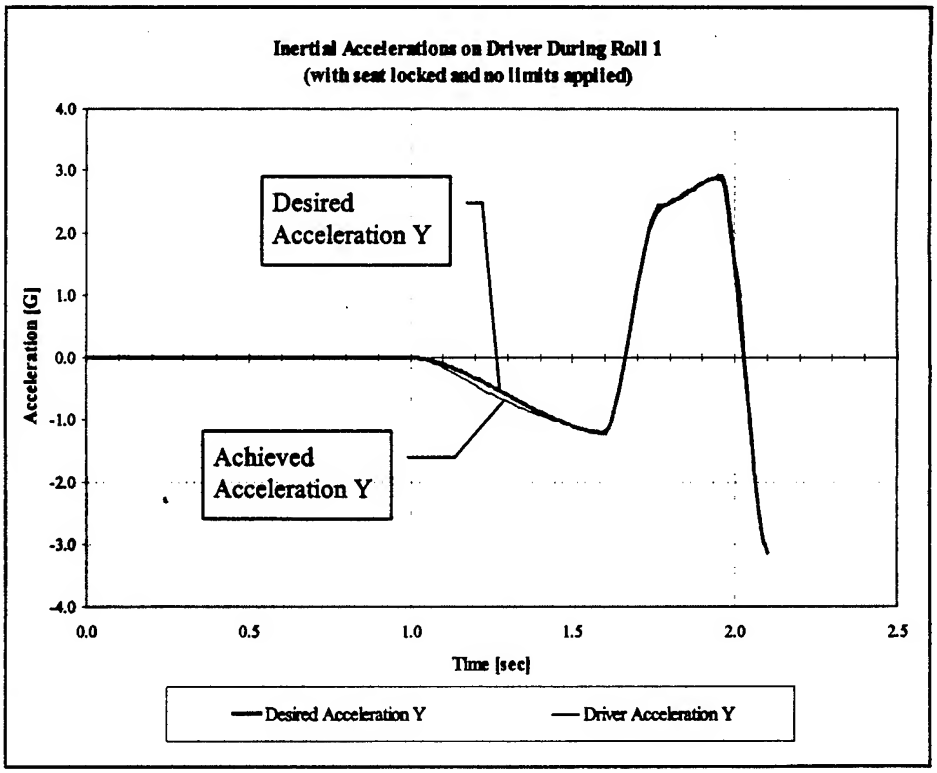

Figure 6-13 Half Roll Accelerations on Driver (z-component) for Roll One

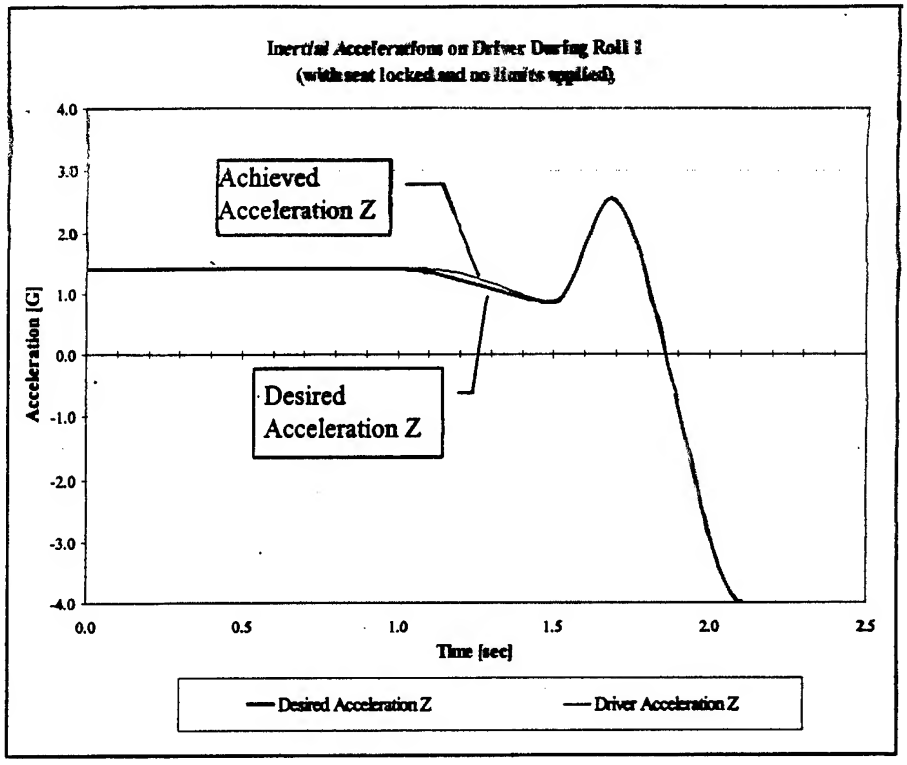

Figure 6-14 Half Roll Accelerations on Passenger (x-component) for Roll One

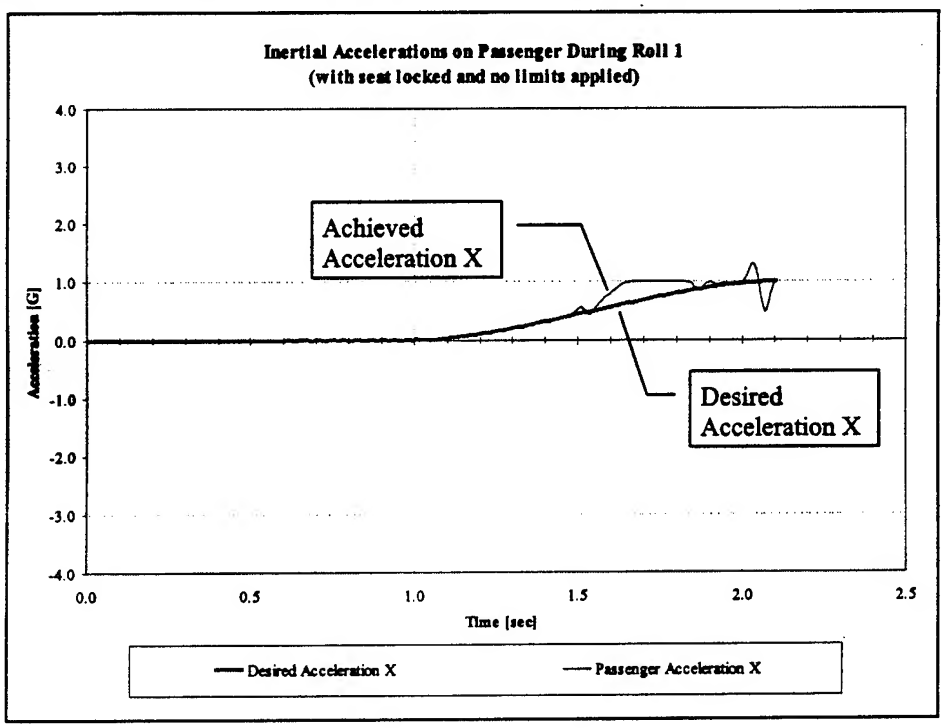

Figure 6-15 Desired vs. Achieved Accelerations on Passenger (y-component) for Roll One

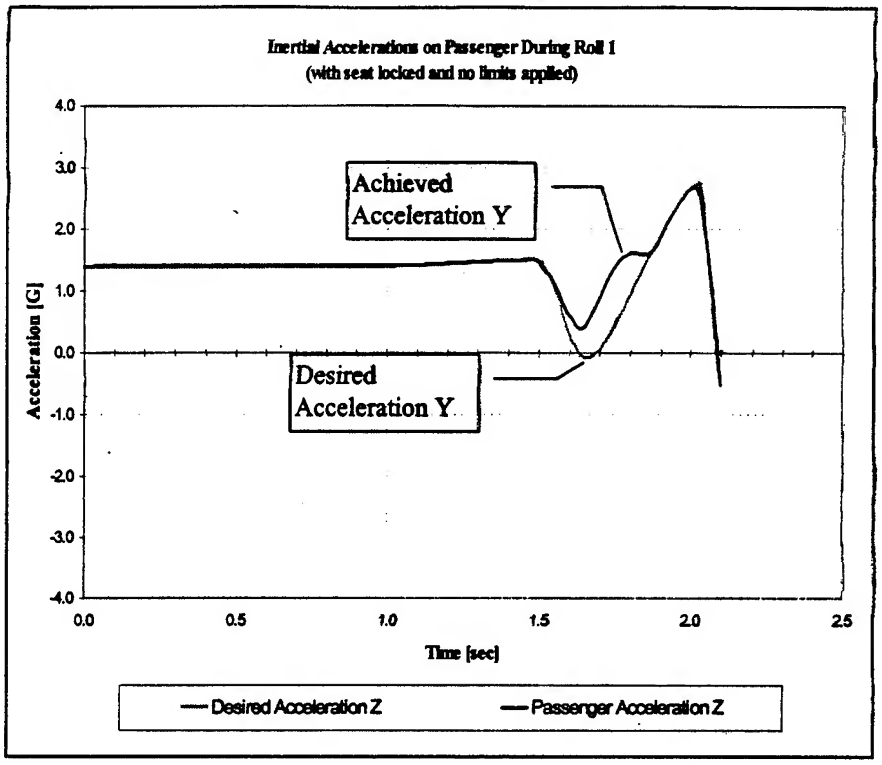

Figure 6-16 Half Roll Accelerations on Passenger (z-component) for Roll One

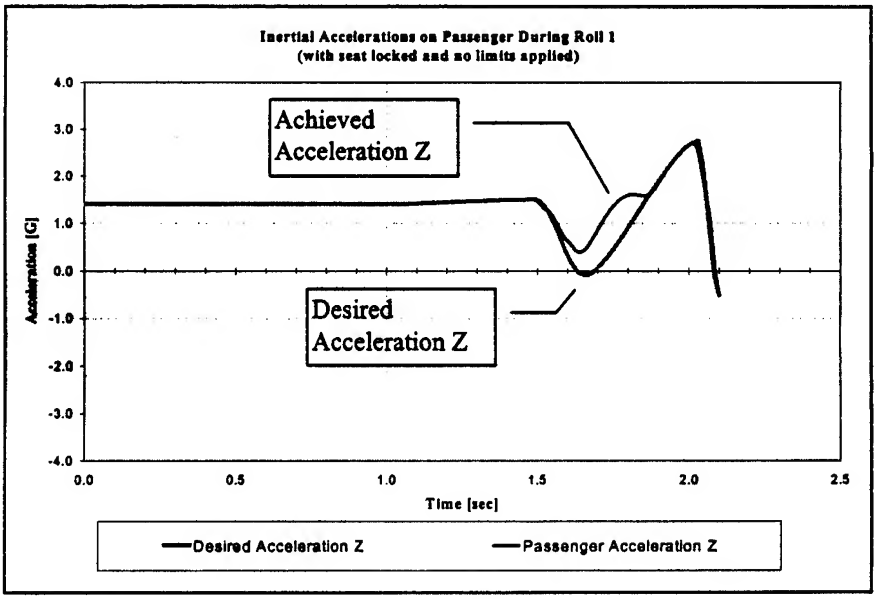

Figure 6-17 Half Roll Accelerations on Driver (x-component) for Roll Two

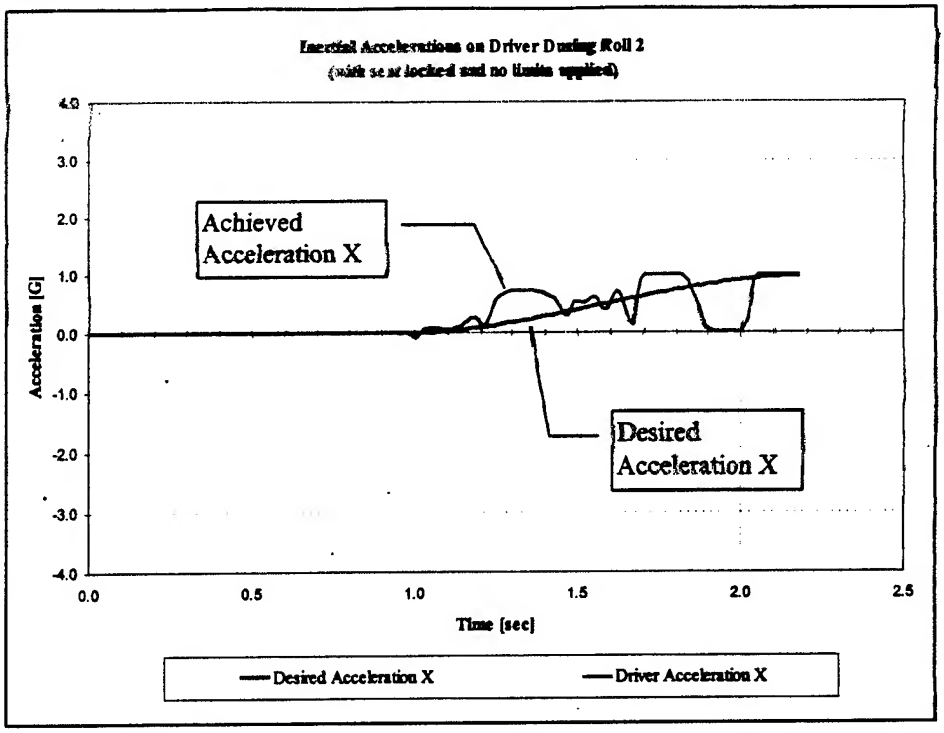

Figure 6-18 Half Roll Accelerations on Driver (y-component) for Roll Two

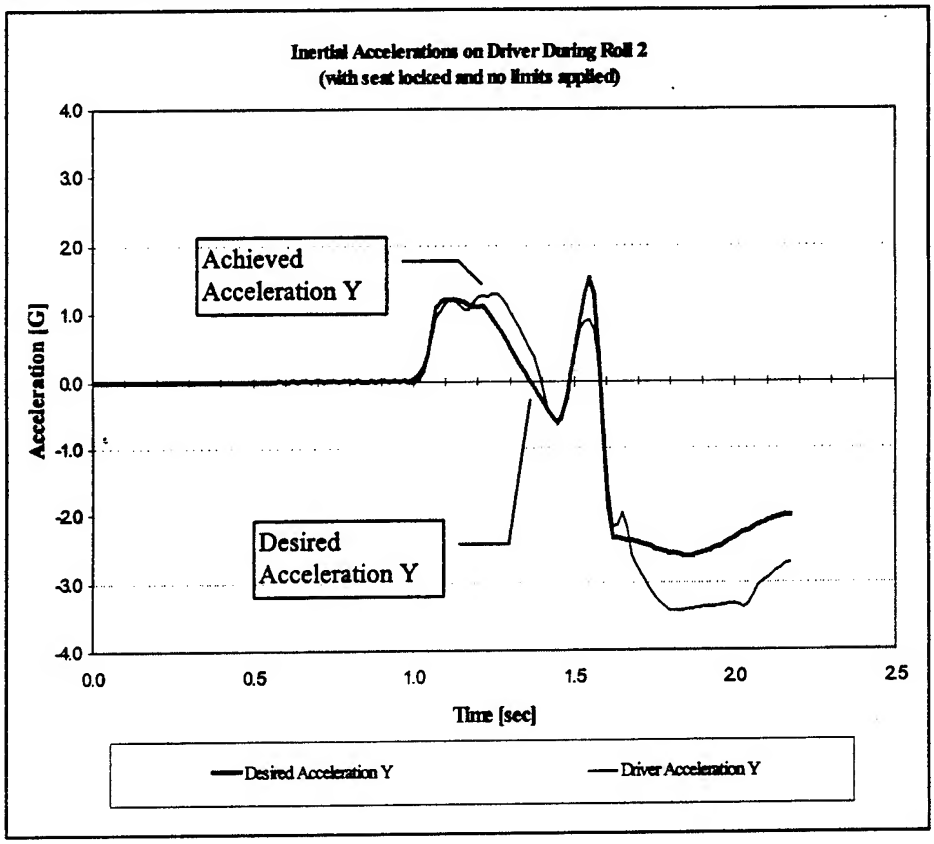

Figure 6-19 Half Roll Accelerations on Driver (z-component) for Roll Two

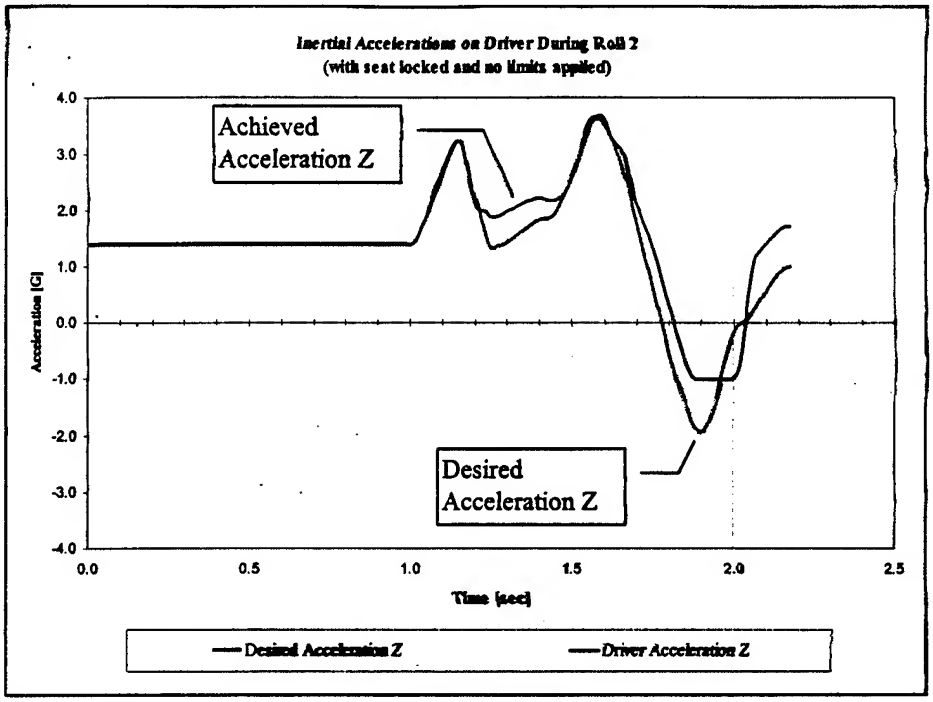

Figure 6-20 Half Roll Accelerations on Passenger (x-component) for Roll Two

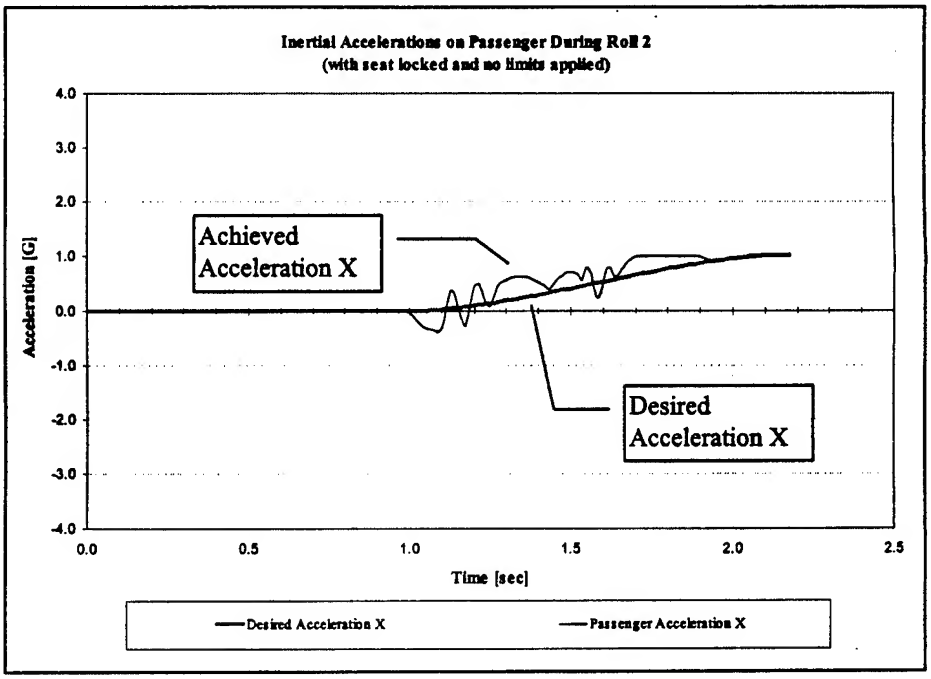

Figure 6-21 Half Roll Accelerations on Passenger (y-component) for Roll Two

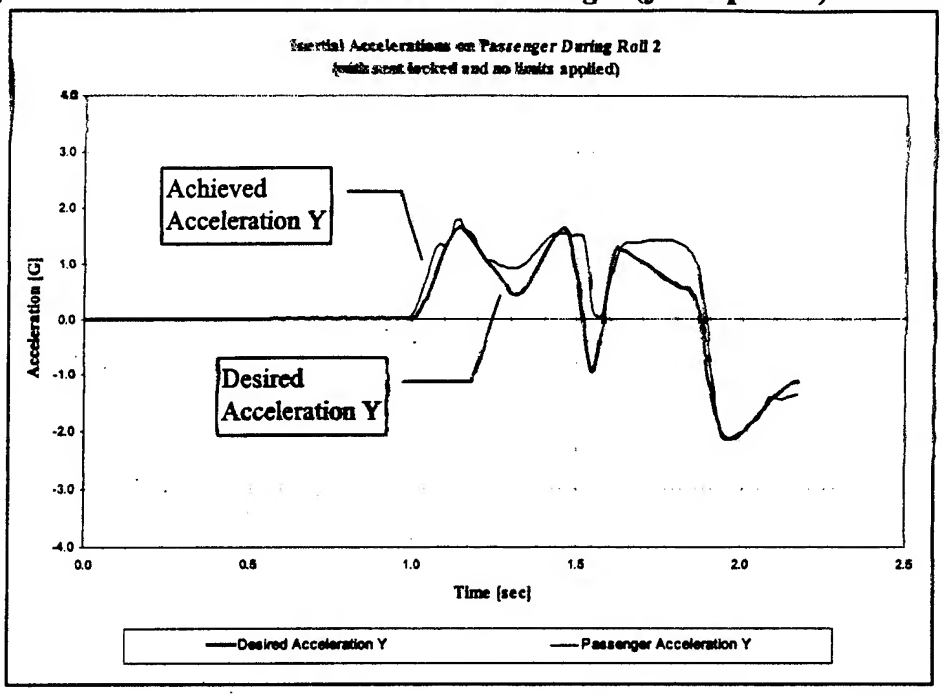

Figure 6-22 Half Roll Accelerations on Passenger (z-component) for Roll Two

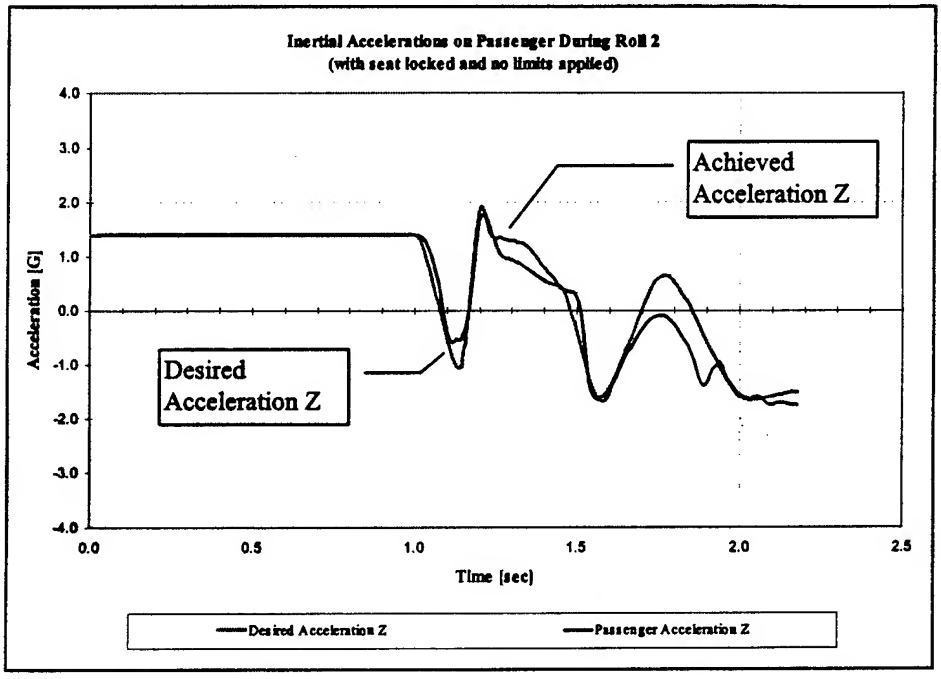

Figure 6-23 Vertical (y-direction) and Lateral (z-direction) Inertial Acceleration Loads

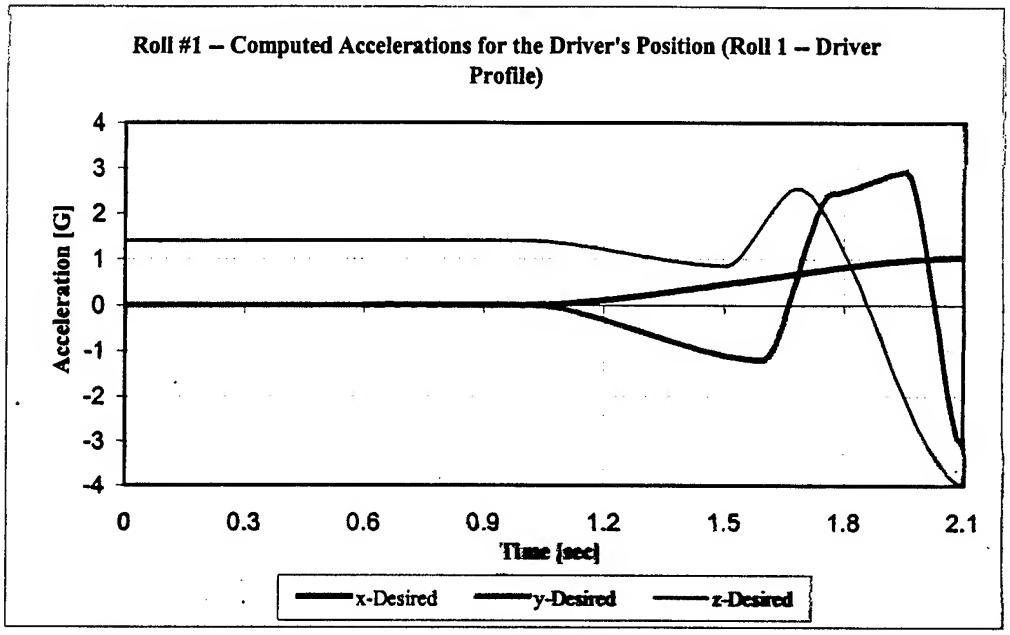

Figure 6-24 Simulated Results after Stylizing Gimbal Movement Curves

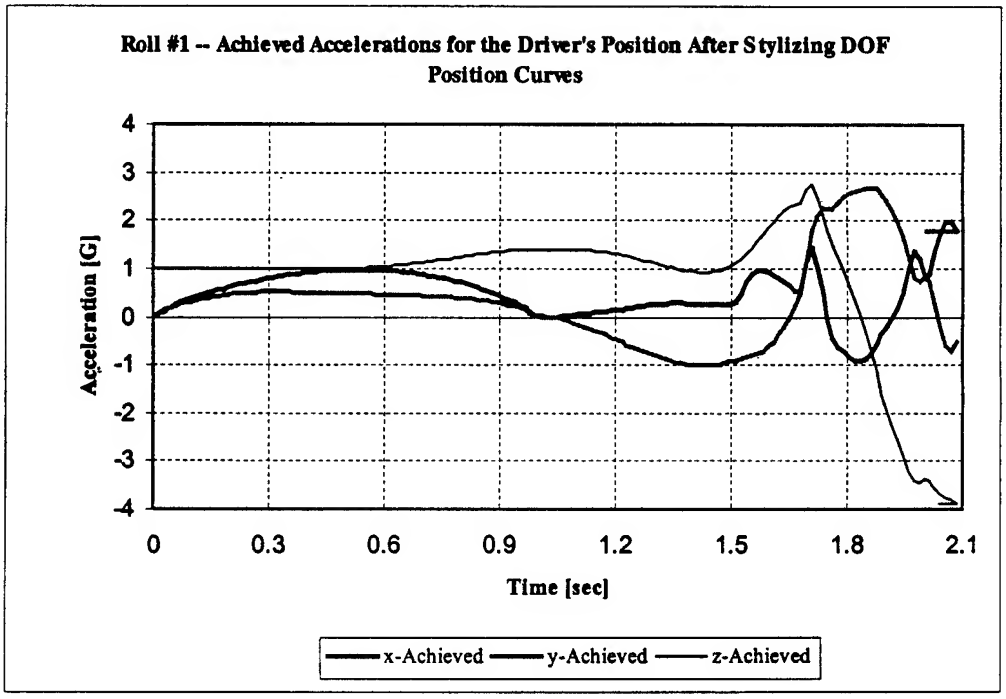

Figure 6-25 Display of the Styfizing of Gimbal Movement Curves

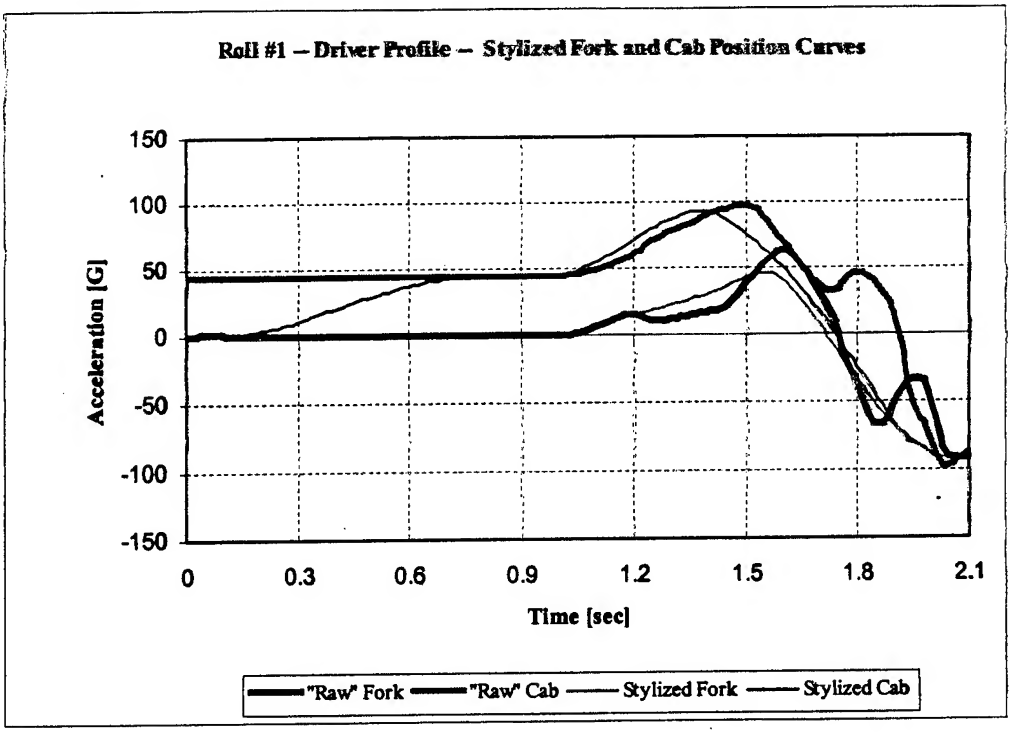

Figure 6-26 Resulting Arm Angular Velocities and Accelerations

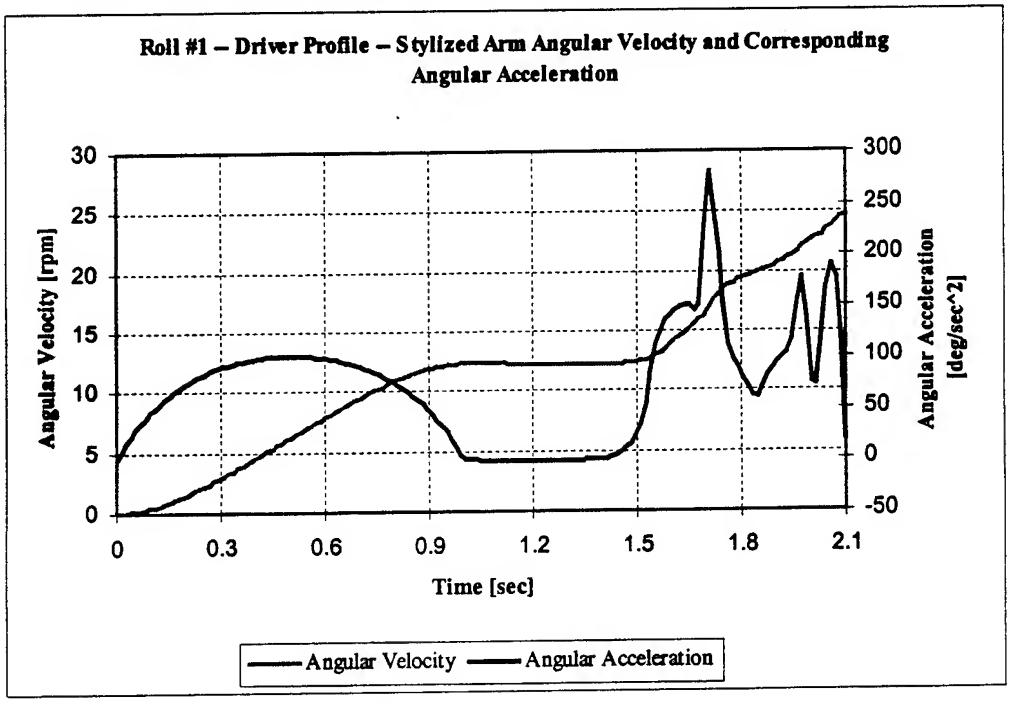

Figure 6-27 Resulting Gimbal Angular Velocities

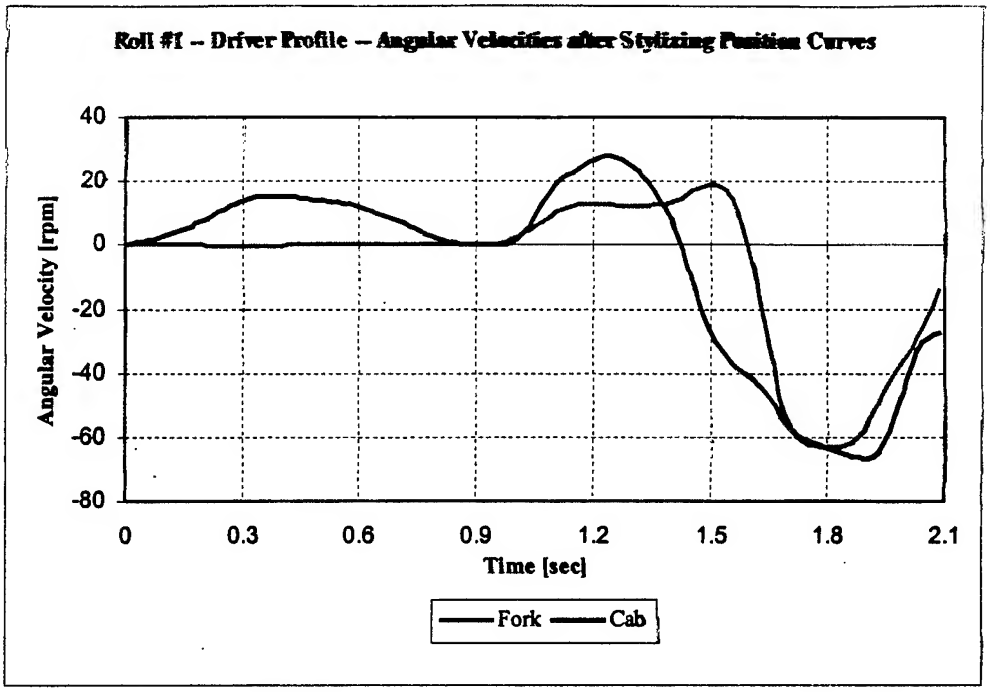

Figure 6-28 Resulting Gimbal Angular Accelerations

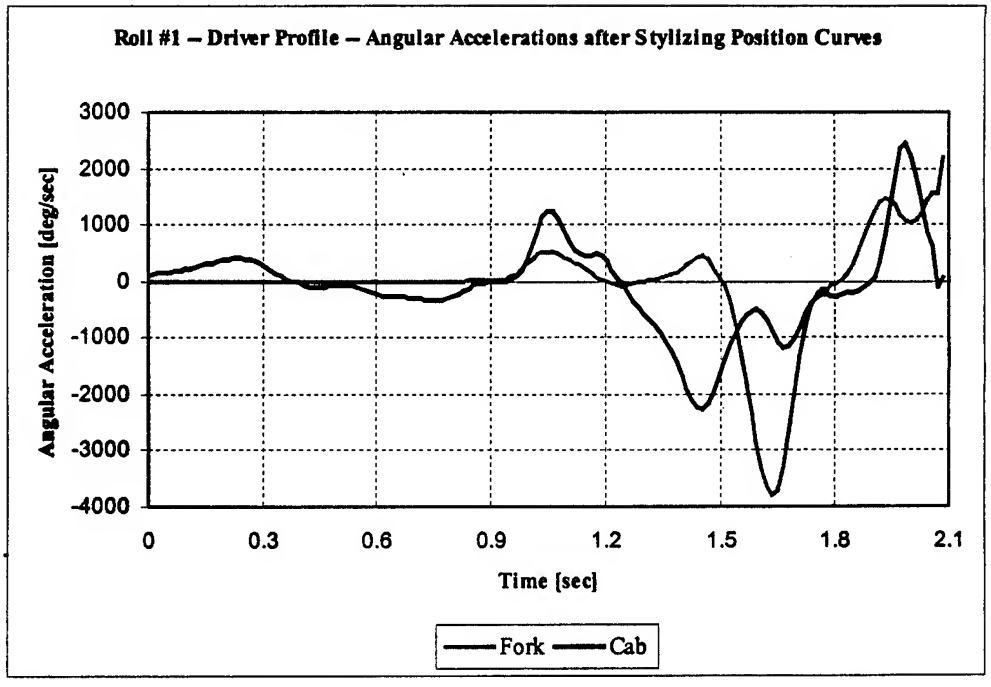

6.6 Conclusions.

As a commercial application for the Dynamic Environment Simulator (DES), it was proposed that the DES be used to simulate a vehicle rollover event. Data was taken from the literature for a soil tripped and a curb tripped experimental roll. The DES software was utilized to develop profiles that could be used to create simulations on an upgraded DES centrifuge. Two experimental rollovers were examined, yielding four sets of typical inertial acceleration profiles that would be experienced by vehicle occupants.

After analyzing the rollover accelerations profiles using the DES Simulation software, the following could be concluded:

- On a pure kinematics basis (i.e., no physical limits applied to the different DOFs), the DES configuration can closely approximate rollover onset acceleration profiles, particularily if the DES were complemented with a seat DOF.

- The study of the rollover onset portion of a full rollover was the principal focus of this section. The rollover onset portion could be considered as the more challenging portion of a rollover to model. Therefore, other portions of a rollover, such as a hypothetical "airborne" portion after the first full roll, or any other comparable situation, should then be within reach of the DES centrifuge as well (again, kinematics only).

- Table 6-1 lists the minimum capabilities that would be required in order to bring the DES within a working range of purposeful rollover analysis studies:

Table 6-1 DES Performance Requirements for Rollover Simulation Tasks

	Angular Velocity [rpm]	Angular Acceleration [deg/sec^2]
Arm	Current is Satisfactory	150
Fork, Cab, and Seat Gimbals	50	1000

As discussed in Section 8, the Level E upgrade would generate an arm angular acceleration of approximately 103 deg/sec^2. If combined with a cab weight reduction (see Section 8.8), the arm acceleration capability could then be brought in near proximity of the requirement stated above. The maximum fork rates are currently quite low (20 rpm, and 120 deg/sec^2), and the cab rate capabilities would need improvements as well. The current maximum capabilities of the cab are 30 rpm

(although, according to DES Technicians, transients of 50 rpm may be possible) and acceleration rates of up to 1140 deg/sec^2 have been measured since the cab upgrade in late 1997[3].

- Although not documented in this report, BRC also performed simulations in which the fork DOF was not enabled, and just the cab DOF was utilized to simulate a rollover. Resulting movements called for performance capabilities similar to the ones reported on in Table 6-1. Consequently, it does not appear to be critical for the fork to necessarily match the requirements stated in Table 6-1.

- The acceleration gradient, as a function of the distance away from the cab centroid, generally did not exceed 1.0 G in the present study. In fact, an in-depth study would likely optimize orientation values for the centrifuge occupant (dummy or human) with repect to gradient requirements. Actual rollovers do indeed impose acceleration gradients on occupants, depending on their location with respect to the vehicle Cg during the rollover event.

- An inherant drawback is that DES occupants (dummy or human) riding through a centrifuge rollover simulation will be exposed and affected by strong rotational artifacts that would generally not occur in actual rollovers.

So, the promising aspects for rollover modeling are that the Level E arm upgrade may satisfactorily increase the arm acceleration rate capability, and rollover acceleration profiles have been shown to be kinematically achievable (i.e., when no motor limitations were applied). Drawbacks are going to be the strong rotational artifacts, inherent to a centrifuge configuration, the demanding cab, fork and/or seat DOF capabilities, and the fact that it may be possible to model only "soil-tripped" types of rollovers (i.e., only the least violent rollover events).

6.7 References.

[1] Cooperrider, Neil K., Thomas, Terry M., and Hammoud, Selim A.. Testing and Analysis of Vehicle Rollerover Behavior. SAE Technical Paper Series 900366. International Congress and Expo

[2] Cooperrider, N.K., Thomas, T.M., Hammoud, S.A., and Woley, P.F. Real World Rollovers- A Crash Test Procedure and Vehicle Kinematics Evaluation. Twelfth International Conference on Experimental Safety Vehicles. May 29- June 1, 1989.

[3] Personal Communication with Veridian, Inc. personnel, Mr. Jeff Bird, on 23 Sept 1998.

7.0 Design Study for DES Performance Improvement.

Veridian Incorporated (formerly Systems Research Laboratories) conducted the Design Study as a subcontractor to BRC. The Design Study encompassed the study of several component subsystems of the DES installation that were candidates for improvements leading to an overall improvement in the DES performance, control, operation and maintenance, and reliability. Thus, each subsystem study considered improvements, which could contribute to reduction in overhead operation costs, as well as strictly performance improvements. Each study included a preliminary review of the current configuration of subsystem and information about its history. The studies conducted by Veridian are summarized individually below. Much of the information in this section was taken directly from Veridian's Reports[1,2,3,4,5,6,7,8,9,10]. The complete text of all of Veridian's reports is available as Annexes 1 through 10 to this report.

7.1 Current Configuration and Background.

The DES was installed in the late 1960's. Much of the original equipment is still in use today. The Arm drive machinery is located below the centrifuge in a machinery room known as "the pit." Along with the arm drive motors and gear boxes, the pit area contains numerous hydraulic pumps and accumulators for the hydrostatic bearings. The floor and walls of the pit are reinforced concrete. A catwalk around the perimeter of the room provides access to the machine support equipment for inspection and maintenance. The machine was originally designed for a G-onset rate in excess of 7 $G \cdot sec^{-1}$ to a maximum of 20G. The centrifuge arm is driven by means of drive pinions mating with a main bull gear. The original arm drive installation included flywheels driving six pinions. Powered by hydraulic motors, the flywheels were connected to the pinions through clutches and right angle 6:1 reduction gearboxes. Designed to be used along with the electric motors, the flywheels would have made G-onset rates in excess of 7G possible. This "Hi-Drive" flywheel system was never used and subsequently removed entirely. There are a total of nine drive pinions. Three of these pinions are driven by 110 HP DC electric motors through reduction gearboxes. The six gearboxes are no longer available, but the six drive pinions remain installed and are unused. The space originally occupied by the flywheels and gearboxes is available for installation of additional motors and gearboxes.

The operator's console has provision for position (Fork and Cab) and velocity (Arm) control with position, velocity, and acceleration feedback loops. An integral part of the control loop is a PDP-11 computer referred to as the Primary Controller. The Primary Controller tailors the drive commands to parameters set in the control software.

The DC current required to operate the drive motors is generated by a motor-generator (Motor/Generator) set. The Motor/Generator set, control transformer, switchgear, and motor drive are all located in the Motor/Generator room. The motor control interface is located in a Cabinet in the Machine Operator room. This interface receives control signals from the Primary Controller and/or the Machine Operator's console producing motor drive command signals, which control the motor drive in the Motor/Generator room. The motor drive responds to these command signals by regulating the arm drive motor current.

The Air Force desires to increase the G-onset rate of the DES. Under normal operating conditions the G-onset rate is limited to $\pm$ 0.6 G·sec^{-1}. There are many upgrade options each offering an increase in utility, performance and/or reliability. Each is discussed separately below.

7.2 Arm Upgrade Study.

Veridian conducted a thorough study of the Arm drive components to form a baseline for proposing upgrade options. Their findings are detailed in the Arm Upgrade Study[2]. The six upgrade options offer incremental improvements in either reliability or performance or both. All offer reduced O&M expenses. The upgrades were labeled by their level and each is described in turn below.

Level A Upgrade. The level A provides an improvement in Arm onset rate to 1.5 G·sec^{-1} via replacement of the Primary Controller and adding some reliability enhancements to the Arm drive machinery. The upgrade is summarized in Figure 8-1.

Figure 7-1 Level A Upgrade

- Performance Improvement
  - G-onset rate increased to 1.5 G·sec^{-1}
- Upgrades
  - Replace Primary Controller
  - Use Existing Motor/Generator Set, but refurbish switch gear and control interface
  - Use existing Drive Motors and Gear Boxes, but install cooling fans
- Total Cost approximately $250,000
- Risk
  - Duty cycle still limited by motor heating
  - Operation of 30 year old equipment above its rated capacity may affect reliability

Level B Upgrade. The Level B upgrade is an extension of the Level A upgrade aimed at improving the reliability of the DES while reducing its O&M costs by replacing the old Motor/Generator Set. Figure 7-2 summarizes the major features of the Level B upgrade.

Figure 7-2 Level B Upgrade

- Performance Improvement
  - G-onset rate increased to 1.5 $G \cdot sec^{-1}$
- Upgrades
  - Replace Primary Controller
  - Replace Motor/Generator Set with solid state motor drive
  - Use existing Drive Motors and Gear Boxes, but install cooling fans
- Total Cost approximately $575,000
- Risk
  - Use of 30 year old gear boxes at increased torque
  - Duty cycle still limited by motor heating
  - Operation of 30 year old motors above their rated capacity may affect reliability

Level C Upgrade. The Level C upgrade improves performance over Levels A and B by replacing the old motors with modern 300 HP motors. See Figure 7-3 for a summary of Level C upgrade features.

Figure 7-3 Level C Upgrade

- Performance Improvement
  - G-onset rate increased to 1.6 $G \cdot sec^{-1}$
- Upgrades
  - Replace Primary Controller
  - Replace Motor/Generator Set with solid state motor drive
  - Replace Drive Motors
- Total Cost approximately $940,000
- Risk
  - Use of 30 year old Gear Boxes at increased torque
  - High cost for limited performance improvement

Level D Upgrade. The Level D upgrade includes Level C, but adds replacement of the old Gear Boxes. Figure 7-4 summarizes its major features.

Figure 7-4 Level D Upgrade

- Performance Improvement
  - G-onset rate increased to 1.6 $G \cdot sec^{-1}$
- Upgrades
  - Replace Primary Controller
  - Replace Motor/Generator Set with solid state motor drive
  - Replace the Drive Motors and Gear Boxes, add brakes to gear couplings and new pinion jack shafts and couplings
- Total Cost approximately $1,290,000
- Risk
  - High cost for limited performance improvement

Level E Upgrade. The installation of the Level E upgrade will substantially improve the G-onset rate of the DES, improve its reliability, and reduce O&M costs. Figure 7-5 outlines the Level E upgrade.

Figure 7-5 Level E Upgrade

- Performance Improvement
  - G-onset rate increased to 3.5 $G \cdot sec^{-1}$
- Upgrades
  - Replace Primary Controller
  - Add 3 additional motor drives.
  - Replace Motor/Generator Set with solid state motor drive
  - Upgrade Power transformer and switch gear
  - Replace the 3 Drive Motors and Gear Boxes with 6 new motors and gear boxes, add brakes to gear couplings and new pinion jack shafts and couplings
- Total Cost approximately $2,130,000
- Risk
  - Crowded pit area may increase maintenance costs

Level F Upgrade. Level F upgrade raises the G-onset to 5 $G \cdot sec^{-1}$ by adding three more motors and gear boxes for a total of nine drive motors. This upgrade further crowds the pit area and may require that the air handler be replaced to cope with the additional heat load. Figure 7-6 displays the major features of the Level F upgrade.

Figure 7-6 Level F Upgrade

- Performance Improvement
  - G-onset rate increased to 5.0 $G \cdot sec^{-1}$
- Upgrades
  - Replace Primary Controller
  - Add 6 additional motor drives
  - Upgrade Power transformer and switch gear
  - Replace Motor/Generator Set with solid state motor drive
  - Replace the 3 Drive Motors and Gear Boxes with 9 new motors and gear boxes, add brakes to gear couplings and new pinion jack shafts and couplings
- Total Cost approximately $2,945,000
- Risk
  - Crowded pit area may increase maintenance costs
  - Additional heat load may require replacement of air handler

7.3 Fork Studies.

The Fork assembly, consisting of the Fork and Fork shaft joined at one end by a flange, is mounted on the centrifuge arm and rotates on a horizontal axis perpendicular to the centrifuge axis. The spherical Cab is attached at the end of the Fork. The Fork drive motor is attached to the other end of the Fork shaft. Large radial roller bearings support the Fork assembly in the main arm trunion allowing it to rotate. The Fork drive motor, a 90 horsepower (@ 15 RPM) DC torque motor, drives the Fork in either direction at up to 20 RPM. Radial and thrust loads are borne by two roller bearings located near each end of the shaft. Rotary joints and slip-rings allow the Fork assembly to rotate continuously in either direction. There is an air-operated brake to hold the Fork in a fixed position. Current to drive the Fork motor is generated by an Amplidyne motor-generator set located in the Motor/Generator room. The Amplidyne is part of the original installation completed in the late 1960's. It is noisy, inefficient, and requires a lot of floor space. Two Fork studies[3,7] were conducted. One was an evaluation of the Fork performance and operational problems. The other report was an upgrade study.

There are several limitations of Fork capability related to the original design, which would be impractical to change. The Fork is dynamically imbalanced, which during arm rotation causes its drive motor to alternately drive and brake every one-quarter Fork rotation. This leads to controllability problems and Fork oscillation in some operational conditions. Moreover, the Fork

will not rotate at all when the Arm rpm exceeds 25. This problem is due to the fork imbalance and an undersized Drive Motor, neither of which can be altered because of the DES's design. Thus, Veridian has concluded that it is not practical to improve the performance of the Fork except by improving its Motor/Generator set and control instrumentation. Figure 7-7 summarizes the improvements recommended by Veridian as a Fork upgrade.

Figure 7-7 Fork Upgrade

- Performance Improvement
  - Reliability and improved control will contribute to improved performance
- Upgrades
  - Replace the Amplidyne Motor/Generator Set with a modern solid-state motor drive
  - Replace the Fork position encoders and the Fork controller
- Total Cost approximately $100,000

The Fork upgrade will depend on replacement of the Primary Controller during the Arm upgrade. Thus, the Fork upgrade should be part of the Arm upgrade.

7.4 Cab Upgrade Studies.

The Cab was part of the late 1960's installation and much of the original equipment is still in use today, including the servo control electronics, Cab motors, trunion bearings, shaft seals, and gear boxes. The Cab is mounted to the Fork by a pair of trunions, one at either side of the Cab. Four servo controlled hydraulic motors rotate the Cab. Four hydraulic motors drive the Cab at a maximum speed of 50 RPM.

The Cab can be controlled from the Machine Operator's console located on the second floor overlooking the centrifuge room. From here the machine operator can observe the Cab in operation. The console has provision for Cab position and velocity control with position, velocity, and acceleration feedback loops. A resolver mounted on the Fork at the Cab trunion provides position feedback. An integral part of the control system is the PDP-11 computer referred to as the Primary Controller. The Primary Controller generates Cab position commands coordinated with the centrifuge arm speed. The control signals must cross two sets of slip rings on their way to and from the Fork.

The Cab drive hydraulic power units are located in the Motor/Generator room. Fluid is pumped from the Motor/Generator room to the Fork through a series of rotary joints. The Cab motor control manifolds and servo valves are mounted on the Fork near the Cab motors. The Cab hydraulic fluid is cooled by a chiller system. The heat exchanger is installed above the Cab pumps in the Motor/Generator room.

Two Cab upgrade studies[4,5] were conducted. The first was aimed at designing a Cab drive upgrade and the second was concerned with improvements of the Cab interior and a brief analysis of a lightweight-Cab design.

Cab Performance Upgrade. The Cab performance upgrade was planned as part of this project and has been completed with external funding. The upgrade consisted of drive motor and interface replacement together with the replacement of the Cab Interface components of the Primary Controller, and the elimination slip rings from the cab control loop, leaving the cab servo controllers in direct electronic contact with the Cab Controller via a Servo Control Card.

Cab Interior Upgrade. The Cab was floor and support ring structures were originally designed to support a heavy shaker table. The current Cab weighs approximately 7,000 lbs. There is no current or anticipated requirement for housing large fixtures in the Cab. The replacement of the Cab with a lightweight design represents a major opportunity for improvement of the performance of all three DES gimbal rates. Many benefits would accrue from a significant reduction in Cab weight. The reader is referred to Veridian's original report[5] for a possible design. The use of modern composite materials offers many advantages over old steel structures without giving up the strength necessary to support experimental equipment under high G. Firms such as Scaled Composites of Mojave, CA, for example, are capable of designing high-strength light-weight spherical structures, which could form the basic Cab structure.[11] Unfortunately, a complete preliminary design of a lightweight-Cab was beyond the scope of this project so that no estimate is available for the cost of design and construction of a Cab replacement. Veridian's report[5] outlines the requirements for housing a simulated aircraft seat, controls, and display projection system.

The addition of a fourth degree-of-freedom to the DES is also possible by incorporating a powered gimbal to yaw the seat about the cab z-axis. BRC included the possibility of simulating a four-DOF DES in its simulation model. Using the model, it was possible to demonstrate gains in flight profile simulation fidelity and a reduction in angular artifact by using three DOF at the Cab rather than the present two.

7.5 Primary Controller Upgrade.

The Primary Controller is responsible for managing the flow of control signals and data between the DES Machine Operator's Console (MOC).

Figure 7-8 Schematic of MOC

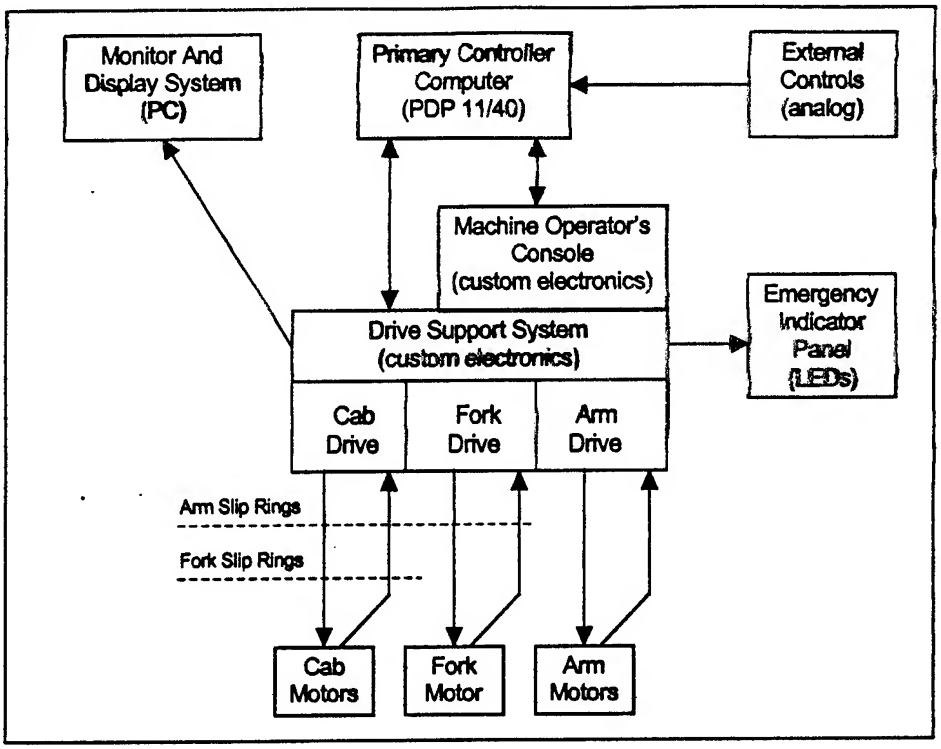

The following descriptions of the component functional blocks of the Primary Controller were extracted from Veridian's report[7].

Monitor And Display System (MADS) - a PC based computer system which monitors, displays and optionally records drive related equipment signals. This system is a fairly recent development which operates as a stand-alone unit and is refined as requirements change.

Primary Controller Computer - a digital computer system which performs the automatic and manual velocity control modes of operation. This is a PDP-11/40 mini-computer system running one of several variations of the same program depending upon the functional requirements of the intended runs.

External Controls - analog based drive command signals coming from an external source (Test Director's Station and Simulation Controller). This provides a wide variety of motion control profiles.

Emergency Indicator Panel - a panel of Light-Emitting Diodes (LED) with fixed labels used to indicate the system or condition which triggered an emergency stop.

Machine Operator's Console - a panel of custom electronics which provide operator monitoring and controls for the DES drive systems. This includes several electro-mechanical components which are make up part of the drive circuits.

Drive Support System - a panel of custom electronics which interpret the drive commands and feedback into a motor control signal. It also provides the Fault Detection and Emergency Stop circuitry. Though listed as a single item, the electronics support each drive system (cab, fork, arm) individually.

Cab, Fork, Arm Motors - individual motor elements which receive a motor control signal, move as commanded and provide a feedback status as to actual position.

The circuitry within MOC, the Drive Support System and the Unit Drives are so closely tied to each other that they act as a single operations circuit. They are shown here as separate components partly due to the physical layout of the equipment and partly to help delineate control paths which will shift as a result of upgrades listed in this report. The MOC also holds a mechanical 3-position mode switch for each drive system. The switch positions are labeled "Manual Position", "Manual Velocity", and "Automatic." Each determines the type of drive control and which system component controls the associated drive system. In "Manual Position" mode, a non-terminated 360° position dial on the MOC is switched into the associated drive circuit. In the "Manual Velocity" and "Automatic" modes, the output from the Primary Controller is modulated and switched into the associated drive circuit. With this method of dual component control, the operator must take great care to align controls when switching modes.

Veridian's proposed upgrade of the Primary Controller comprises four possible upgrade packages. The Packages are described separately below.

Upgrade Package #1. This Package has already been completed in conjunction with the recent Cab upgrade. The Cab Drive Interface was upgraded to move the servo control signals closer to the drive system and to eliminate all sets of slip rings.

Upgrade Package #2. This upgrade would accompany the upgrade of the Fork drive controller and would be directed toward the Fork Drive Interface. The older electronic components would be replaced with modern solid state electronics and made compatible with the new Fork motor controller. Upgrade Package #2 is summarized in Figure 7-9.

Figure 7-9 Upgrade Package #2

Fork Interface Upgrade

- Features
  - Design and Code New Controller Software
  - Install New Hardware (PC with A/D, D/A and Digital I/O)
  - Acceptance Testing of New System
  - Document New System
- Cost Estimate - $73,000

Upgrade Package #3. The major feature of this Package is the replacement of the PDP-11/40 computer system and its software with a modern fully equipped PC based computer system. The primary features of the Package #3 are shown in Figure 7-10.

Figure 7-10 Upgrade Package #3

Control Computer Replacement

- Features
  - Upgrade Package #2 Features (Design and Code New Interface Software, Install New Hardware, Acceptance Testing of New System, Document New System)
  - Remove and Replace Old PDP-11 Computer
- Cost Estimate - $157,500

Upgrade Package #4. This final upgrade level will remove the Machine Operators Console (MOC) and replace it with a modern PC based system which will comprise a new interface for the operator. The upgrade includes a new Instrument Panel and the existing custom electronics that perform the DES safety interlocks. Figure 7-11 summarizes the Upgrade Package #4.

Figure 7-11 Upgrade Package #4

MOC Upgrade

- Features
  - Upgrade Package #2 Features (Design and Code New Interface Software, Install New Hardware, Acceptance Testing of New System, Document New System, Remove and Replace Old PDP-11 Computer)
  - New Instrument Panel and Operator Interface
- Cost Estimate - $240,000

7.6 DES Instrumentation and Data Transmission Systems Upgrade.

The Instrumentation and Data Transmission systems system descriptions were contained in two Veridian reports[6,9], which are summarized in this section.

The DES data acquisition system comprises 36 data channels from the Cab to a patch panel located in the Medical Monitor Room. There are 32 twisted pairs and four 75 ohm coax channels. Of the 32 twisted pairs, 8 channels are dedicated to physiological monitoring leaving

24 channels for data. Of the four coax channels, three are dedicated to the closed loop tracking target display and the 4th to the subject monitor video.

In the Cab Colbourn amplifiers/signal conditioners are used for data collection. The data types range from ECG & EMG data to Strain Gage data. These devices are mounted in racks and can be interchanged as needed. Additional racks can be installed as needed. Additional physiological data is obtained from off the shelf medical devices such as Cerebral Oximeters, Pulse Oximeters, and Blood Pressure monitoring devices.

The video display system consists of two InFocus DLP projectors for the out the window display and two Citizen projectors for the Heads Up Display (HUD) and instrument panel displays.

The Monitor And Display System (MADS) monitors the machine operational parameters such as bearing pressures, fluid temperatures, motor current, arm speed, etc. This system provides real time monitoring of system parameters as well as data logging capability.

The test data collection system records test related data such as pressure, temperature, and acceleration. Historically, data originating in the Cab is conditioned (filtered and amplified) in the Cab and returned to the patch panel in the Medical Monitor room as high level analog signals. These signals cross 3 sets of slip rings on the way to the patch panel. This method is limited by the number of available channels and requires a signal conditioner for each channel. The quality of the slip-ring path also impacts the quality of the data. The numerous slip-ring crossings are a potential source of noise and signal degradation.

The proposed upgrade to the instrumentation system would be relatively inexpensive and improve the reliability, signal quality, and capacity of the system. The DES data acquisition system can be upgraded using the distributed data acquisition system technology. Distributed data acquisition refers to the technique of placing signal conditioning equipment and digitizers near the transducer and transmitting the digitized data to a host computer over a digital data link. Using the RS-232/RS-485 communication protocol, the digitizer can be located up to 4,000 feet from the host. Numerous digitizers in remote locations can be networked using this method. The per channel sample rate is limited by the number of channels being digitized and the speed of the serial link.

The modern distributed system approach, as applied to the DES, involves placing an intelligent data acquisition box in the cab or on the arm. The smart box provides signal conditioning and as well as signal digitizing. The digitized results are transmitted across the slip-rings to a host computer via digital data link. This methodology has been used on the DES in the past. Figure 7-12 summarizes the proposed upgrade.

Figure 7-12 Data Acquisition

- Distributed Data Acquisition Technology
- Increase Capacity from 36 to 64 Channels
- Three Specialized Data Acquisition Workstations
- High Capacity Data Archiving Storage
- Total Cost: $30,000 (Hardware and Materials Only)

7.7 Integration of BRC Model with DES Control System.

Veridian has studied the task of integration of the BRC Profile Design and Simulation Model with the existing Simulation Controller Program. BRC's program produces output files that can be directly employed by the Simulation Controller without further editing. However, the MATLAB version of BRC's Profile Design and Simulation program will be difficult to integrate into the Simulation Controller which is written in the C computer language. Part of BRC's program has already been converted to C, but more work will be required to create a completely integrated system. To aid in the integration of the packages which are now written in different languages, Veridian is creating a Profile Manager program which can accept input profiles from several sources, manage a database of previously created profiles and provide an interface with the Simulation Controller Program. The programs will all operate under the Microsoft Windows environment so they can communicate via "drag and drop" or the "clip board" features in that operating environment.

7.8 Summary.

The possible DES upgrades range from relatively minor improvements to the DES control software all the way to expensive hardware and software upgrades. Most of the improvements can be made incrementally as resources become available. Reliability, reduced operation and maintenance costs and increased performance would result from implementing the Level E upgrade with the addition of a lightweight-Cab modification. These improvements could be obtained for much less than the cost of a new centrifuge facility. They would improve the ability of the DES to simulate modern and emerging agile fighter flight profiles as well as improving its utility in physiological research, development of new aircraft instrumentation, and aircrew training.

7.9 References.

[1] Veridian Corporation, Dayton OH. Dynamic Environment Simulator Estimate of Future Test and Research Requirements. (Sept, 1997).

[2] Veridian Corporation, Dayton OH. Dynamic Environment Simulator Arm Drive Upgrade. (Sept, 1997).

[3] Veridian Corporation, Dayton OH. Dynamic Environment Simulator Fork Drive Upgrade. (Sept, 1997).

[4] Veridian Corporation, Dayton OH. Dynamic Environment Simulator Cab Drive Upgrade. (Sept, 1997).

[5] Veridian Corporation, Dayton OH. Dynamic Environment Simulator Cab Interior Upgrade. (Sept, 1997).

[6] Veridian Corporation, Dayton OH. Dynamic Environment Simulator DES Instrumentation Upgrade. (Sept, 1997).

[7] Veridian Corporation, Dayton OH. Dynamic Environment Simulator Primary Controller Upgrade. (Sept, 1997).

[8] Veridian Corporation, Dayton OH. Dynamic Environment Simulator Fork Drive Evaluation. (Jul, 1998).

[9] Veridian Corporation, Dayton OH. Dynamic Environment Simulator Data Transmission Methods. (Jul, 1998).

[10] Veridian Corporation, Dayton OH. Dynamic Environment Simulator BRC Model Integration. (Jul, 1998).

[11] Personal Communication with Mr. Bob Morgan. February 1997.

8.0 Cost-Benefit Study.

One of the major aims of the DES design improvement study was to evaluate feasible design improvements for their benefits. We decided to estimate the performance benefits in terms of the ability of the DES to simulate typical high-agility aircraft maneuvers. By simulating the DES performance with the improved gimbal drive capability, an objective measure of the performance benefits of a design improvement can be associated with its financial costs. The Cost-Benefit Study combined the products of several technical studies that were conducted in parallel. Figure 8-1 presents a schematic of the major steps in the process. The component studies are briefly described in the following paragraphs. More detailed discussions of the individual studies are described elsewhere in this report.

8.1 Design Improvement Study.

Veridian Incorporated (formerly Systems Research Laboratories) conducted the Design Improvement Study as a subcontractor to BRC. The study consisted of documenting the current design and then systematically analyzing the DES subsystem components for possible upgrades, which would contribute to improved performance of the DES and/or improved maintenance and reduced costs of operation. The product of the study comprised suggested design improvements and their estimated costs together with estimates of the improved performance of the particular subsystem component. The major finding of the study was that G-onset of the DES could be improved significantly. However, significant improvement of the Fork and Cab gimbal rates were not feasible without major redesign of the DES that would be cost prohibitive. Moreover, the performance benefits obtained would be insignificant compared to the benefits on increasing G-onset by modification of the Arm drive. An intriguing finding related to additional G-onset, Fork, and Cab gimbal rates could be achieved by reducing the mass of the Cab. Unfortunately, no performance improvement estimates could be made without a Cab redesign analysis, which was beyond the scope of this study. The interested reader is referred to Section 7.0 for summaries of the subsystem studies.

8.2 DES Testing.

BRC and Veridian conducted a five sets of tests of the DES to help determine dynamic parameters, and to generally validate the mathematical model of the DES. The commanded control inputs for the Arm, Fork, and Cab are, respectively, angular velocity, angular position, and angular position.

Section 5.1 contains a summary of the tests conducted by Veridian and BRC on the centrifuge.

Figure 8-1 Schematic of Cost-Benefit Analysis Process

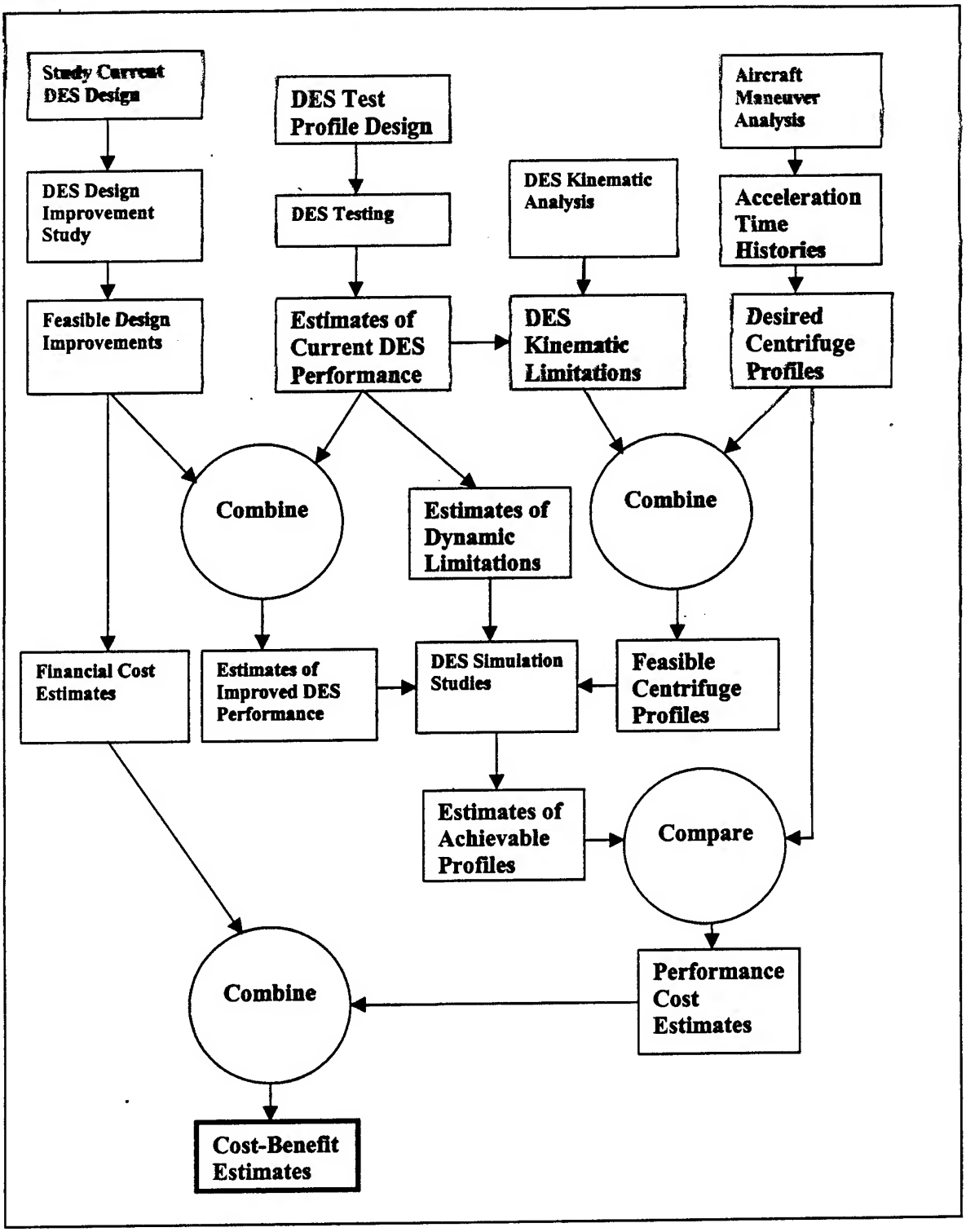

8.3 DES Kinematic Analysis.

BRC created a geometric model of the DES by employing drawings and actual measurements of the relationships in space between the major axes. Within the Cab, the relationships between the seat, occupant's head, and the Cab's tri-axial accelerometer were also measured in relation to the Cab gimbal axis and geometric center. From these measurements, series of coordinate frames were devised to enable the computation of inverse and forward kinematic analysis for the DES. These analyses resulted in computation of the necessary angular accelerations and velocities required creating a given translational acceleration profiles specified at a particular point of interest in the Cab. The kinematic models also allow the computation of angular velocities and accelerations within each coordinate frame. Refer to Section 4.0 for a complete description of the model coordinate frames.

8.4 Centrifuge Profile Creation.

Certain aircraft maneuvers, for example, basic flight maneuvers (BFMs) are common and repeatedly executed in flight. For high-performance (high-agility, fighter, attack, and air superiority) aircraft these maneuvers may involve rapidly changing translational and angular accelerations, which are stressful to the aircrew. Several of these profiles were described in detail in Section 3. The design of desired acceleration profiles begins with the analysis of a particular aircraft maneuver that the research-analyst wishes to simulate.

8.5 Centrifuge Profile Simulation.

Three aircraft profiles were chosen for the Cost-Benefit Study: (1) High-G turn; (2) Push-Pull effect maneuver; and (3) Herbst maneuver. These profiles were created by studying time histories of aircraft acceleration and then creating stylized approximations to the time histories of the profiles. Finally, acceleration magnitude excursions below +1 G were eliminated for these profiles to create kinematically feasible profiles. The x-, y-, and z-axis acceleration time histories for these profiles are illustrated in Figures 8-2, 8-3, and 8-4.

Figure 8-2 High G-turn Profile

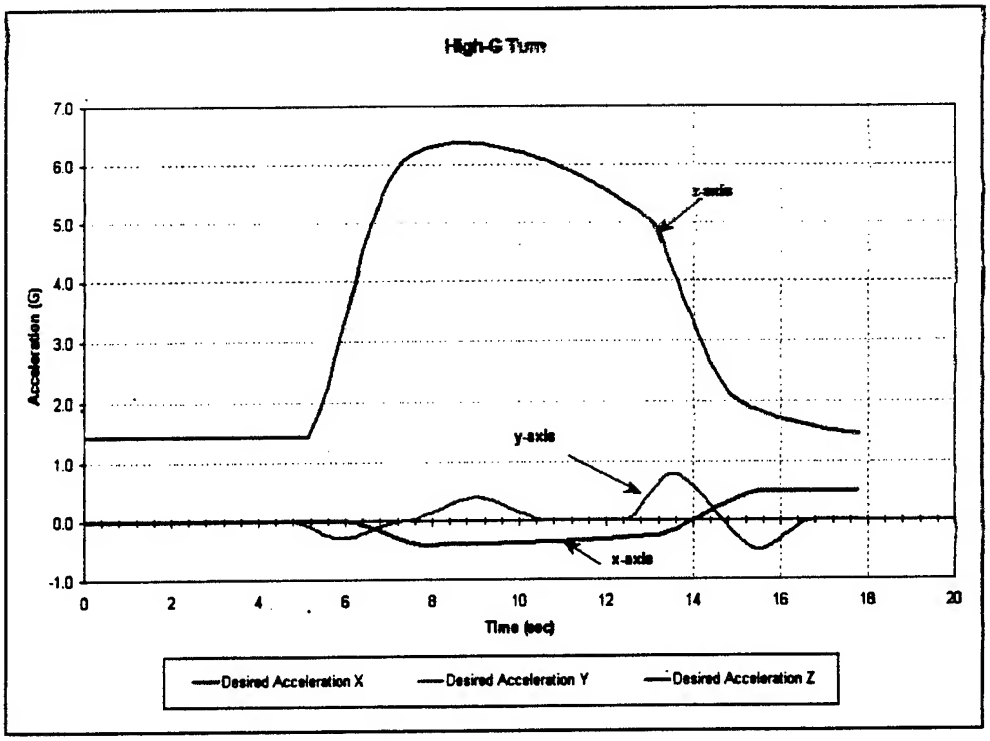

Figure 8-3 Push-Pull Profile

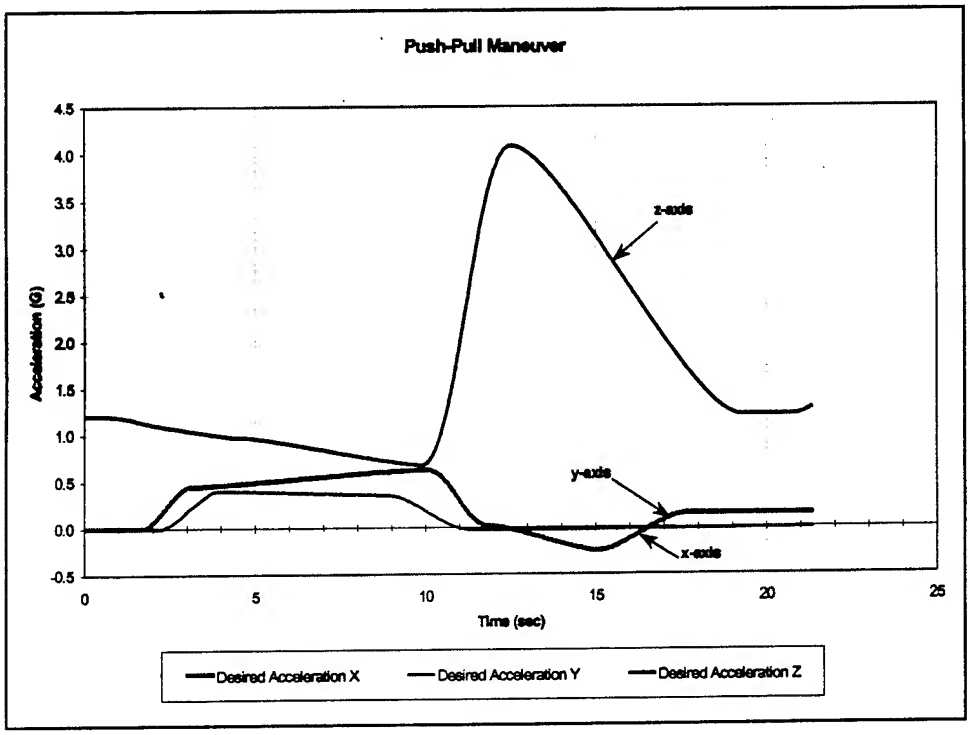

Figure 8-4 Herbst Maneuver Profile

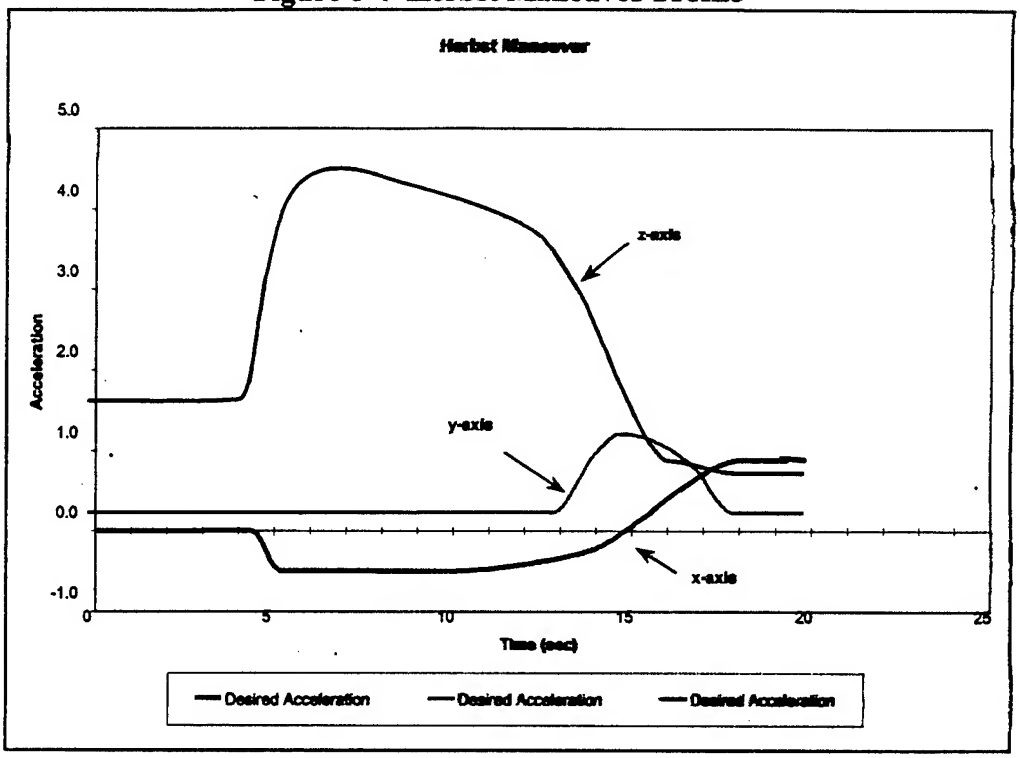

The DES kinematic and dynamic models were employed to simulate the execution of these profiles using the performance estimates derived from testing plus the estimates for the various upgrade levels. Table 8-1 summarizes the limits applied. Where estimates of dynamic response of the DES were available they were used in the DES simulations. Otherwise, the limits were applied to the kinematic model to limit the rates and velocity capabilities of each axis. In addition to the three existing axes, an additional axis capable of rotating the occupant seat was simulated to illustrate the advantage of adding a fourth degree of freedom to the DES.

8.6 Performance Cost Estimates.

Because of the short radius of the DES, it is impossible to simultaneously simulate both the translational and angular acceleration of an aircraft maneuver. Therefore, the usual practice in profile design is to attempt to duplicate the translational acceleration time-history of a particular maneuver while accepting the concomitant angular artifacts. For our Cost-Benefit Analysis, only the translational accelerations were considered. The angular acceleration costs were not considered in the profile performance cost algorithm.

The Total Performance Cost for a profile is computed as a sum of the individual sources of error that contribute to the total error in a profile. The following components make up the Total Cost.

8.6.1 Arm Cost.

This cost is defined as the absolute difference in magnitude of the G achieved and the G desired. The Arm cost assumes that all acceleration magnitude is generated by the angular velocity of the Arm. This is not strictly true for points which are displaced from the Fork or Cab axes as their rotation generates small transient acceleration during Fork and Cab gimbal rotation. Mathematically, Arm Cost is defined by the following equation.

$$\text{Arm Cost} = \left(\sqrt{G_x^2 + G_y^2 + G_z^2}\right)_{\text{Achieved}} - \left(\sqrt{G_x^2 + G_y^2 + G_z^2}\right)_{\text{Desired}} \qquad \text{Eq. 8-1}$$

8.6.2 Degree-of-Freedom (DOF) Cost.

The DOF cost is the absolute value of the vector difference in the achieved and desired acceleration. Mathematically, DOF Cost is defined by the following Equation.

$$\text{DOF Cost} = \sqrt{(G_{x_{\text{Achieved}}} - G_{x_{\text{Desired}}})^2 + (G_{y_{\text{Achieved}}} - G_{y_{\text{Desired}}})^2 + (G_{z_{\text{Achieved}}} - G_{z_{\text{Desired}}})^2} \qquad \text{Eq. 8-2}$$

Note that the DOF cost does not include effects due to Fork or Cab physical limitations—it was created solely for the purpose of comparing 3-DOF and 4-DOF simulations.

8.6.3 Fork Cost.

The Fork Cost is the absolute value of the vector difference in the achieved and desired acceleration with only the Fork and Arm physical limits applied during the simulation.

8.6.4 Cab Cost.

The Cab Cost is the absolute value of the vector difference in the achieved and desired acceleration with only the Cab and Arm physical limits applied during the simulation.

8.6.5 Seat Cost.

The Seat Cost is the absolute value of the vector difference in the achieved and desired acceleration with only the Seat and Arm physical limits applied during the simulation. Only kinematic limits could be applied to the Seat gimbal, as there were no estimates of the Seat dynamics available.

Then, the Total Cost is the sum of the Arm, DOF, Fork, Cab, and Seat costs. For comparison purposes the Total Cost was reduced by 25% when the Seat is added to the simulation to allow comparison with simulations when no Seat DOF is available.

8.7 Simulation of "Cost-Benefit" Profiles.

Tables 8-1, 8-2, and 8-3 and Figures 8-5 through 8-7, present the results of the simulations conducted for estimating the benefit of the various improvement levels. To remove the variability related to the choice of axis weighting, all the simulations were done using the "Pointing Method." The simulation program proved to be very useful for illustrating the effects of manipulating the physical limits on DES profile fidelity. A review of the simulation cost results shows that profile extension reduces the total cost of all the profiles by extending the length of the profiles so that G-magnitudes can be achieved although not at the rates of the original profile. When comparing extended length profiles with fixed length profiles the difference in total cost differences become less as the Arm G-onset rate increases. The performance cost for all three profiles plateau at the Level E upgrade (3.5 $G \cdot sec^{-1}$). No further improvement is possible through Arm onset rate increases because all the performance cost is related to the Fork and Cab gimbal performance. All profiles show a slight improvement, *i.e.* decrease in performance cost, associated with allowing the seat to yaw about the Cab z-axis. The degree of improvement may be limited by the relatively low kinematic limits chosen for the seat. These limits were chosen primarily to allow ease of positioning of the seat for fixed orientation operation. Based on the results of this study, there does not appear to be a substantial advantage to increasing the arm G-onset beyond 3.5 $G \cdot sec^{-1}$. Time extension of profiles improves the total cost of all profiles at the expense of reducing the fidelity of the acceleration onset rates during those phases of a profile that exceed the physical limits on the gimbals acceleration onset.

8.8 DES Performance Sensitivity to Cab Weight Reduction.

The DES Centrifuge is an extremely heavy piece of machinery characterized by a multitude of complex shapes. Its overall mass moment of inertia (MOI) is not precisely known, but a commonly accepted value, based on various tests performed over time, has been of 6.5×10^6 $in \cdot lbf \cdot sec^2$ (in metric units, 7.37×10^5 $kg \cdot m^2$).

BRC performed calculations based on a number of the centrifuge runs, which were carried out throughout the course of this project. As a results, BRC bracketed the MOI of the DES to values laying somewhere between 6.0×10^5 and 11.0×10^5 kg·m^2.

The weight of the fork assembly (including its shaft, and excluding the cab) was roughly estimated at 35,000 lbs.

Best estimates for the weights of various cab components could be itemized as follows:

Cab Ring	5,400 lbs (weighted January '98)
Cab Shells	1,000 lbs (500 lbs each)
Floor Assembly	400 lbs
Seat and Misc Equipment	200 lbs
Total	7,000 lbs

A set of counterbalance weights, acting against the cab weight on the other end of the arm, are located at approximately 78" away from the arm center of rotation. The cab is of course located at 228" (19 ft) away from the center of rotation.

Figure 8-8 displays the expected increase in the arm angular acceleration capability as a function of the cab weight, assuming cab weight reduction scenarios ranging from 8,000 lbs down to 2,000 lbs. The value of 8,000 lbs was chosen over the estimated 7,000 lbs to account for possible errors in weight estimates. Figure 8-9 displays the expected maximum possible increase in the G-onset rate of the DES, for the lightest possible cab (refer back to Figure 8-8). A maximum increase of approximately 35% can be achieved for the G-onset rate, for an increase of 27% in the arm angular acceleration capability. An important note here is that the net benefit of any cab weight reduction would be considerably greater if the arm angular acceleration capability were higher. Namely, a 27% increase around the 15.5 deg/sec^2 level is proportionally greater for any given higher angular acceleration capability. For example, the Level E upgrade would generate 103 deg/sec^2 which would rise to 131 deg/sec^2 for the maximum cab weight reduction – a net increase of 27.8 deg/sec^2, to be compared to the 4.8 deg/sec^2 gained in Figure 8-8 because the DES is currently at a 15.5 deg/sec^2 capability.

Figure 8-10 needs to be examined in tandem with Figure 8-9 since onset rates vary depending on the G-level.

The fork performance may, at best, improve by 15% with the maximum cab weight reduction. However, if the geometry of a new cab is such that its center of gravity is closer to the fork center of rotation axis than what it is now, then the fork handicap, which restricts the fork to a stand-still at the 3.5 to 4 G-level, may well be eliminated.

Finally, the cab performance would be increased by a directly proportional factor since the cab angular acceleration and the cab inertia are directly proportional to its mass.

8.9 Conclusion.

To summarize, no short-arm centrifuge can duplicate the acceleration forces experienced by the aircrew in an agile aircraft. For this reason, only translational acceleration fidelity was considered in this study. Angular acceleration artifact may be more noticeable in profiles optimized for translational acceleration. However, only with large sacrifices in translational acceleration fidelity can the angular artifacts produced by a centrifuge be reduced significantly. In addition, it is possible that with alternate initial conditions and/or the addition of a fourth degree of freedom at the cab, that the fidelity of the translational acceleration simulation could be improved while the angular motion artifact was reduced. That study was beyond the scope of the present effort.

In most cases, time extension of the profiles made significant reductions in total profile cost. This was seen even during simulation of higher acceleration onset rate capability for the Arm. Time extensions were not excessive—they amounted to at most about one-third duration increases in the 20-second profiles we simulated. Part of the reason that time extension made such a large difference in total cost was that time extension errors are not weighted as high as acceleration magnitude errors by the cost algorithm. Therefore as time extension allows the simulation to achieve the magnitudes closely albeit at lower onset rates, the total costs are reduced significantly. The true cost of large profile time extension versus the conduct of profiles with higher onset rates with shorter extensions is a judgment better made by the research scientists in view of the relative effect of the errors on the data being sought in the simulation.

The major conclusions from the Cost-Benefit Analysis were: (1) Arm G-onset rates above 3.5 $G \cdot sec^{-1}$ will not improve DES simulation of the translational acceleration fidelity in typical high-agility aircraft profiles; (2) Time extension improves the acceleration magnitude simulation of all profiles at the expense of sacrificing acceleration onset fidelity; (3) The addition of a fourth degree of freedom at the cab is likely to improve profile fidelity in many profiles of interest, and (4) a reduction in cab weight of 50-75% will result in a 25-35% increase in the G-onset of the DES, a 10-15% increase in the fork angular acceleration, and a 50-75% increase in the cab angular acceleration.

Table 8-1 Summary of Simulation Costs for High-G Profiles

Configuration	Approximate G-Onset Rate (G/sec)	Maximum Arm Angular Acceleration (deg/sec^2)	Seat Configuration (L[deg]/U)	Cost Function of Simulation					
				Arm (G-sec)	BOF (G-sec)	Fork (G-sec)	Cab (G-sec)	Seat (G-sec)	Total (G-sec)
Current Fixed Duration Profile	0.5	25.5	L [0 deg]	50.8	50.8	56.2	55.4	NA	213.2
			L [90 deg]	50.8	50.8	56.7	55.8	NA	214.0
			Unlocked	50.8	50.8	56.7	55.4	56.7	202.8
Extended Duration Profile	0.5	15.5	L [0 deg]	8.6	2.0	4.1	3.6	NA	18.2
			L [90 deg]	8.0	3.0	5.7	5.6	NA	22.3
			Unlocked	8.7	0.6	5.8	5.2	5.3	19.3
Upgrade Level A and B Fixed Duration Profile	1.5	35.5	L [0 deg]	31.1	31.5	32.2	33.1	NA	127.9
			L [90 deg]	31.1	31.3	34.8	33.9	NA	131.1
			Unlocked	31.1	31.2	34.7	33.8	34.8	123.7
Extended Duration Profile	1.5	35.5	L [0 deg]	3.9	1.4	4.2	3.3	NA	12.8
			L [90 deg]	3.9	1.8	4.7	3.8	NA	14.2
			Unlocked	4.3	0.5	5.9	6.3	4.2	14.2
Fixed Duration Profile	1.6	53.3	L [90 deg]	13.9	14.4	14.7	14.9	NA	57.8
			Unlocked	13.9	14.0	14.1	15.1	15.5	54.4
Extended Duration Profile	1.6	53.3	L [0 deg]	1.3	1.9	2.4	2.8	NA	7.7
			L [90 deg]	1.4	1.8	3.8	2.8	NA	9.9
			Unlocked	1.5	0.6	4.2	3.7	2.6	9.1
Upgrade Level E Fixed Duration Profile	3.5	104.9	L [0 deg]	0.9	3.3	21.7	1.3	NA	27.1
			L [90 deg]	0.9	2.5	13.5	1.6	NA	18.5
			Unlocked	0.9	0.4	15.7	2.4	0.9	15.2
Extended Duration Profile	3.5	104.9	L [0 deg]	0.7	2.6	1.8	1.9	NA	7.0
			L [90 deg]	0.7	2.1	1.7	2.3	NA	6.8
			Unlocked	0.7	0.3	1.2	3.5	1.3	5.3
Upgrade Level F Fixed Duration Profile	5.0	155.8	L [0 deg]	0.9	3.3	21.7	1.3	NA	27.1
			L [90 deg]	0.9	2.5	13.5	1.6	NA	18.5
			Unlocked	0.9	0.4	15.7	2.4	0.9	15.2
Extended Duration Profile	5.0	155.8	L [0 deg]	0.7	2.6	1.8	1.9	NA	7.0
			L [90 deg]	0.7	2.1	1.7	2.3	NA	6.8
			Unlocked	0.7	0.3	1.2	3.5	1.3	5.3

Figure 8-5a Chart of Costs for Fixed Length High-G Profiles

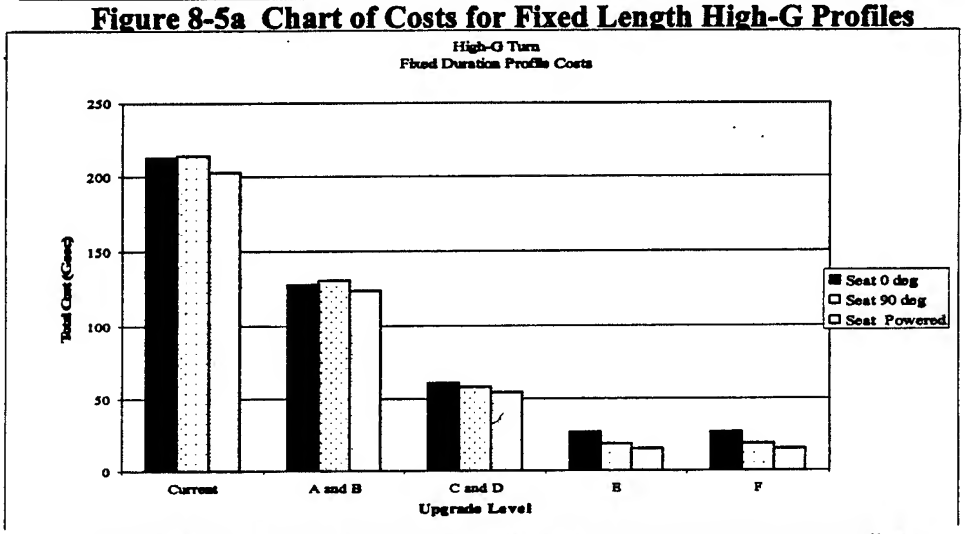

Figure 8-5b Chart of Costs for Extended Length High-G Profiles

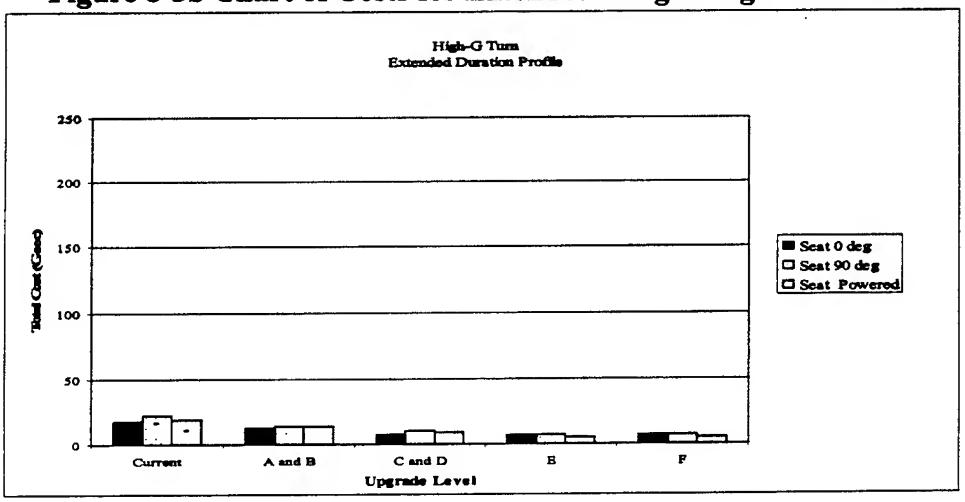

Table 8-2 Summary of Simulation Costs for Push-Pull Profiles

Configuration	Approximate G-Onset Rate (G/sec)	Maximum Arm Angular Acceleration (deg/sec^2)	Seat Configuration (L[deg]/U)	Cost Function of Simulation					
				Arm (G-sec)	DOF (G-sec)	Fork (G-sec)	Cab (G-sec)	Seat (G-sec)	Total (G-sec)
Current Fixed Duration Profile	0.5	15.5	L [0 deg]	21.0	21.0	23.9	24.4	NA	114.3
			L [90 deg]	21.0	21.0	23.9	24.1	NA	90.0
			Unlocked	21.0	21.0	23.9	24.4	24.0	85.7
Extended Duration Profile	0.5	15.5	L [0 deg]	8.3	1.8	7.1	6.5	NA	23.7
			L [90 deg]	8.3	1.8	7.2	6.5	NA	23.8
			Unlocked	8.4	1.8	6.9	6.6	6.5	22.6
Upgrade Level A and B Fixed Duration Profile	1.5	35.5	L [0 deg]	16.9	16.9	22.4	19.1	NA	75.3
			L [90 deg]	16.9	16.9	19.3	17.9	NA	70.9
			Unlocked	16.9	16.9	20.7	19.1	19.2	69.6
Extended Duration Profile	1.5	35.5	L [0 deg]	3.3	0.9	3.3	2.7	NA	10.1
			L [90 deg]	3.4	0.9	3.0	2.9	NA	10.2
			Unlocked	3.3	0.8	3.3	2.6	2.6	9.3
Fixed Duration Profile	1.6	53.3	L [90 deg]	11.5	11.6	13.1	8.9	NA	45.1
			Unlocked	11.5	11.6	11.3	12.9	13.1	45.1
Extended Duration Profile	1.6	53.3	L [0 deg]	1.6	0.7	2.3	1.8	NA	6.4
			L [90 deg]	1.6	0.7	2.1	2.3	NA	6.7
			Unlocked	1.5	0.6	2.6	1.8	2.4	6.7
Upgrade Level E Fixed Duration Profile	3.5	104.9	L [0 deg]	0.6	0.9	14.1	1.3	NA	16.9
			L [90 deg]	0.6	1.5	11.7	13.3	NA	27.0
			Unlocked	0.6	0.8	17.2	1.1	0.7	15.4
Extended Duration Profile	3.5	104.9	L [0 deg]	0.5	0.8	1.3	1.6	NA	5.0
			L [90 deg]	0.5	1.2	1.3	2.0	NA	4.9
			Unlocked	0.5	0.7	1.3	2.0	1.8	4.2
Upgrade Level F Fixed Duration Profile	5.0	155.8	L [0 deg]	0.6	0.9	14.1	1.3	NA	16.9
			L [90 deg]	0.6	1.5	11.7	13.3	NA	27.0
			Unlocked	0.6	0.8	17.2	1.1	0.7	15.4
Extended Duration Profile	5.0	155.8	L [0 deg]	0.5	0.8	1.3	1.6	NA	4.2
			L [90 deg]	0.5	1.2	1.3	2.0	NA	4.9
			Unlocked	0.5	0.7	1.3	2.0	1.8	4.2

Figure 8-6a Chart of Costs for Fixed Length Push-Pull Profiles

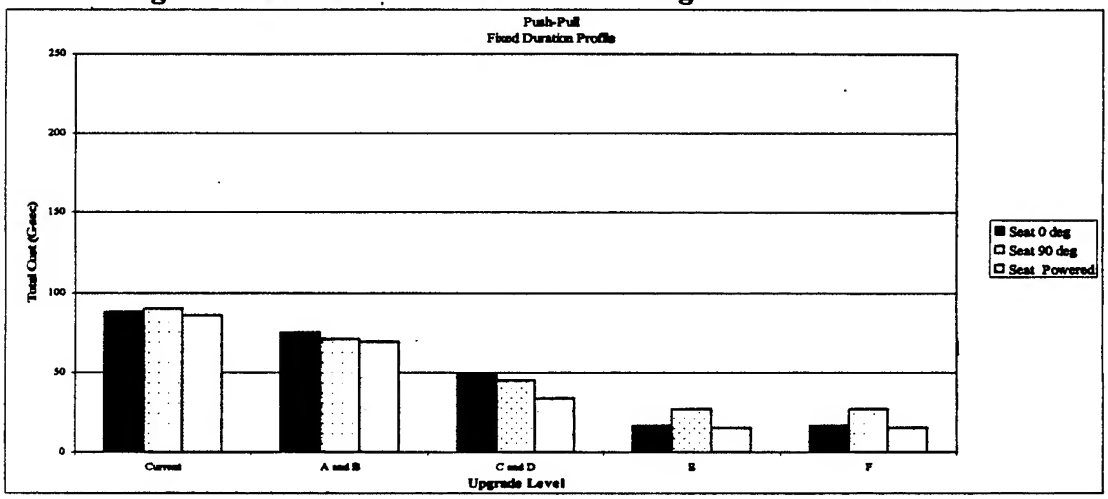

Figure 8-6b Chart of Costs for Extended Length Push-Pull Profiles

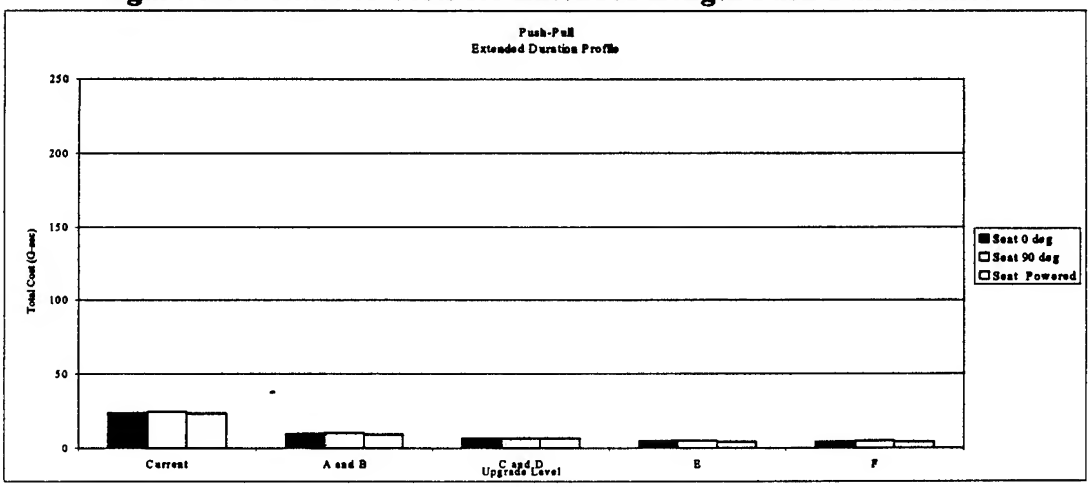

Table 8-3 Summary of Simulation Costs for Herbst Profiles

Configuration	Approximate G-Onset Rate (G/sec)	Maximum Arm Angular Acceleration (deg/sec^2)	Seat Configuration (L/deg/SP)	Cost Function of Simulation					
				Arm (G-sec)	HOF (G-sec)	Neck (G-sec)	Chk (G-sec)	Seat (G-sec)	Total (G-sec)
Current Fixed Duration Profile	0.5	15.5	L [0 deg]	33.1	33.4	37.6	37.6	NA	141.3
			L [90 deg]	32.8	33.8	37.2	36.9	NA	139.0
			Unlocked	33.1	33.3	37.6	34.2	37.5	235.6
Extended Duration Profile	0.5	15.5	L [0 deg]	7.1	5.5	9.3	10.6	NA	32.5
			L [90 deg]	6.8	5.0	9.0	8.6	NA	29.4
			Unlocked	7.4	5.6	9.9	21.5	9.9	40.7
Upgrade Level A and B Fixed Duration Profile	1.5	35.5	L [0 deg]	23.3	23.8	26.7	24.3	NA	108.1
			L [90 deg]	23.0	23.4	26.1	25.0	NA	97.5
			Unlocked	23.3	23.6	26.7	23.2	26.3	92.6
Extended Duration Profile	1.5	35.5	L [0 deg]	5.3	5.0	9.7	10.1	NA	30.0
			L [90 deg]	4.8	4.6	3.4	19.6	NA	28.6
			Unlocked	5.3	5.5	9.6	16.1	9.6	34.6
Fixed Duration Profile	1.6	53.3	L [90 deg]	14.5	14.7	17.2	16.8	NA	62.7
			Unlocked	14.4	14.5	29.0	15.8	16.5	68.3
Extended Duration Profile	1.6	53.3	L [0 deg]	4.8	5.6	9.5	18.6	NA	38.4
			L [90 deg]	4.8	4.7	7.5	12.1	NA	27.7
			Unlocked	4.7	5.3	9.2	17.7	9.5	34.8
Upgrade Level E Fixed Duration Profile	3.5	104.9	L [0 deg]	5.3	6.3	27.6	5.7	NA	44.9
			L [90 deg]	4.1	4.9	26.7	6.8	NA	41.7
			Unlocked	5.3	6.1	28.5	11.0	6.8	42.6
Extended Duration Profile	3.5	104.9	L [0 deg]	4.4	5.3	9.6	10.0	NA	29.4
			L [90 deg]	3.6	4.4	8.8	10.8	NA	26.8
			Unlocked	4.4	5.0	9.5	17.9	9.9	35.1
Upgrade Level F Fixed Duration Profile	5.0	156.8	L [0 deg]	5.3	6.3	27.6	5.7	NA	44.9
			L [90 deg]	4.1	4.9	26.7	6.8	NA	41.7
			Unlocked	5.3	6.1	28.5	11.0	6.8	42.6
Extended Duration Profile	5.0	156.8	L [0 deg]	4.4	5.3	9.6	10.0	NA	29.4
			L [90 deg]	3.6	4.4	8.8	10.8	NA	26.8
			Unlocked	4.4	5.0	9.5	17.9	9.9	35.1

Figure 8-7a Chart of Costs for Fixed Length Herbst Profiles

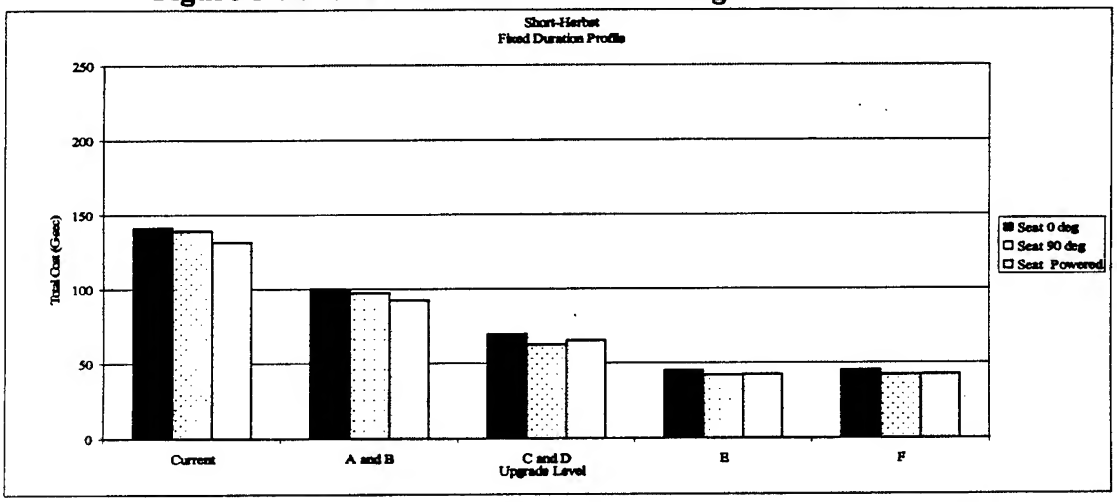

Figure 8-7b Chart of Costs for Extended Length Herbst Profiles

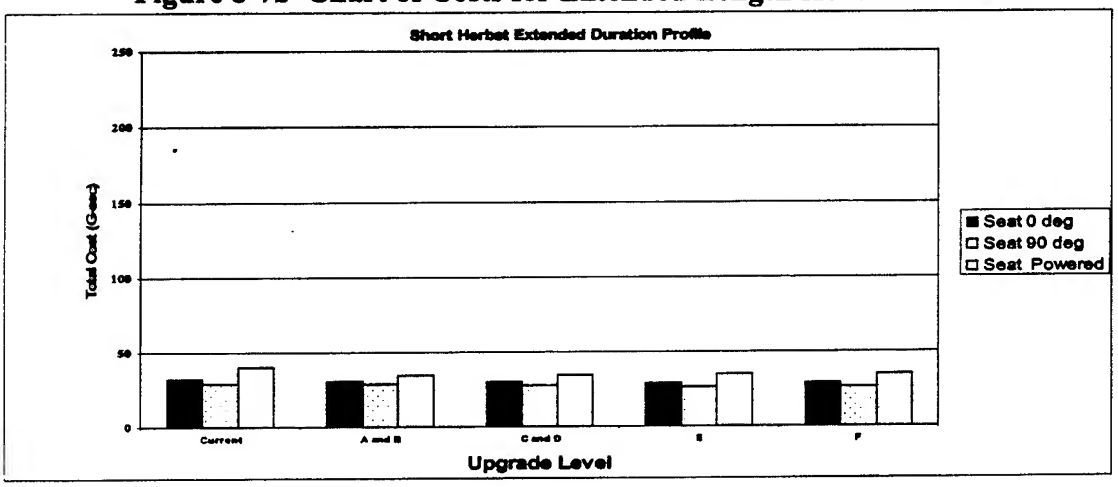

Figure 8-8 DES Parametric Study- The Effects of Cab Weight Reduction on the Arm Angular Acceleration

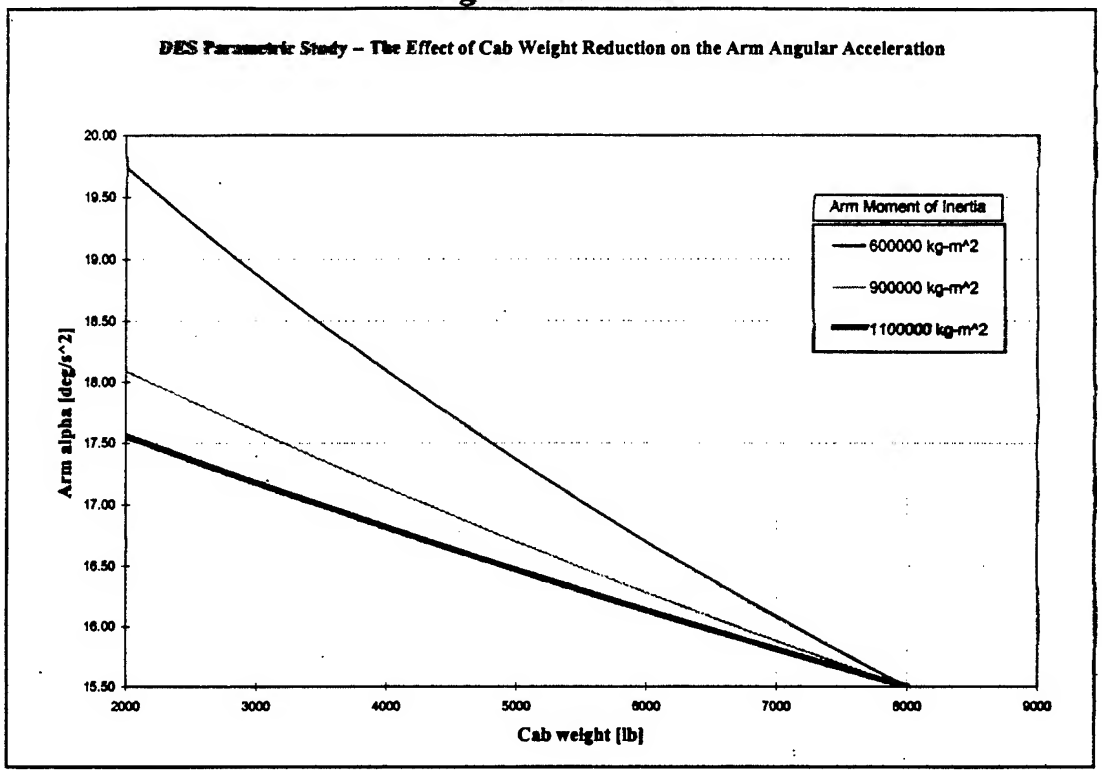

Figure 8-9 Comparison of Pilot G-Onset- Existing Arm Angular Acceleration vs. 27% Increase in Arm Angular Acceleration

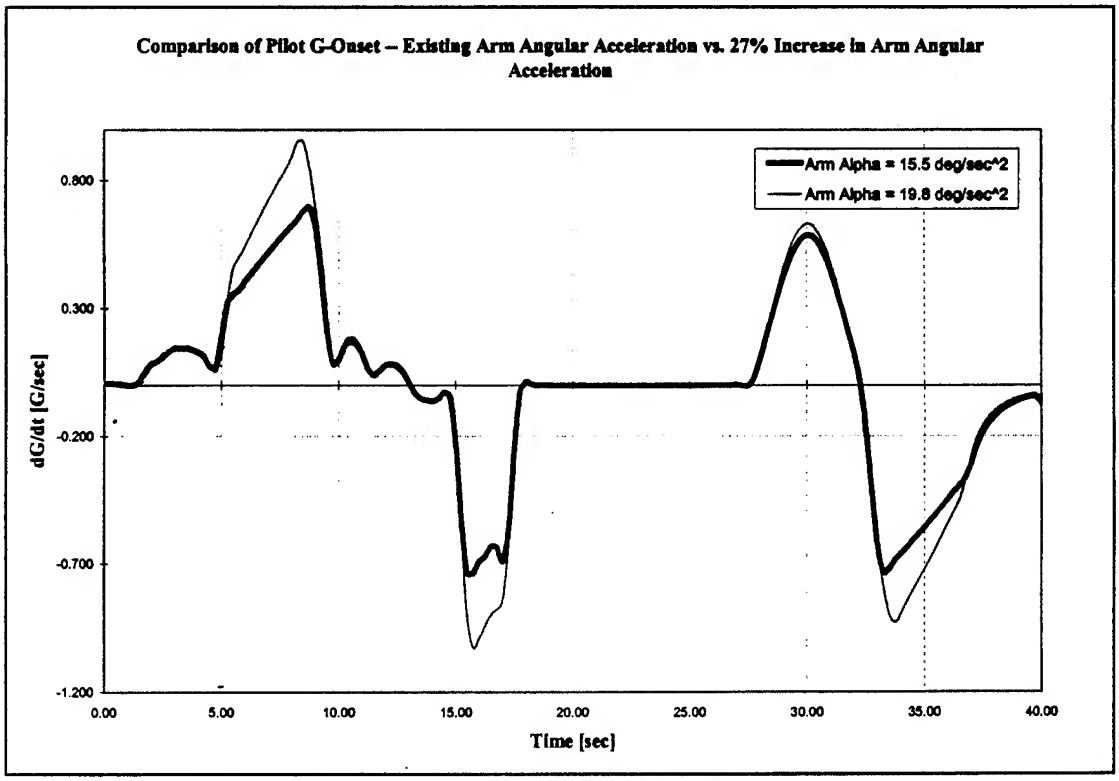

Figure 8-10 Comparison of Pilot Acceleration- Existing Arm Angular Acceleration vs. 27% Increase in Arm Angular Acceleration

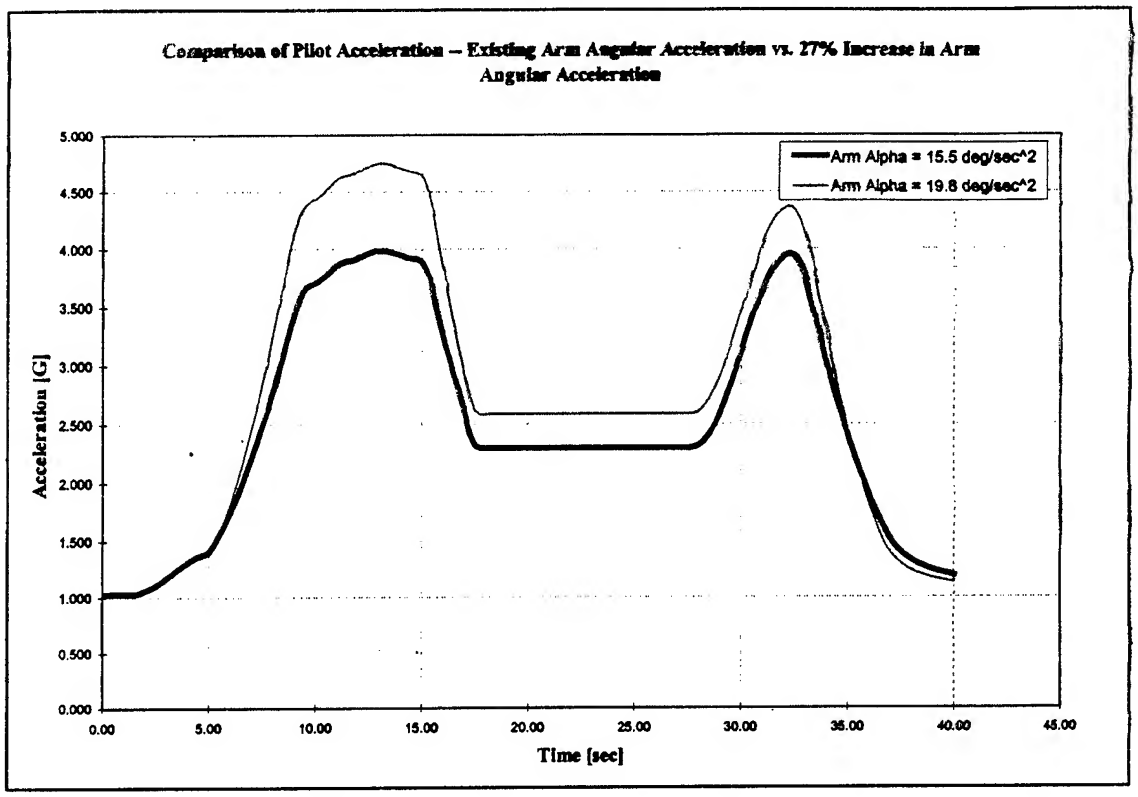

9.0 Recommendations.

- **Level "E" Arm Upgrade:** Based on the aircraft simulations that were modeled with the DES Simulation software, it appears that the Level E upgrade for the arm drive motors would yield the best performance to cost ratio.

- **Lighter Cab Structure:** Because of the synergistic effect on the performance of the arm, fork, and cab, BRC would also recommend the whole cab structure to be revised, and rebuilt. This is desirable because the current fork and cab drives have been shown to limit the performance of the DES as a whole, when more powerful arm motors were modeled. (The final report will include BRC's calculation with regard to the effects of a weight decrease in the cab).

- **Seat Degree of Freedom:** During the development of the DES, BRC engineers created and solved for many random acceleration profiles. More specifically, these profiles could generally not be labeled as "flight profiles", but their particularity was that they appeared to be difficult to solve for (i.e., neither one of the three acceleration components would stagnate near 0 or 1 G). As a result, BRC engineers observed that a motorized seat would contributed tremendously to the capability of the DES to match difficult desired profiles. Many acceleration profiles were matched nearly perfectly. Therefore, BRC would also recommend the seat located within the cab to be motorized.

- **Software:** The performance of the DES Simulation software is rather adequate as is. However, it currently does not optimize profiles over the whole time span of a given profile. An overall optimization scheme has not yet been devised, but it could likely be incorporate into the four solvers that are currently available. On the other hand, if a seat DOF was ever implemented, the performance of the DES, together with the DES Simulation software, would be such that the need for an overall optimization scheme would be greatly reduced (see the "Seat Degree of Freedom" note).

9.1 Business Plan.

This section presents the preliminary BRC Business Plan for commercializing the technology developed during the DES Phase II SBIR. This preliminary plan details how BRC largely intends to use the DES technology as part of its normal commercial activities.

9.1.1 Introduction and Background.

It is possible that BRC may be able to use the DES simulation as a basis for developing a MATLAB® [i] Simulator Toolbox designed to provide the basic software tools necessary to model, simulate and predict the time variation in position, velocity, and acceleration of motion-base simulators and mechanical rides. The MATLAB® Toolbox concept will be researched and its feasibility explored in a Phase III SBIR by BRC. If feasible, BRC will sponsor the development of a MATLAB® Simulator Toolbox software to be transferred under license to Injury Sciences Incorporated (ISI), a wholly owned subsidiary licensee of BRC. ISI will, in turn, market the Toolbox through the Math Works, Incorporated to commercial customers and provide a commercial consulting service based on application of the Toolbox software to solve the

equations of motion for motion base simulators and mechanical rides. ISI will also provide training, maintenance, and software support under contract to the USAF and other users in the Government and to The Math Works, Inc.

9.1.2 Potential Technology Applications.

Military

Centrifuge Profiles. The USAF and USN employ human centrifuges to recreate the acceleration/inertial force environment associated with high performance flight. The advent of highly agile supermaneuvering aircraft has recently generated interest in simulating high agility fighter maneuvers on centrifuges. Of course, it is impossible to reproduce the motion of a six-degree of freedom aircraft with an earth bound three-degree of freedom centrifuge. However, an accurate model of the centrifuge can be employed to create an optimal approximation to the actual force-motion environment. When combined with high fidelity visual displays, the centrifuge can be employed to good benefit in training and research programs supporting development of high agility aircraft.

The MATLAB® tools developed in the DES Phase II SBIR will be a valuable technology in creating models of centrifuge simulators and in understanding how to optimize those profiles to create motion profiles designed to simulate the force-motion stimuli associated with conducting the maneuvers in the actual aircraft.

Design of Motion Base Simulators. All three DOD services and other government agencies employ motion base simulators in training and research. Simulators are safer and more cost-effective to operate than the actual aircraft, boat, or wheeled vehicle being simulated.

BRC's consulting service will employ the MATLAB® tools developed under the SBIR could be employed to create a model of a particular motion base simulator. Once completed, the model can be used to create motion profiles aimed at recreating the acceleration and force stimuli produced by the real vehicle undergoing the same maneuvers.

9.1.3 Private Sector Applications.

Automotive Seating Design. Automobile seating designers are faced with a number of difficult choices in the design of seating for modern automobiles and light trucks. The seats must: (1) be comfortable and functional for the driver and passengers during long duration travel; (2) contribute to the restraint of occupants during normal or emergency maneuvering; (3) aid in occupant protection and restraint during crash events; and finally and significantly, (4) accommodate the entire driving population. For example, seats must damp out vibration and provide soft, low friction surfaces for comfort, while providing support and head restraint in rear-end collisions. They must cushion and stabilize the occupants in violent off-road maneuvers while suppressing the effects of large movements in the vehicle's suspension system. These characteristics are difficult to design and optimize since optimal performance of one requirement often means large compromises in achieving good performance in another. Presently, seats and

restraint designs are tested using humans in benign acceleration environments and using manikins in hazardous acceleration or impact tests.

Human centrifuges with multiple degrees of freedom can be employed to simulate the acceleration-inertial force environment of certain automobile motions. BRC has investigated the utility of the DES in that role in during the latter phases of the SBIR project. The MATLAB® model of the DES will play an enabling role in understanding how to create DES simulations of the acceleration events accompanying violent automobile motions. If this capability of the DES can be validated, the DES can employed to create simulations of automobile accelerations during loss of control or roll-over. Using controlled simulations, the motions of manikins or human subjects could be studied to aid in the design of more effective automotive seating and restraint systems. Once a simulation is validated, it could be employed with occupant simulation packages to elucidate differences in the responses of different size people to the various seat/restraint designs in representative simulations.

Seating and Restraint in Other Transportation Systems. The seating and restraint systems provided for occupants of boats, aircraft, heavy trucks, heavy construction vehicles, and buses is often implicated in accidental injuries. Most of the compromises in the design of seating and restraint systems for automobiles also must be made by designers of vehicles for these modes of transportation. The application of centrifuge simulation to vehicles employed in recreational and commercial transportation, and in the construction industries, would be similar and might be easier to accomplish than the automotive applications noted above.

Amusement Park Mechanical Ride Design. Presently, the amusement and theme park industry is a target of litigation related to alleged personal injuries sustained by riders of mechanical rides. In general, the designers of such systems have little or no background in occupant tolerance, occupant protection, or the biomechanics of acceleration-related injuries. In fact, some mechanical rides do produce injuries in susceptible passengers. The designers who seek to create ever-increasing "thrills" build rides, which are overly aggressive in the acceleration or rate of change in acceleration imposed on the riders. Despite warnings and disclaimers, suits are filed and won against the owner-operators of the rides.

The MATLAB® simulation tools could be employed to simulate the motions of a mechanical ride "car." This use would enable the computation of accurate input acceleration-force profiles for occupant simulators such as MADYMO™ or ATB which could estimate the biomechanical response to acceleration imposed by mechanical rides. The design of the ride itself, passenger compartments, and seating, as well as restraint systems, could be optimized to create the desired entertainment effects without exposing the "customers" to unduly harsh vibration or acceleration environments. This is an untapped market.

9.3.1 Potential Customers for Selected Applications.

Selected Application: Creation of Centrifuge Profiles for Agile Flight Simulation.

Both the USAF and USN desire to employ centrifuge flight simulators in investigating the physiology of highly agile flight. The development of high agility aircraft is presently underway,

but there are no simulators presently dedicated to simulating agile flight profiles on the ground. A computer model of the centrifuge-simulator will aid in the creation of optimal simulations of supermaneuverable flight profiles such as the "Cobra" and "Herbst" maneuvers among others.

How Customer Presently Fills this Need: The Human Effectiveness Directorate (HE) formerly employed robotics concepts in a custom developed model to design profiles for the DES. Their recent efforts have been directed toward creating optimal profiles for the simulations of the force-motion environment produced by tactical aircraft conducting high-agility maneuvers. These simulations and their optimizations have been solved using a Cray super computer. The creation of the DES simulation tools during the Phase II SBIR will facilitate the design and refinement of simulated high-agility profiles.

The USAF and USN require research and development studies to understand the physiology of high-agility flight and to ensure its safety without exposing pilots to hazardous in-flight situations. The expense of flight test is very high, costing millions of dollars to build high-agility aircraft and fly them in test maneuvers. Every effort is being made to make the best informed decision related to the safety high agility flight without placing test pilots at unduly high risks. The study of the aircrew's physiological responses to high-agility maneuvers in flight is severely circumscribed by physical limitations and flight safety considerations. Thus, the ability to study the physiology and training requirements in a controlled, safe environment would be a much more cost-effective and perhaps safer solution to the development of countermeasures for adverse physiological responses and for development of training protocols.

The MATLAB® simulation tools will also be a valuable addition to the existing research and development tools. A validated model would be valuable to the R&D community in making such decisions now and into the future. Because the development of Toolbox is sponsored by the USAF, US Government agencies would have a Government Purpose License to use or modify the Toolbox code without payment of royalties.

9.1.4 Commercial Market Development.

BRC intends to offer a commercial consulting service related to employment of the Simulator Toolbox and the Phase II model of the HE DES to employ the DES as an automobile simulator. The MATLAB® simulation of the DES, validated in the Phase II SBIR program, will be employed to design the automobile simulation profiles.

Using a mockup of a typical passenger car interior with representative restraint systems, BRC will study occupant motions and restraint system-occupant interaction with anthropomorphic manikins. These controlled studies will provide data which will enable the development of improved restraint systems, seating, and interior design for automotive applications. Currently, tests such as rollovers are done by rolling actual instrumented vehicles.

BRC expects the automobile industry will find the DES simulations attractive for a number of reasons:

a. The simulations will be repeatable and controlled, but with dynamics within the range of actual violent automobile maneuvers.

b. The use of the DES is relatively inexpensive compared to actual automobile testing.

c. Restraint system or seating modifications can be studied systematically and new designs can be studied independently of the other confounding features of the actual automobile design.

Finally, BRC envisions a role for its subsidiary IS in marketing the use of motion base simulators as substitutes for actual vehicle testing. IS can act as a consultant-middle man between the automotive industry and the HE in marketing the automobile simulation capabilities of the DES. This will encourage the transfer of the government's technology to the private sector and provide a flow of industry funding to the HE to support other projects. Separately, ISI will encourage the use of the MATLAB® technique by the automotive industry in modeling and design of simulations for the DES and other motion base simulators.

REFERENCES SECTION 9

[1] The Math Works, Incorporated. MATLAB®, Natick, MA. (1995).

Appendix A- Test Grids for Test Series 1,2, and 3 (Test Series #4 is a partial repeat of #3 and no test grids for the 25 test of test series #5)

06/13/76.

DES Test Matrix (draft)

Table 1 shows the proposed DES test matrix. Shaded areas indicate a test in which the arm moves at constant angular velocity, the cab is allowed to autovector, and then the arm motor is turned off, allowing the DES to come to rest under the influence of wind drag and other frictional effects.

Table 1: Proposed DES Test Matrix

Test #	Arm Angular Velocity [rpm]	Radial Acceleration [g]	Step Arm [rpm]	Step Fork [deg]	Step Cab [deg]
1	12.5	1	5	0	0
2	12.5	1	-5	0	0
3	12.5	1	0	5	0
4	12.5	1	0	-5	0
5	12.5	1	0	0	5
6	12.5	1	0	0	-5
7	12.5	1	5	5	0
8	12.5	1	5	0	5
9	12.5	1	0	5	5
10	12.5	1	10	0	0
11	12.5	1	20	0	0
12	12.5	1	0	10	0
13	12.5	1	0	20	0
14	12.5	1	0	0	10
15	12.5	1	0	0	20
16	12.5	1	0	0	0
17	17.5	2	10	0	0
18	17.5	2	20	0	0
19	17.5	2	0	10	0
20	17.5	2	0	20	0
21	17.5	2	0	0	10

22	17.5	2	0	0	20
23	17.5	2	0	0	0
24	21.5	3	10	0	0
25	21.5	3	20	0	0
26	21.5	3	0	10	0
27	21.5	3	0	20	0
28	21.5	3	0	0	10
29	21.5	3	0	0	20
30	21.5	3	0	0	0
31	25	4	10	0	0
32	25	4	20	0	0
33	25	4	0	10	0
34	25	4	0	20	0
35	25	4	0	0	10
36	25	4	0	0	20
37	25	4	0	0	0
38	27.8	5	10	0	0
39	27.8	5	20	0	0
40	27.8	5	0	0	0
41	32.9	7	10	0	0
42	32.9	7	20	0	0
43	32.9	7	0	0	0
44	37.3	9	10	0	0
45	37.3	9	20	0	0
46	37.3	9	0	0	0

BRC Second Series of DES Tests

961011

BRC Phase 2 Tests 10/18/96

Profile Name	Data Filename	Profile # (pf) Test #	Cab/Fork Velocity Limit (deg/sec)	Start Radial G	Change in Arm Velocity (RPM)	Type of Arm Input	Change in Fork Angle (degrees)	Type of Fork Input	Change in Cab Angle (degrees)	Type of Cab Input	Notes	Initial G Total	Radius 19.0 ft Initial RPM	Final RPM	Final G Total
p2_1	961007DB.000	1		1	10	ramp					Ramp up 10 rpm at 0.5G/s	1.414	12.430	22.43	3.40
p2_2	961007DB.001	2		1	20	ramp					Ramp up 10 rpm at 0.5G/s	1.414	12.430	32.43	6.90
p2_3	961007DB.002	3		3	10	ramp					Ramp up 10 rpm at 0.5G/s	3.160	21.530	31.53	6.50
p2_4		4		5	10	ramp					Ramp up 10 rpm at 0.5G/s	5.100	27.800	37.80	9.30
p2_5	961007DB.003	5		1	15	step						1.414	12.430	27.43	5.00
p2_6		6		1	25	step						1.414	12.430	37.43	9.10
p2_7		7		3	15	step						3.160	21.530	36.53	8.70
p2_8		8		5	8	step					Ramp down 10 rpm at 0.5G/s	5.100	27.800	35.80	8.35
p2_9	961007DB.004	9		3	-10	ramp					Ramp down 10 rpm at 0.5G/s	3.160	21.530	11.53	1.30
p2_10	961007DB.005	10		5	-20	ramp						5.100	27.800	7.80	?
p2_11	961007DB.006	11		3	-15	step						3.160	21.530	6.53	?
p2_12	961007DB.007	12		5	-25	step						5.100	27.800	2.80	?
p2_13	961007DB.008	13	30	1			-30	step				1.414	12.430		
p2_14	961007DB.009	14	30	1			+30	step				1.414	12.430		
p2_15	961007DB.012	15	30	3			-30	step				3.160	21.530		
p2_16	961007DB.013	16	30	3			+30	step				3.160	21.530		
p2_17	961007DB.014	17	30	1			-60	step				1.414	12.430		
p2_18	961007DB.015	18	30	1			+60	step				1.414	12.430		
p2_19	961007DB.017	19	30	3			-60	step				3.160	21.530		
p2_20	961007DB.018	20	30	3			+60	step				3.160	21.530		
p2_21	961007DB.019	21	30	1			-90	step				1.414	12.430		
p2_22	961007DB.020	22	30	1			+90	step				1.414	12.430		
p2_23	961007DB.021	23	30	3			-90	step				3.160	21.530		
p2_24	961007DB.022	24	30	3			+90	step				3.160	21.530		
p2_25	961007DB.023	25	30	1					30	step		1.414	12.430		
p2_26	961007DB.024	26	30	1					-30	step	Nominal - 38° → 14° = 24°	1.414	12.430		
p2_27	961007DB.025	27	30	3					30	step		3.160	21.530		
p2_28	961007DB.026	28	30	3					-30	step	Good.	3.160	21.530		
p2_29	961007DB.027	29	30	5					30	step	OK, 10 1/2	5.100	27.800		
p2_30	961010DB.000	30	30	5					-30	step	OK. Spike	5.100	27.800		
p2_31	961010DB.001	31	30	1					60	step	OK	1.414	12.430		
p2_32	961010DB.002	32	30	1					-60	step	OK	1.414	12.430		
p2_33	961010DB.003	33	30	3					60	step	OK.	3.160	21.530		
p2_34	961010DB.004	34	30	3					-60	step	Good	3.160	21.530		
p2_35	961010DB.005	35	30	5					60	step	Good	5.100	27.800		
p2_36	961010DB.006	36	30	5					-60	step	Good	5.100	27.800		
p2_37	961010DB.007	37	30	1					90	step	Good	1.414	12.430		
p2_38	961010DB.008	38	30	1					-90	step	Good	1.414	12.430		
p2_39	961010DB.009	39	30	3					90	step	"	3.160	21.530		
p2_40	961010DB.010	40	30	3					-90	step	"	3.160	21.530		
p2_41	961010DB.011	41	30	5					90	step	"	5.100	27.800		
p2_42	961010DB.012	42	30	5					-90	step	"	5.100	27.800		
p2_43	961010DB.013	43	30	1			-45	step	45	step	OK	1.414	12.430		
p2_44	961010DB.014	44	30	1			+45	step	-45	step	OK	1.414	12.430		
p2_45	961010DB.015	45	30	3			-45	step	45	step	OK	3.160	21.530		
p2_46	961010DB.016	46	30	3			+45	step	-45	step	OK.	3.160	21.530		

BRC Phase 2 Tests 10/18/96

Profile Name	Data Filename	Profile # (pf) Test #	Cab/Fork Velocity Limit (deg/sec)	Start Radial G	Change in Arm Velocity (RPM)	Type of Arm Input	Change in Fork Angle (degrees)	Type of Fork Input	Change in Cab Angle (degrees)	Type of Cab Input	Notes	Initial G Total	Radius 19.0 ft Initial RPM	Final RPM	Final G Total
p2_95	961010DB.065	95	40	1	10	step	-60	step	60	step		1.414	12.430	22.43	3.40
p2_96		96	40	1	20	step	-60	step	-60	step		1.414	12.430	32.43	6.90
p2_97	961010DB.066	97	40	1	10	step	-90	step	90	step		1.414	12.430	22.43	3.40
p2_98		98	40	1	20	step	-90	step	-90	step		1.414	12.430	32.43	6.90
p2_99		99	40	3	10	step	30	step	30	step		3.160	21.530	31.53	6.50
p2_100		100	40	3	10	step	-30	step	-30	step		3.160	21.530	31.53	6.50
p2_101		101	40	3	10	step	60	step	60	step		3.160	21.530	31.53	6.50
p2_102		102	40	3	10	step	-60	step	-60	step		3.160	21.530	31.53	6.50
p2_103		103	40	3	10	step	90	step	90	step		3.160	21.530	31.53	6.50
p2_104		104	40	3	10	step	-90	step	-90	step		3.160	21.530	31.53	6.50
p2_105	961010DB.067	105	50	1			-60	step				1.414	12.430		
p2_106	961010DB.068	106	50	1			+60	step				1.414	12.430		
p2_107	961010DB.069	107	50	3			-60	step				3.160	21.530		
p2_108	961010DB.070	108	50	3			+60	step				3.160	21.530		
p2_109	961010DB.071	109	50	1			-90	step				1.414	12.430		
p2_110	961010DB.072	110	50	1			+90	step				1.414	12.430		
p2_111	961010DB.073	111	50	3			-90	step				3.160	21.530		
p2_112	961010DB.074	112	50	3			+90	step				3.160	21.530		
p2_113	961010DB.075	113	50	1					60	step		1.414	12.430		
p2_114	961010DB.076	114	50	1					-60	step		1.414	12.430		
p2_115	961010DB.077	115	50	3					60	step		3.160	21.530		
p2_116	961010DB.078	116	50	3					-60	step		3.160	21.530		
p2_117	961010DB.079	117	50	5					60	step		5.100	27.800		
p2_118	961010DB.080	118	50	5					-60	step		5.100	27.800		
p2_119	961010DB.081	119	50	1					90	step		1.414	12.430		
p2_120	961010DB.082	120	50	1					-90	step		1.414	12.430		
p2_121	961010DB.083	121	50	3					90	step		3.160	21.530		
p2_122	961010DB.084	122	50	3					-90	step		3.160	21.530		
p2_123	961010DB.085	123	50	5					90	step		5.100	27.800		
p2_124	961010DB.086	124	50	5					-90	step		5.100	27.800		
p2_125	961010DB.087	125	50	1			-45	step	45	step		1.414	12.430		
p2_126	961010DB.088	126	50	1			+45	step	-45	step		1.414	12.430		
p2_127	961010DB.089	127	50	3			-45	step	45	step		3.160	21.530		
p2_128	961010DB.090	128	50	3			+45	step	-45	step		3.160	21.530		
p2_129	961010DB.091	129	50	1	10	step	-60	step	60	step		1.414	12.430	22.43	3.40
p2_130		130	50	1	20	step	-60	step	-60	step		1.414	12.430	32.43	6.90
p2_131	961010DB.092	131	50	1	10	step	-90	step	90	step		1.414	12.430	22.43	3.40
p2_132		132	50	1	20	step	-90	step	-90	step		1.414	12.430	32.43	6.90
p2_133		133	50	3	10	step	60	step	60	step		3.160	21.530	31.53	6.50
p2_134		134	50	3	10	step	-60	step	-60	step		3.160	21.530	31.53	6.50
p2_135		135	50	3	10	step	90	step	90	step		3.160	21.530	31.53	6.50
p2_136		136	50	3	10	step	-90	step	-90	step		3.160	21.530	31.53	6.50

BRC Phase 2 Tests 10/18/96

Profile Name	Data Filename	Profile # (pf) Test #	Cab/Fork Velocity Limit (deg/sec)	Start Radial G	Change in Arm Velocity (RPM)	Type of Arm Input	Change in Fork Angle (degrees)	Type of Fork Input	Change in Cab Angle (degrees)	Type of Cab Input	Notes	Initial G Total	Radius 19.0 ft Initial RPM	Final RPM	Final G Total
p2_47	961010DB.017	47	30	1	10	step	-30	step	30	step		1.414	12.430	22.43	3.40
p2_48	961010DB.018	48	30	1	20	step	+30	step	-30	step		1.414	12.430	32.43	6.90
p2_49	961010DB.019	49	30	1	10	step	-60	step	60	step		1.414	12.430	22.43	3.40
p2_50	961010DB.020	50	30	1	20	step	+60	step	-60	step	FORK UNSTABLE@END	1.414	12.430	32.43	6.90
p2_51	961010DB.021	51	30	1	10	step	-90	step	90	step		1.414	12.430	22.43	3.40
p2_52	961010DB.022	52	30	1	20	step	+90	step	-90	step		1.414	12.430	32.43	6.90
p2_53	961010DB.024	53	30	3	10	step	30	step	-30	step	FORK MOVES	3.160	21.530	31.53	6.50
p2_54	961010DB.025	54	30	3	10	step	+30	step	-30 ok	step	? SHOULD BE NEG FORK	3.160	21.530	31.53	6.50
p2_55	961010DB.026	55	30	3	10	step	-60 +30	step	-60 -30	step		3.160	21.530	31.53	6.50
p2_56	961010DB.027	56	30	3	10	step	-60	step	-60 +60	step		3.160	21.530	31.53	6.50
p2_57	961010DB.028	57	30	3	10	step	-90 +60	step	-90 -60	step		3.160	21.530	31.53	6.50
p2_58	961010DB.029	58	30	3	10	step	-90	step	-90 90	step		3.160	21.530	31.53	6.50
p2_59	961010DB.030	59	40 30	1 3	10		30 90	step?	-90	step		1.414	12.430		
p2_60	961010DB.031	60	40	1			-30	step				1.414	12.430		
p2_61	961010DB.032	61	40	3			30	step				3.160	21.530		
p2_62	961010DB.033	62	40	3			-30	step				3.160	21.530		
p2_63	961010DB.034	63	40	1			-60 30	step				1.414	12.430		
p2_64	961010DB.035	64	40	1			-60 ok	step				1.414	12.430		
p2_65	961010DB.036	65	40	57			60	step				3.160	21.530		
p2_66	961010DB.037	66	40	3			-60 ok	step				3.160	21.530		
p2_67	961010DB.038	67	40	1			-90 +60	step				1.414	12.430		
p2_68		68	40	1			-90	step				1.414	12.430		
p2_69	961010DB.039	69	40	21			90 -90	step				3.160	21.530		
p2_70	961010DB.040	70	40	3			-90	step				3.160	21.530		
p2_71	961010DB.041	71 72	40 35	1					30	step		1.414	12.430		
p2_72	961010DB.042	72 73	40 35	1					-30	step		1.414	12.430		
p2_73	961010DB.043	73 74	40 "	3					30	step		3.160	21.530		
p2_74	961010DB.044	74 75	40 "	3					-30	step		3.160	21.530		
p2_75	961010DB.045	75 76	40 "	5					30	step		5.100	27.800		
p2_76	961010DB.046	76 77	40 35	5					-30	step		5.100	27.800		
p2_77	961010DB.047	77 78	40 ok	1					60	step		1.414	12.430		
p2_78	961010DB.048	78 79	40 "	1					-60	step		1.414	12.430		
p2_79	961010DB.049	79 80	40 "	3					60	step		3.160	21.530		
p2_80	961010DB.050	80 81	40 "	3					-60	step	Arm was still accelerating	3.160	21.530		
p2_81	961010DB.051	81 82	40 "	5					60	step		5.100	27.800		
p2_82	961010DB.052	82 83	40 "	5					-60	step		5.100	27.800		
p2_83	961010DB.053	83 84	40 "	1					90	step		1.414	12.430		
p2_84	961010DB.054	84 85	40 "	1					-90	step		1.414	12.430		
p2_85	961010DB.055	85 86	40 "	3					90	step		3.160	21.530		
p2_86	961010DB.056	86 87	40 "	3					-90	step		3.160	21.530		
p2_87	961010DB.057	87 88	40 "	5					90	step		5.100	27.800		
p2_88	961010DB.058	88	40 "	5					-90	step		5.100	27.800		
p2_89	961010DB.060	89	40 "	1			-45	step	45	step		1.414	12.430		
p2_90	961010DB.061	90	40 "	1			+45	step	-45	step		1.414	12.430		
p2_91	961010DB.062	91	40 "	3			-45	step	45	step		3.160	21.530		
p2_92	961010DB.063	92	40 "	3			+45	step	-45	step		3.160	21.530		
p2_93	961010DB.064	93	40 35	1	10	step	-30	step	30	step	Cab flew [illegible] right [illegible]	1.414	12.430	22.43	3.40
p2_94		94	40 !	1	20	step	-30	step	-30	step		1.414	12.430	32.43	6.90

BRC Second Series of DES Tests

961011

BRC Phase 2 Tests 10/18/96

Profile Name	Data Filename	Profile # (pf) Test #	Cab/Fork Velocity Limit (deg/sec)	Start Radial G	Change in Arm Velocity (RPM)	Type of Arm Input	Change in Fork Angle (degrees)	Type of Fork Input	Change in Cab Angle (degrees)	Type of Cab Input	Notes	Initial G Total	Radius 19.0 ft Initial RPM	Final RPM	Final G Total
p2_1	961007DB.000	1		1	10	ramp					Ramp up 10 rpm at 0.5G/s	1.414	12.430	22.43	3.40
p2_2	961007DB.001	2		1	20	ramp					Ramp up 10 rpm at 0.5G/s	1.414	12.430	32.43	6.90
p2_3	961007DB.002	3		3	10	ramp					Ramp up 10 rpm at 0.5G/s	3.160	21.530	31.53	6.50
p2_4		4		5	10	ramp					Ramp up 10 rpm at 0.5G/s	5.100	27.800	37.80	9.30
p2_5	961007DB.003	5		1	15	step						1.414	12.430	27.43	5.00
p2_6		6		1	25	step						1.414	12.430	37.43	9.10
p2_7		7		3	15	step						3.160	21.530	36.53	8.70
p2_8		8		5	8	step					Ramp down 10 rpm at 0.5G/s	5.100	27.800	35.80	8.35
p2_9	961007DB.004	9		3	-10	ramp					Ramp down 10 rpm at 0.5G/s	3.160	21.530	11.53	1.30
p2_10	961007DB.005	10		5	-20	ramp						5.100	27.800	7.80	?
p2_11	961007DB.006	11		3	-15	step						3.160	21.530	6.53	?
p2_12	961007DB.007	12		5	-25	step						5.100	27.800	2.80	?
p2_13	961007DB.008	13	30	1			-30	step				1.414	12.430		
p2_14	961007DB.009	14	30	1			+30	step				1.414	12.430		
p2_15	961007DB.012	15	30	3			-30	step				3.160	21.530		
p2_16	961007DB.013	16	30	3			+30	step				3.160	21.530		
p2_17	961007DB.014	17	30	1			-60	step				1.414	12.430		
p2_18	961007DB.015	18	30	1			+60	step				1.414	12.430		
p2_19	961007DB.017	19	30	3			-60	step				3.160	21.530		
p2_20	961007DB.018	20	30	3			+60	step				3.160	21.530		
p2_21	961007DB.019	21	30	1			-90	step				1.414	12.430		
p2_22	961007DB.020	22	30	1			+90	step				1.414	12.430		
p2_23	961007DB.021	23	30	3			-90	step				3.160	21.530		
p2_24	961007DB.022	24	30	3			+90	step				3.160	21.530		
p2_25	961007DB.023	25	30	1					30	step		1.414	12.430		
p2_26	961007DB.024	26	30	1					-30	step	Nervous - 38° → 14° = 84°	1.414	12.430		
p2_27	961007DB.025	27	30	3					30	step		3.160	21.530		
p2_28	961007DB.026	28	30	3					-30	step	Good	3.160	21.530		
p2_29	961007DB.027	29	30	84.5					30	step	OK, 10 1a	5.100	27.800		
p2_30	961010DB.000	30	30	5					-30	step	OK. Spike	5.100	27.800		
p2_31	961010DB.001	31	30	1					60	step	OK	1.414	12.430		
p2_32	961010DB.002	32	30	1					-60	step	OK	1.414	12.430		
p2_33	961010DB.003	33	30	3					60	step	OK.	3.160	21.530		
p2_34	961010DB.004	34	30	3					-60	step	Good	3.160	21.530		
p2_35	961010DB.005	35	30	5					60	step	Good	5.100	27.800		
p2_36	961010DB.006	36	30	5					-60	step	Good	5.100	27.800		
p2_37	961010DB.007	37	30	1					90	step	Good	1.414	12.430		
p2_38	961010DB.008	38	30	1					-90	step	Good	1.414	12.430		
p2_39	961010DB.009	39	30	3					90	step	"	3.160	21.530		
p2_40	961010DB.010	40	30	3					-90	step	"	3.160	21.530		
p2_41	961010DB.011	41	30	5					90	step	"	5.100	27.800		
p2_42	961010DB.012	42	30	5					-90	step	"	5.100	27.800		
p2_43	961010DB.013	43	30	1			-45	step	45	step	OK	1.414	12.430		
p2_44	961010DB.014	44	30	1			+45	step	-45	step	OK	1.414	12.430		
p2_45	961010DB.015	45	30	3			-45	step	45	step	OK	3.160	21.530		
p2_46	961010DB.016	46	30	3			+45	step	-45	step	OK	3.160	21.530		

BRC Second Series of DES Tests

961011

BRC Phase 2 Tests 10/18/96

Profile Name	Data Filename	Profile # (pf) Test #	Cab/Fork Velocity Limit (deg/sec)	Start Radial G	Change in Arm Velocity (RPM)	Type of Arm Input	Change in Fork Angle (degrees)	Type of Fork Input	Change in Cab Angle (degrees)	Type of Cab Input	Notes	Initial G Total	Radius 19.0 ft Initial RPM	Final RPM	Final G Total
p2_1	961007DB.000	1		1	10	ramp					Ramp up 10 rpm at 0.5G/s	1.414	12.430	22.43	3.40
p2_2	961007DB.001	2		1	20	ramp					Ramp up 10 rpm at 0.5G/s	1.414	12.430	32.43	6.90
p2_3	961007DB.002	3		3	10	ramp					Ramp up 10 rpm at 0.5G/s	3.160	21.530	31.53	6.50
p2_4		4		5	10	ramp					Ramp up 10 rpm at 0.5G/s	5.100	27.800	37.80	9.30
p2_5	961007DB.003	5		1	15	step						1.414	12.430	27.43	5.00
p2_6		6		1	25	step						1.414	12.430	37.43	9.10
p2_7		7		3	15	step						3.160	21.530	36.53	8.70
p2_8		8		5	8	step					Ramp down 10 rpm at 0.5G/s	5.100	27.800	35.80	8.35
p2_9	961007DB.004	9		3	-10	ramp					Ramp down 10 rpm at 0.5G/s	3.160	21.530	11.53	1.30
p2_10	961007DB.005	10		5	-20	ramp						5.100	27.800	7.80	?
p2_11	961007DB.006	11		3	-15	step						3.160	21.530	6.53	?
p2_12	961007DB.007	12		5	-25	step						5.100	27.800	2.80	?
p2_13	961007DB.008	13	30	1			-30	step				1.414	12.430		
p2_14	961007DB.009	14	30	1			+30	step				1.414	12.430		
p2_15	961007DB.012	15	30	3			-30	step				3.160	21.530		
p2_16	961007DB.013	16	30	3			+30	step				3.160	21.530		
p2_17	961007DB.014	17	30	1			-60	step				1.414	12.430		
p2_18	961007DB.015	18	30	1			+60	step				1.414	12.430		
p2_19	961007DB.017	19	30	3			-60	step				3.160	21.530		
p2_20	961007DB.018	20	30	3			+60	step				3.160	21.530		
p2_21	961007DB.019	21	30	1			-90	step				1.414	12.430		
p2_22	961007DB.020	22	30	1			+90	step				1.414	12.430		
p2_23	961007DB.021	23	30	3			-90	step				3.160	21.530		
p2_24	961007DB.022	24	30	3			+90	step				3.160	21.530		
p2_25	961007DB.023	25	30	1					30	step		1.414	12.430		
p2_26	961007DB.024	26	30	1					-30	step		1.414	12.430		
p2_27	961007DB.025	27	30	3					30	step		3.160	21.530		
p2_28	961007DB.026	28	30	3					-30	step		3.160	21.530		
p2_29	961007DB.027	29	30	5					30	step		5.100	27.800		
p2_30	961010DB.000	30	30	5					-30	step		5.100	27.800		
p2_31	961010DB.001	31	30	1					60	step		1.414	12.430		
p2_32	961010DB.002	32	30	1					-60	step		1.414	12.430		
p2_33	961010DB.003	33	30	3					60	step		3.160	21.530		
p2_34	961010DB.004	34	30	3					-60	step		3.160	21.530		
p2_35	961010DB.005	35	30	5					60	step		5.100	27.800		
p2_36	961010DB.006	36	30	5					-60	step		5.100	27.800		
p2_37	961010DB.007	37	30	1					90	step		1.414	12.430		
p2_38	961010DB.008	38	30	1					-90	step		1.414	12.430		
p2_39	961010DB.009	39	30	3					90	step		3.160	21.530		
p2_40	961010DB.010	40	30	3					-90	step		3.160	21.530		
p2_41	961010DB.011	41	30	5					90	step		5.100	27.800		
p2_42	961010DB.012	42	30	5					-90	step		5.100	27.800		
p2_43	961010DB.013	43	30	1			-45	step	45	step		1.414	12.430		
p2_44	961010DB.014	44	30	1			+45	step	-45	step		1.414	12.430		
p2_45	961010DB.015	45	30	3			-45	step	45	step		3.160	21.530		
p2_46	961010DB.016	46	30	3			+45	step	-45	step		3.160	21.530		

THIRD SERIES OF TESTS

Cumulative Profile Test Name Matrix

Profile Number	File Name	Base G (G's)	Descriptive Profile Name
1	prof3_01	1.4	1.4G w+5 A+0.1
2	prof3_02	1.4	1.4G w-5 A-0.1
3	prof3_03	1.4	1.4G w+5 A+0.25
4	prof3_04	1.4	1.4G w-5 A-0.25
5	prof3_05	2.5	2.5G w+5 A+0.1
6	prof3_06	2.5	2.5G w-5 A-0.1
7	prof3_07	2.5	2.5G w+5 A+0.25
8	prof3_08	2.5	2.5G w-5 A-0.25
9	prof3_09	3.2	3.2G w+5 A+0.1
10	prof3_10	3.2	3.2G w-5 A-0.1
11	prof3_11	3.2	3.2G w+5 A+0.25
12	prof3_12	3.2	3.2G w-5 A-0.25
13	prof3_13	4.2	4.2G w+5 A+0.1
14	prof3_14	4.2	4.2G w-5 A-0.1
15	prof3_15	4.2	4.2G w+5 A+0.25
16	prof3_16	4.2	4.2G w-5 A-0.25
17	prof3_17	1.4	1.4G CA1 F-0 C-180
18	prof3_18	1.4	1.4G CA2 F-0 C-270
19	prof3_19	1.4	1.4G CA3 F-0 C-90
20	prof3_20	1.4	1.4G CA4 F-0 C-180
21	prof3_21	1.4	1.4G CF1 F-0 C-180
22	prof3_22	1.4	1.4G CF2 F-0 C-270
23	prof3_23	1.4	1.4G CF3 F-0 C-90
24	prof3_24	1.4	1.4G CF4 F-0 C-180

25	prof3_25	1.4	1.4G FA1 F-180 C-0
26	prof3_26	1.4	1.4G FA2 F-270 C-0
27	prof3_27	1.4	1.4G FA3 F-90 C-0
28	prof3_28	1.4	1.4G FA4 F-180 C-0
29	prof3_29	1.4	1.4G FF1 F-180 C-0
30	prof3_30	1.4	1.4G FF2 F-270 C-0
31	prof3_31	1.4	1.4G FF3 F-90 C-0
32	prof3_32	1.4	1.4G FF4 F-180 C-0
33	prof3_33	3.2	3.2G CA5 F-0 C-180
34	prof3_34	3.2	3.2G CA6 F-0 C-270
35	prof3_35	3.2	3.2G CA7 F-0 C-90
36	prof3_36	3.2	3.2G CA8 F-0 C-180
37	prof3_37	3.2	3.2G CF5 F-0 C-180
38	prof3_38	3.2	3.2G CF6 F-0 C-270
39	prof3_39	3.2	3.2G CF7 F-0 C-90
40	prof3_40	3.2	3.2G CF8 F-0 C-180
41	prof3_41	3.2	3.2G FA5 F-180 C-0
42	prof3_42	3.2	3.2G FA6 F-270 C-0
43	prof3_43	3.2	3.2G FA7 F-90 C-0
44	prof3_44	3.2	3.2G FA8 F-180 C-0
45	prof3_45	3.2	3.2G FF5 F-180 C-0
46	prof3_46	3.2	3.2G FF6 F-270 C-0
47	prof3_47	3.2	3.2G FF7 F-90 C-0
48	prof3_48	3.2	3.2G FF8 F-180 C-0
49	prof3_49	2.9	Cobra Arm
50	prof3_50	2.2	Cobra Fork1
51	prof3_51	2.2	Cobra Cab1
52	prof3_52	2.2	Cobra Fork2
53	prof3_53	2.2	Cobra Cab2